ote technical note technical

Reflective Cracking Outdoor Phase I Comprehensive Report
Part B –Test Report

August 2020

DOT/FAA/TC-TNxx/xx

This document is available to the U.S. public through the National Technical Information Services (NTIS), Springfield, Virginia 22161.

This document is also available from the Federal Aviation Administration William J. Hughes Technical Center at actlibrary.tc.faa.gov.

U.S. Department of Transportation
Federal Aviation Administration

NOTICE

This document is disseminated under the sponsorship of the U.S. Department of Transportation in the interest of information exchange. The United States Government assumes no liability for the contents or use thereof. The United States Government does not endorse products or manufacturers. Trade or manufacturer's names appear herein solely because they are considered essential to the objective of this report. The findings and conclusions in this report are those of the author(s) and do not necessarily represent the views of the funding agency. This document does not constitute FAA policy. Consult the FAA sponsoring organization listed on the Technical Documentation page as to its use.

This report is available at the Federal Aviation Administration William J. Hughes Technical Center's Full-Text Technical Reports page: actlibrary.tc.faa.gov in Adobe Acrobat portable document format (PDF).

Technical Report Documentation Page

1. Report No.	2. Government Accession No.	3. Recipient's Catalog No.
DOT/FAA/TC-TNxx/xx	DOT/FAA/TC-TNxx/xx	

4. Title and Subtitle	5. Report Date
Reflective Cracking Outdoor Phase I Comprehensive Report Part B –Test Report	July 31, 2020
	6. Performing Organization Code
7. Author(s) Mesbah Ahmed, Mir Arefin, Hao Yin	8. Performing Organization Report No.
9. Performing Organization Name and Address GDIT 600 Aviation Research Blvd. Egg Harbor Township, NJ 08234	10. Work Unit No. (TRAIS)
	11. Contract or Grant No. DTFACT-15-D-00007
12. Sponsoring Agency Name and Address U.S. Department of Transportation Federal Aviation Administration Airport Engineering Division 800 Independence Ave., SW Washington, DC 20591	13. Type of Report and Period Covered Technical Note
	14. Sponsoring Agency Code AAS-100

15. Supplementary Notes

The Federal Aviation Administration Airport Technology Research and Development COR is Jeffrey Gagnon.

16. Abstract

The crack propagation rate derived from the previous six indoor full-scale tests conducted at the FAA (Federal Aviation Administration) National Airport Pavement Test Facility (NAPTF), needed to be validated and calibrated to the field conditions that involves both aircraft and temperature loads. To address, the Reflective Cracking Outdoor Phase I test pavement section was constructed at the FAA National Airport Pavement and Material Research Center (NAPMRC), to isolate and compare aircraft gear load and temperature effects on the initiation and propagation of reflection cracks. The FAA Heavy Vehicle Simulator-Airfields (HVS-A) was used on the Temperature and Traffic (TT) section to simulate the mixed loading (aircraft gear load and temperature variation), while the Temperature Only (TO) section was subjected to the temperature loads only.

During the response test, asphalt strain gage data showed the occurrence of maximum tensile strains at the overlay bottom and therefore, leading to an anticipation of Mode I fracture at the overlay bottom. During the formal full-scale testing, several reflection cracks were observed along joint TT34, TT45, and TT56 of the TT section. The pass number corresponding to crack initiation was estimated based on a strain energy analysis. The temperature profile on the TO section recorded the lowest overlay temperature at the surface, which was in opposition to the bottom-up cooling scheme resulted in negative temperature gradient in the Indoor Reflective Cracking Tests.

17. Key Words	18. Distribution Statement
	This document is available to the U.S. public through the National Technical Information Service (NTIS), Springfield, Virginia 22161. This document is also available from the Federal Aviation Administration William J. Hughes Technical Center at actlibrary.tc.faa.gov.

19. Security Classif. (of this report)	20. Security Classif. (of this page)	21. No. of Pages	22. Price
Unclassified	Unclassified	55	

Form DOT F 1700.7 (8-72) Reproduction of completed page authorized

TABLE OF CONTENTS

	Page
EXECUTIVE SUMMARY	IX
INTRODUCTION	1
DESIGN AND CONSTRUCTION OF THE TEST SECTION	2
Description Of Test Section	2
Construction	5
Subgrade (P-152MR) Preparation	5
Subbase (P-154MR) Construction	5
Concrete (P-501MR) Paving	6
Shoulder (P-209MR) Construction	6
Surface HMA (P-401MR) Paving	7
Instrumentation	7
DESCRIPTION OF TESTING METHODS AND EQUIPMENT	12
Testing Equipment	12
Test Description	12
Estimation of Wheel Load	12
Test Procedure	15
Response Test	18
Monitoring	18
FULL SCALE TEST	19
Response Test	19
Traffic Test	21
Observations	22
BASELINE MEASUREMENT ANALYSIS	24
HWD Data	24
Initial Analysis	24
Backcalculation of Layer Moduli	27
LWD Data	32
TRAFFIC DATA ANALYSIS	34

Preliminary Analysis 34

Critical Track 34
Strain Response 36
Overlay Temperature 39

Advanced Analysis 40

Crack Characterization 40
Joint Movement 43

SUMMARY 45

REFERENCES 46

APPENDICES

Appendix A—Distress Photos A-1

Appendix B—Distress Maps B-1

Appendix C—LWD Results C-1

Appendix D—HMA Overlay Modulus D-1

Appendix E—Joint Displacement Gage Plots E-1

LIST OF FIGURES

Figure	Page
1 Mechanisms of Reflective Cracking (Yin, 2016)	1
2 RC Outdoor Phase I Pavement Cross-Section (Mandal and Yin, 2019)	2
3 Reflective Cracking Outdoor Phase I, Test Item Layout (Mandal and Yin, 2019)	3
4 Reflective Cracking Outdoor Phase I, Test Item Cross-section (Mandal and Yin, 2019)	4
5 Reflective Cracking Outdoor Phase I Instrumentation Layout (Mandal and Yin, 2019)	11
6 HVS-A with SWL on RC Outdoor Phase I Pavement Section	12
7 Horizontal Tensile Strain at HMA Overlay Bottom (Traffic & Temperature Load) (GDIT, 2019)	13
8 Cumulative Strain Energy at HMA Overlay Bottom (Traffic & Temperature Load) (GDIT, 2019)	14
9 Pass to Crack Initiation vs. Wheel Load (Traffic & Temperature Loads) (GDIT, 2019)	14
10 Wander Pattern (GDIT, 2019)	16
11 Sample Distress map (Portion)	23
12 Sample Log (Portion)	23
13 HWD and LWD Test Layout	25
14 HWD Deflection Basin: (a) TO, and (b) TT	26
15 Dynamic Modulus of P-401MR	31
16 Determination of Critical Track from Strain Responses (TT34-SG7-3.0)	35
17 Strain Profile in the HMA Overlay (TO34)	37
18 Strain Distribution along Joint (TO34)	37
19 Strain Responses at the Overlay Edge (Doweled vs Undoweled)	38
20 Strain Responses in the Middle of the Overlay (Doweled vs Undoweled)	38
21 Temperature Variations in HMA overlay (5 day of Trafficking)	39
22 Temperature Variation in HMA Overlay (Yin, 2017)	40
23 1st Bottom-up Crack on the West Edge of TT45 (February 12, 2020)	41
24 SG Response over Pass Number at the West Edge of TT45	41
25 Joint Displacement at the West Edge of TT45	42
26 Cumulative Strain Energy Calculated from TT45-SG7-3.0 along West Edge of TT45	42
27 Joint Displacement along Doweled Joint (over 5-days of Trafficking)	43
28 Joint Displacement along Undoweled Joint (over 5-days of Trafficking)	44
29 Joint Opening in Response to HMA Temperature Differential	45

LIST OF TABLES

Table	Page
1 Timeline for Construction of P-152MR Layer	5
2 Timeline for Construction of P-154MR Layer	6
3 HVS-A Carriage Positions for a Full Wander Pattern (GDIT, 2019)	16
4 HVS-A Carriage Positions for Response Test (GDIT, 2019)	18
5 RC Outdoor Phase I Sensor Response Test Data Summary for TT Section	19
6 RC Outdoor Phase I Sensor Response Test Data Summary for TO Section	20
7 Traffic History on TT Section	22
8 Traffic History and Distress Observation on TT Section	24
9 Summary of ISM (TO and TT)	27
10 Pavement Structure and Layer Seed Moduli Used for Backcalculation	28
11 Summary of HWD Load and Deflection Corresponding to 12,000 lbs Load Level	29
12 Summary of Backcalculated Layer Modulus	30
13 ANOVA Analysis of Backcalculated Layer Moduli	32
14 Summary of Combined Modulus from LWD Test	34
15 ANOVA Analysis of Combined Modulus	34
16 Critical Track based on Response Test Data	35

LIST OF ACRONYMS

ANOVA	Analysis of Variation
ASTM	American Standard for Testing and Materials
DAQ	Data Acquisition Unit
DCP	Dynamic Cone Penetrometer
D-PSPA	Portable Seismic Pavement Analyzer for Unbound Material
EG	Strain Gages
FAA	Federal Aviation Administration
HVS-A	Heavy Vehicle Simulator-Airfields
HMA	Hot Mix Asphalt
HWD	Heavy Weight Deflectometer
JDG	Joint Displacement Gages
LWD	Light Weight Deflectometer
NAPTF	National Airport Pavement Test Facility
NAPMRC	National Airport Pavement and Material Research Center
PI	Principal Investigator
PSPA	Portable Seismic Pavement Analyzer
RC	Reflective Cracking
SG	Surface Strain Gages
SWL	Single Wheel Load
T	Thermocouple
TESS	Temperature Effect Simulation System
TO	Temperature Load Only
TT	Traffic and Temperature Load

EXECUTIVE SUMMARY

Reflective cracking is considered a major challenge in maintenance and rehabilitation of rigid airfield pavements with asphalt overlay, which is not addressed in the current Federal Aviation Administration (FAA) airport pavement design. Previously at the FAA National Airport Pavement Test Facility (NAPTF), six full-scale tests were conducted to understand the mechanism of reflective cracking under mechanically simulated temperature load using the Temperature Effect Simulation System (TESS). The crack propagation rate derived from these indoor tests needed to be validated and calibrated to the field conditions that involves both aircraft and temperature loads.

At the FAA National Airport Pavement and Material Research Center (NAPMRC), the main objective of the Reflective Cracking Outdoor Phase I test was to isolate and compare aircraft gear load and temperature effects on the initiation and propagation of reflection cracks. The test pavement is 155 feet long by 15 feet wide, which comprised two test lanes: Temperature Only (TO) section and Temperature and Traffic (TT) section with a 30 foot long transition in between. The pavement structure included a 3 inch thick P-401MR (HMA overlay with PG 64-22), a 9 inch thick P-501MR (PCC slab), an 8 inch thick P-154MR (granular aggregate subbase), all on a prepared P-152MR subgrade. The P-501MR layer of both TO and TT sections comprised six 10 foot by 10 foot slabs with transverse joints, either Type C (Doweled Contraction Joint) or Type D (Undoweled/Dummy Contraction Joint). The FAA Heavy Vehicle Simulator-Airfields (HVS-A) was used on the TT section to simulate the mixed loading (aircraft gear load and temperature variation), while the TO section was subjected to the temperature loads only. Key pavement instrumentation included surface strain gages (SG), asphalt strain gages (EG), joint displacement gages (JDG), and thermocouples (T) at multiple depths.

Field testing confirmed that the TO and TT sections are replicates. The response data verified the functionality of the most of the SGs, while only three EGs in the TT section and two EGs in the TO section survived during the construction. During the response test, asphalt strain gage data showed the occurrence of maximum tensile strains at the overlay bottom, leading to an anticipation of Mode I fracture at the overlay bottom. During the formal full-scale testing, several reflection cracks were observed on the east and west edges along joint TT34, TT45, and TT56 of the TT section. The pass number corresponding to crack initiation was estimated from a strain energy analysis. The temperature profile on the TO section recorded the lowest overlay temperature at the surface, which was in opposition to the bottom-up cooling scheme that resulted in negative temperature gradient in the Indoor Reflective Cracking Tests.

INTRODUCTION

The objective of reflective cracking research is to develop a set of fully validated equations (the failure model) that can be directly implemented in the overlay design procedure in all future versions of FAARFIELD (Yin, 2016). The failure model will relate the required thickness of an asphalt overlay to several input variables, including projected traffic, climatic data (temperature cycles), and the condition of the existing pavement.

Reflection cracks are caused by discontinuities (cracks or joints) in underlying layers that propagate through a hot mix asphalt (HMA) overlay. This propagation is due to continuous movement at the crack prompted by thermal expansion and traffic loadings. If the new overlay is bonded to the distressed layer, cracks in the existing pavement propagate to the surface after a period of time, which is generally a function of the thickness of the overlay.

Most reflective cracking is caused by the combination of two mechanisms, as illustrated in figure 1: (a) Horizontal Movement of Slab – usually temperature associated and causes tensile and bending stresses to develop in the overlay, and (b) Vertical Movement at the Joint/Crack Area – primarily load induced and creates shear and tensile stresses within the overlay (figure 1). In addition, crack initiation and propagation are influenced by the existing pavement structure and conditions, reflective cracking countermeasures (e.g. reinforcing, interlayers), HMA mixture properties, the degree of load transfer at joints and cracks, and others.

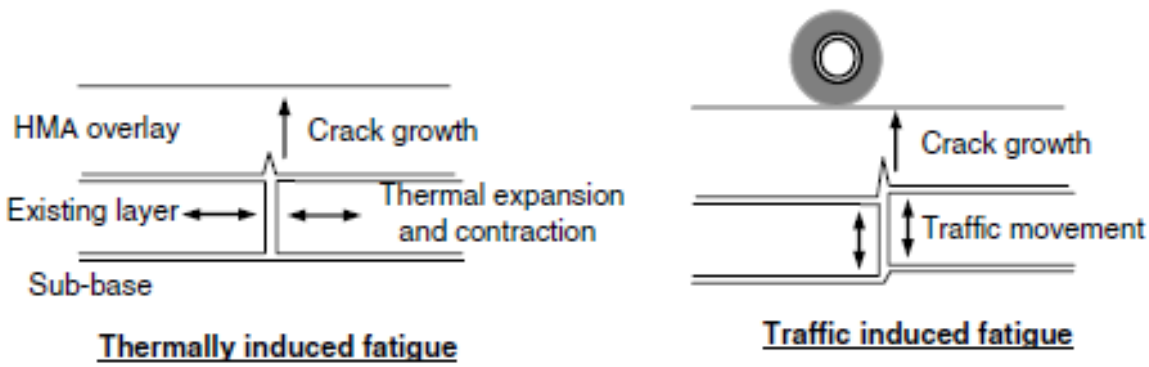

Figure 1. Mechanisms of Reflective Cracking (Yin, 2016).

Comprehensive full-scale tests under different aircraft and temperature loads are needed so that the crack propagation model derived from Reflective Cracking Rig tests can be validated and calibrated to the field conditions. The Heavy Vehicle Simulator-Airfields (HVS-A) provides a unique opportunity to isolate and compare aircraft gear load and temperature effects on reflective cracking (Yin, 2016).

The negative temperature gradient (i.e., cooler on bottom) in the overlay resulting from the bottom-up cooling scheme integrated in the Temperature Effect Simulation System (TESS) during the previous Indoor Reflective Cracking Rig tests in National Airport Pavement Test Facility (NAPTF) does not reflect the temperature cycles occurring in nature realistically. Therefore, two identical pavement cross-sections were built at the National Airport Pavement and Material

Research Center (NAPMRC) to perform experiments using Temperature Load only (TO) and Traffic and Temperature Load (TT).

DESIGN AND CONSTRUCTION OF THE TEST SECTION

DESCRIPTION OF TEST SECTION.

Reflective Cracking (RC) Outdoor Phase I test pavement is 155 feet long by 15 feet wide, consisting of two test areas, Temperature Only (TO) section, Temperature and Traffic (TT) section, and a 30 foot long transition. As shown in figure 2, the pavement structure includes a 3 inch thick P-401MR HMA overlay, a 9 inch thick P-501MR concrete layer, an 8 inch thick P-154MR granular subbase, all on a prepared P-152MR subgrade. The P-501MR layer of each section (TO and TT) consists of six 10 × 10 foot slabs (figure 3). All transverse joints were either Type C (Doweled Contraction Joint) or Type D (Undoweled/Dummy Contraction Joint), as illustrated in figure 4. Since no stabilized base is present and the HMA overlay is relatively thin (3"), this overlaid rigid pavement structure may be considered representative of a non-hub or general aviation facility, i.e., not intended to handle heavy aircraft loads.

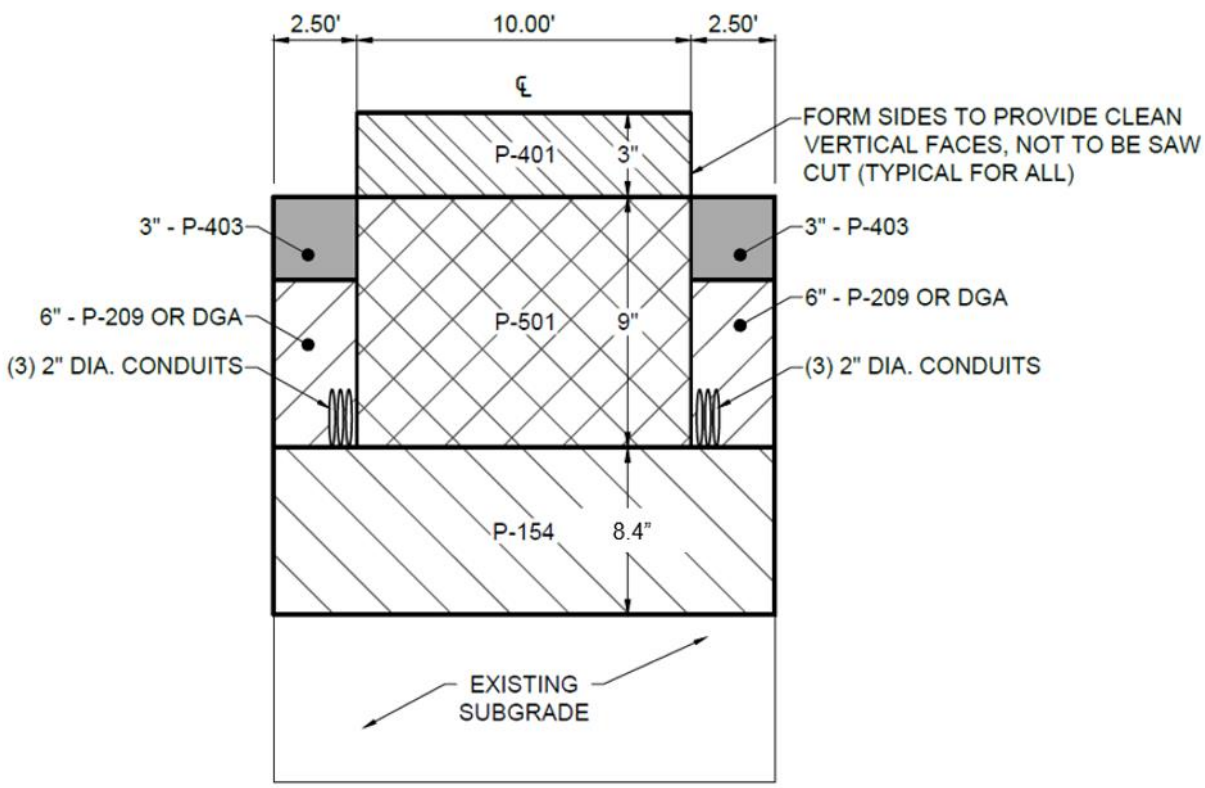

Figure 2. RC Outdoor Phase I Pavement Cross-Section (Mandal and Yin, 2019).

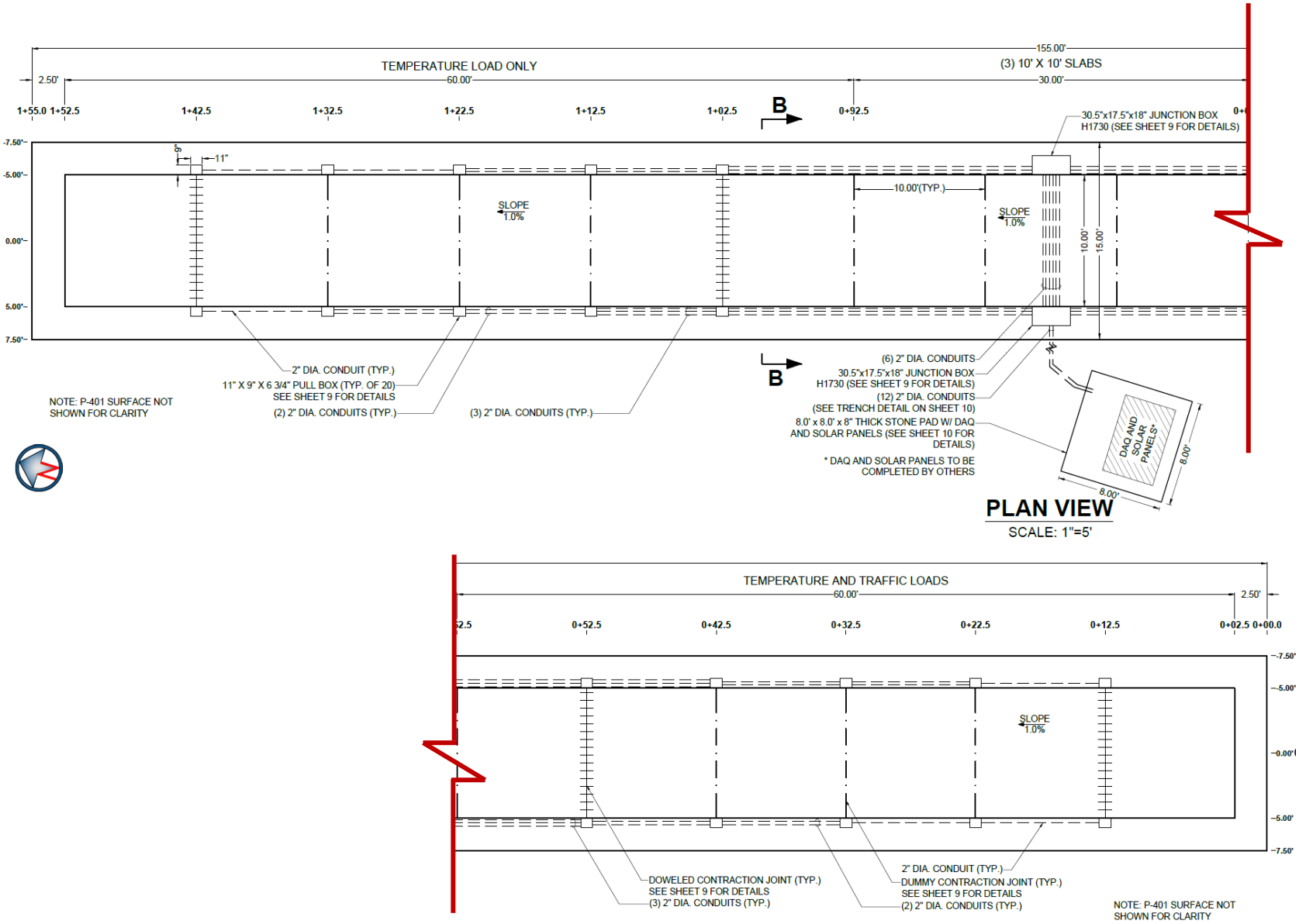

Figure 3. Reflective Cracking Outdoor Phase I, Test Item Layout (Mandal and Yin, 2019).

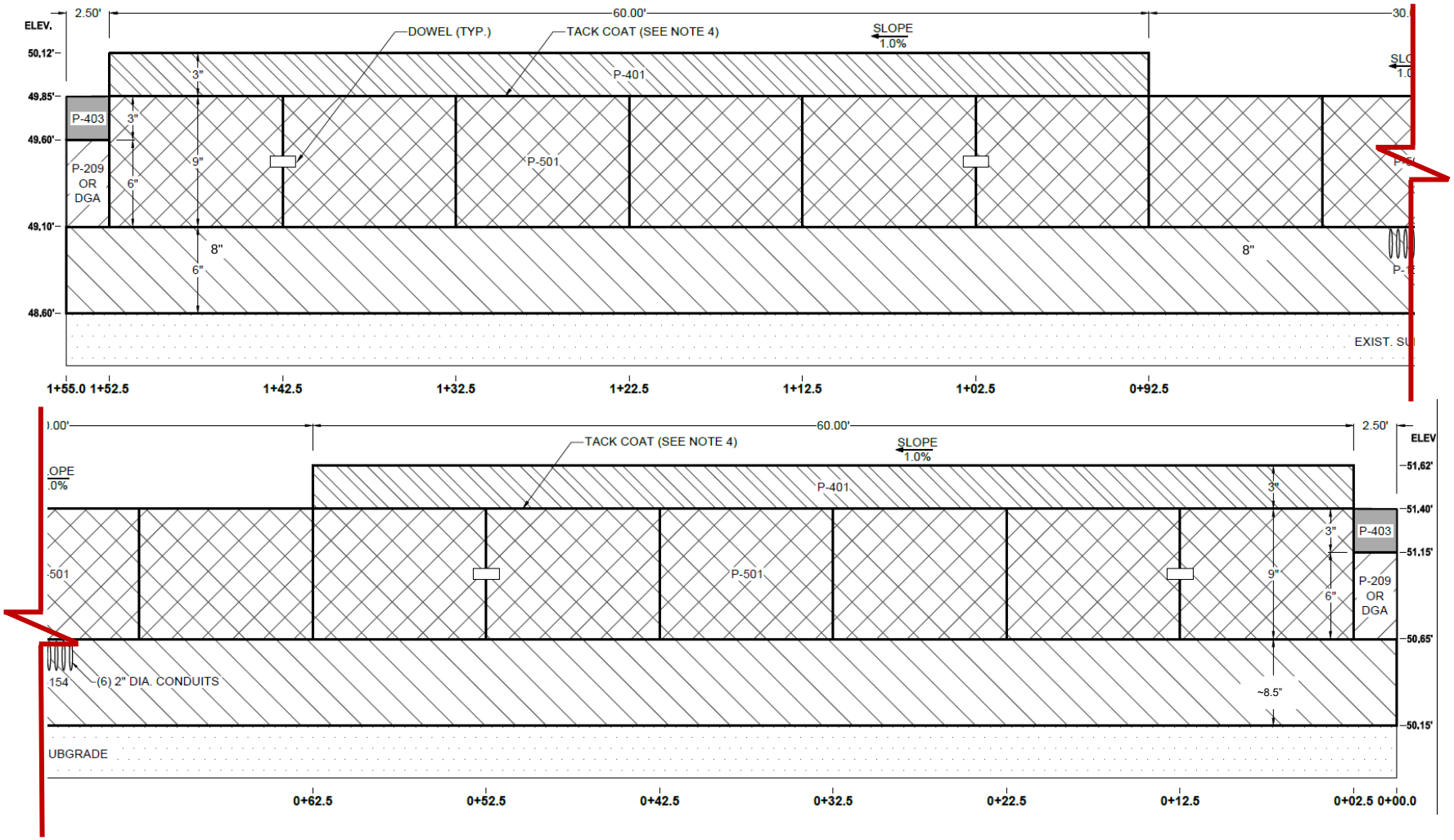

Figure 4. Reflective Cracking Outdoor Phase I, Test Item Cross-section (Mandal and Yin, 2019).

CONSTRUCTION.

The construction of RC Outdoor Phase I required the support and services of several contractors and industry professionals. The construction team consisted of General Dynamics Information Technology (GDIT) personnel, L. Feriozzi Concrete Co (Feriozzi), Atlantic City, NJ; A.E. Stone, Inc. (AE Stone), Egg Harbor Township, NJ; and JBT, Grafton, WI. Material testing and sampling were completed by the FAA's NextGen Materials Testing Laboratory. The nuclear gage density tests were conducted by Craig Testing Laboratories, Inc. (Craig), Mays Landing, NJ, whereas, the 3D scanning for grading slope and elevation for each layer was conducted by Rodriguez Consulting, LLC (Rodriguez), Philadelphia, PA. The construction of RC Outdoor Phase I started on June 18, 2018 and finished on April 30, 2019.

SUBGRADE (P-152MR) PREPARATION. The construction of the subgrade started on June 19, 2018 and finished on June 29, 2018. Table 1 shows the breakdown for the construction of the P-152MR layer, including the field testing. The NextGen Materials Testing Laboratory determined the maximum density of the existing subgrade was 125.7 pcf at a moisture content of 8.9% and the soil classification was SM. Four thermocouples (T) were also installed in the subgrade and covered with a bucket. P-152MR layer construction was accepted on June 29, 2018. Then, field tests such as LWD, D-PSPA, and Dynamic Cone Penetrometer (DCP) were conducted according to the Material Characterization Plan. The results of the field tests are reported in Appendix F of RC Outdoor Phase I Construction History Report (Mandal and Yin, 2019).

Table 1. Timeline for Construction of P-152MR Layer

Item	June 2018										
	19	20	21	22	23	24	25	26	27	28	29
Modified Proctor Curve in Laboratory					*	*					
Compaction					*	*					
Field Tests					*	*					
3D Laser Scan (Leica Model P20)					*	*					
Re-grade Subgrade					*	*					
Re-do 3D Laser Scan					*	*					
Re-do Field Tests					*	*					

** Weekend*

SUBBASE (P-154MR) CONSTRUCTION.

Placement of the P-154MR material commenced on July 2, 2018 and the construction of the P-154MR layer was completed on July 26, 2018. Table 2 shows the breakdown for the construction of the P-154MR layer, including the field testing. The gradation samples showed the materials were within the P-154 specification limits. Results from compaction testing at depths of 4", 6", and 8" all passed the required 100% of the maximum dry density value. Average moisture content values at 4", 6", and 8" depths were 7.3%, 7.4%, and 7.4% respectively. Once the P-154MR layer was accepted by the FAA, field tests such as LWD, DCP, and D-PSPA were conducted on top of P-154MR according to Material Characterization Plan. The LWD and D-PSPA tests were again conducted on November 14, 2018 to verify the test results prior to pouring concrete. A summary

of the testing results is documented in Appendix G of RC Outdoor Phase I Construction History Report (Mandal and Yin, 2019).

Table 2. Timeline for Construction of P-154MR Layer

Item	July 2018																									Nov.
	2	3	4	5	6	7	8	9	10	11	12	13	14	15	16	17	18	19	20	21	22	23	24	25	26	14
P-154MR Material Placement			•			*	*						*	*						*	*					
Proctor Compaction Curve in Laboratory			•			*	*						*	*						*	*					
Watering and Compaction			•			*	*						*	*						*	*					
Trim to Grade After Meeting Density @ 6-in. Depth			•			*	*						*	*						*	*					
Manual Survey			•			*	*						*	*						*	*					
Trim and Skin-patch to Required Elevation			•			*	*						*	*						*	*					
3D Laser Scan			•			*	*						*	*						*	*					
Straight Edge Test			•			*	*						*	*						*	*					
Water to Adjust Moisture Content			•			*	*						*	*						*	*					
Scarify P-154MR Layer			•			*	*						*	*						*	*					
Water and Compact Scarified P-154MR Layer			•			*	*						*	*						*	*					
Manual Survey			•			*	*						*	*						*	*					
Excavate Area to Rectify Soft Spot Area			•			*	*						*	*						*	*					
Compact Excavated Area			•			*	*						*	*						*	*					
Scarify Top Layer of Excavated Area			•			*	*						*	*						*	*					
Manual Survey			•			*	*						*	*						*	*					
Trim to Grade After Meeting Density @ 8-in. Depth			•			*	*						*	*						*	*					
Manual Survey			•			*	*						*	*						*	*					
Re-do Streight Edge Test			•			*	*						*	*						*	*					
Re-do 3D Laser Scan			•			*	*						*	*						*	*					
Field Tests			•			*	*						*	*						*	*					
Field Tests (verification prior to pouring concrete)			•			*	*						*	*						*	*					

• *Holiday*
* *Weekend*

CONCRETE (P-501MR) PAVING. The P-501MR material used for RC Outdoor Phase I was the same as used in Construction Cycle 8 (900 Flex Mix Design) and the mix design is provided in Appendix H of RC Outdoor Phase I Construction History Report. During the installation of the formwork, the thermocouples were also installed on top of the P-154MR layer. Upon completion of the acceptance testing, the P-501MR was placed on December 4, 2018. The results of the acceptance testing are provided in Appendix I of RC Outdoor Phase I Construction History Report. On December 12, 2018 (after 7 days of curing), the formwork for the P-501MR layer was removed. The next day, the joints were saw cut and sealed per the construction plans. Once the P-501MR concrete was cured for 28 days, field tests including the Heavy Weight Deflectometer (HWD) and Portable Seismic Pavement Analyzer (PSPA) were conducted on January 3, 2019. A summary of both material characterization, field test results, and outcomes from the analysis can be found in Appendix I of RC Outdoor Phase I Construction History Report.

SHOULDER (P-209MR) CONSTRUCTION. On April 4, 2019, 58.32 tons of P-209MR material were placed all around the concrete slabs and compacted using a plate compactor. The P-209MR material was placed 3 inches below the edge of the P-501MR layer. The maximum density and moisture content for the P-209MR shoulder material was 162.8 pcf and 5.4%, respectively as determined in the FAA NextGen Pavement Materials Laboratory. Once the P-209MR shoulder met the acceptance requirements, HMA (PG 64-22) was installed all around the concrete slab. The plate compactor was used to compact the HMA material on top of the P-209MR shoulder. The Nuclear Gage was then used to verify the compaction requirements for the HMA material. Testing

was conducted at four random locations and the average density was 92.4% of the maximum dry density. The results of the acceptance testing and laboratory testing on the P-209MR and the HMA material were reported in Appendix J of RC Outdoor Phase I Construction History Report (Mandal and Yin, 2019).

SURFACE HMA (P-401MR) PAVING. Placement of the P-401MR HMA surface layer occurred on April 30, 2019. The P-401MR lift was placed in a single lift directly on the underlying P-501MR layer at a compacted thickness of 3 inches in the 10 foot wide paving lane. Prior to spreading the HMA material using the paver, the project team covered the installed embedded sensors (on top of P-501MR) with the HMA material using shovels. Compaction, using rollers, continued as needed until field densities met the P-401MR specification. At the end, the P-401MR layer achieved an average density of 95.5% after a total of 10 passes. The detailed test results of the field density are documented in Appendix L of RC Outdoor Phase I Construction History Report (Mandal and Yin, 2019). After compaction, the edges of the P-401MR layer were saw cut on May 22, 2019 to create a smooth vertical edge. Loose HMA samples were also obtained from the asphalt plant to verify HMA mix design. The P-401MR mix verification was conducted at the asphalt plant (A.E. Stone) as well as in the NextGen Materials Testing Laboratory. After compaction, core samples were extracted from the transition areas for density acceptance testing. All the laboratory and field test results are summarized in Appendix L of RC Outdoor Phase I Construction History Report (Mandal and Yin, 2019). However, PSPA testing on top of the P-401MR layer was not conducted per the Material Characterization plan as the equipment was not functional at the time.

INSTRUMENTATION.

Figure 5 shows the instrumentation layout. On the TO section, a total of 10 joint displacement gages (JDG) were installed on the side of concrete slab. A total of 10 asphalt strain gages (EG) were embedded at HMA overlay bottom directly above the joint. These gages were placed at two offset locations (+/- 0.67feet) from the centerline. There were also surface strain gages (SG) installed at the overlay surface. Thermocouples (T) were installed with the following arrangement: (a) one array of six at the south-west corner of Slab TO1, and (b) one array of six at the north-east corner of Slab TO6. Thermocouples were placed at depths as shown in figure 5(b) and (d). The TT section has an identical instrumentation layout, as shown in figure 5.

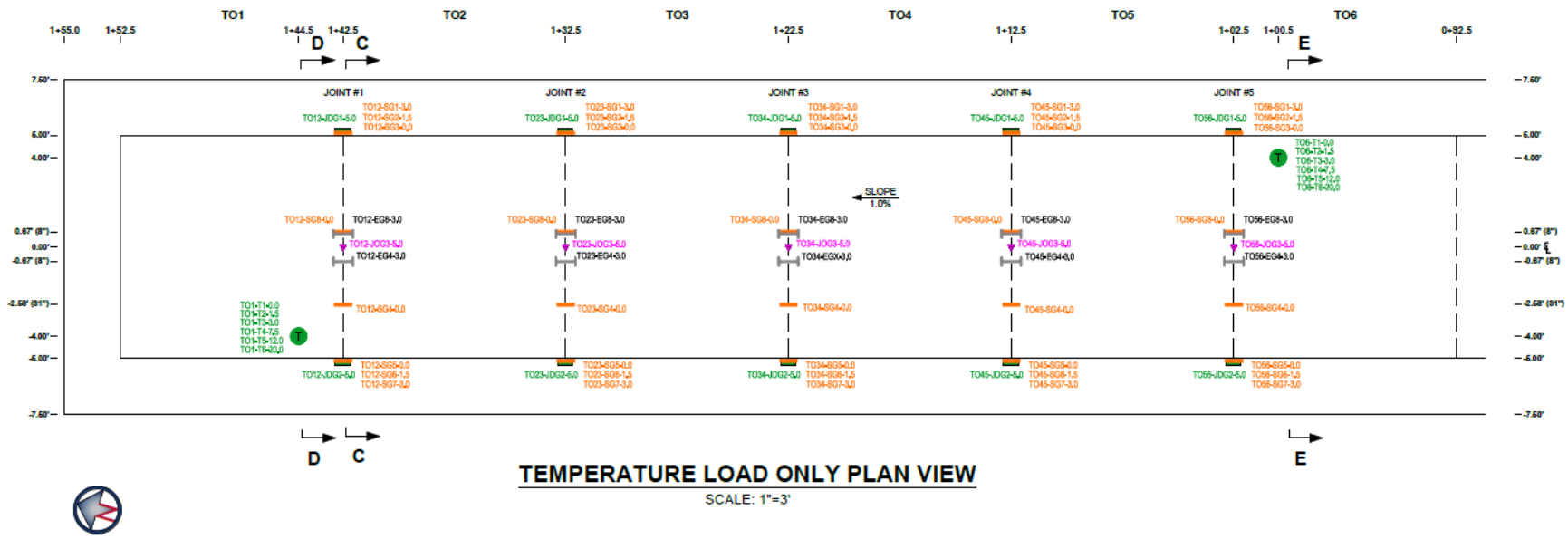

TEMPERATURE LOAD ONLY PLAN VIEW

SCALE: 1"=3'

(a)

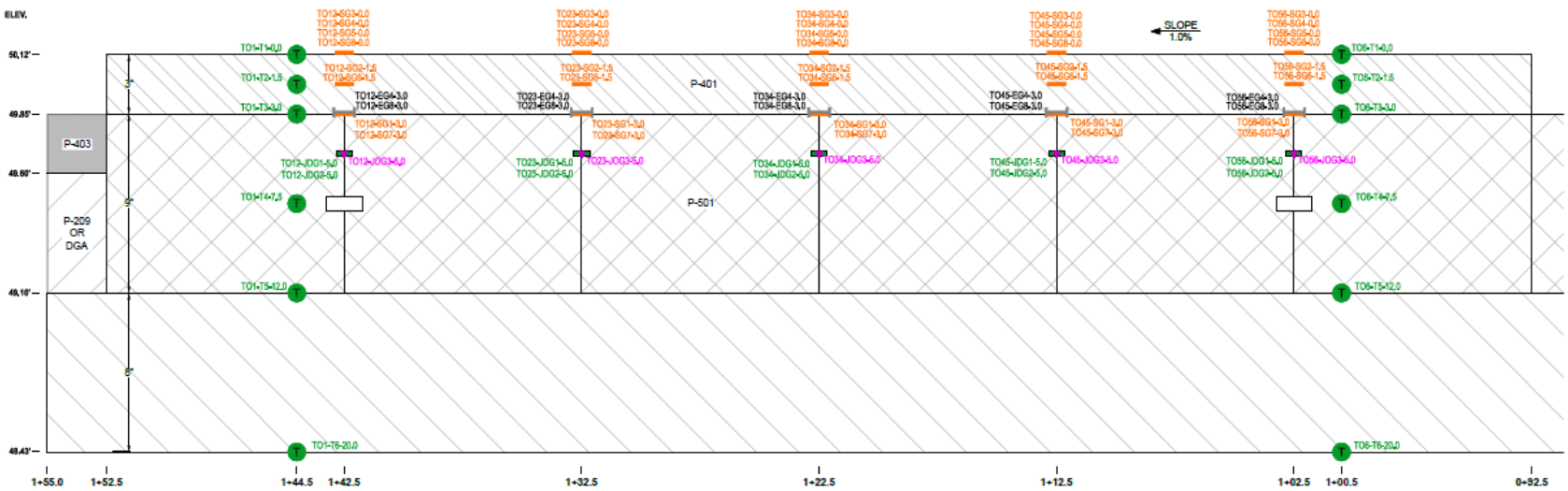

TEMPERATURE LOAD ONLY PROFILE VIEW

(b)

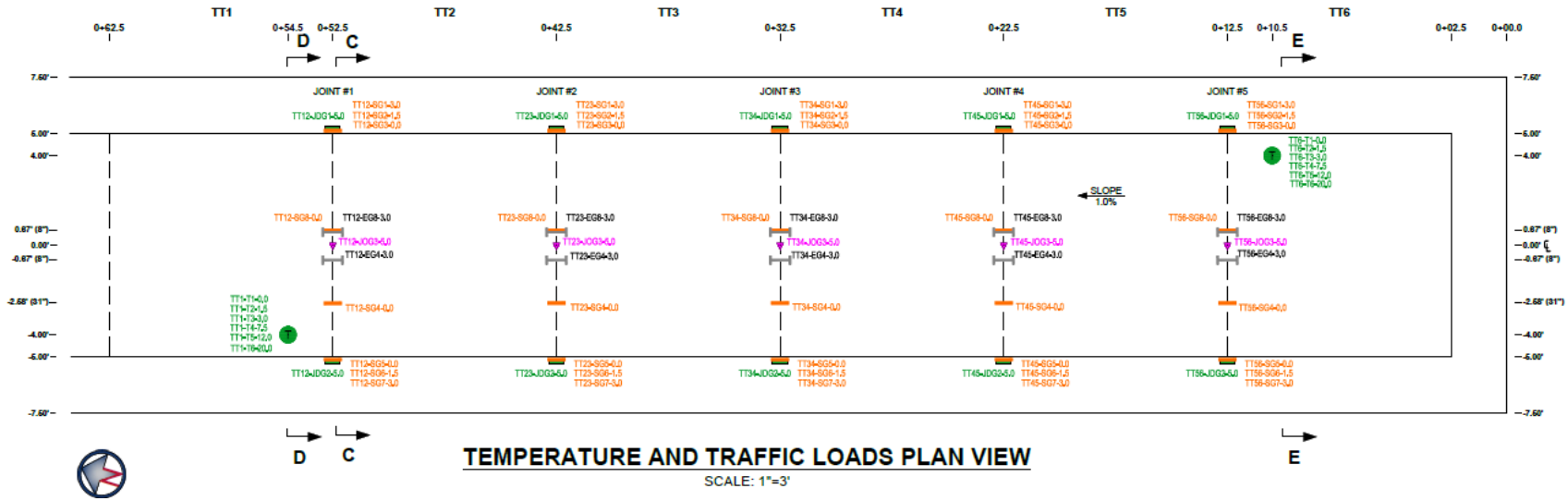
TT1
TT2
TT3
TT4
TT5
TT6
0+62.5
0+54.5
0+52.5
0+42.5
0+32.5
0+22.5
0+12.5
0+10.5
0+02.5
0+00.0
D
C
E
JOINT #1
JOINT #2
JOINT #3
JOINT #4
JOINT #5
SLOPE
1.0%
7.50'
6.00'
4.00'
0.67' (8")
0.00'
-0.67' (8")
-2.58' (31")
-4.00'
-6.00'
-7.50'
TEMPERATURE AND TRAFFIC LOADS PLAN VIEW
SCALE: 1"=3'

(c)

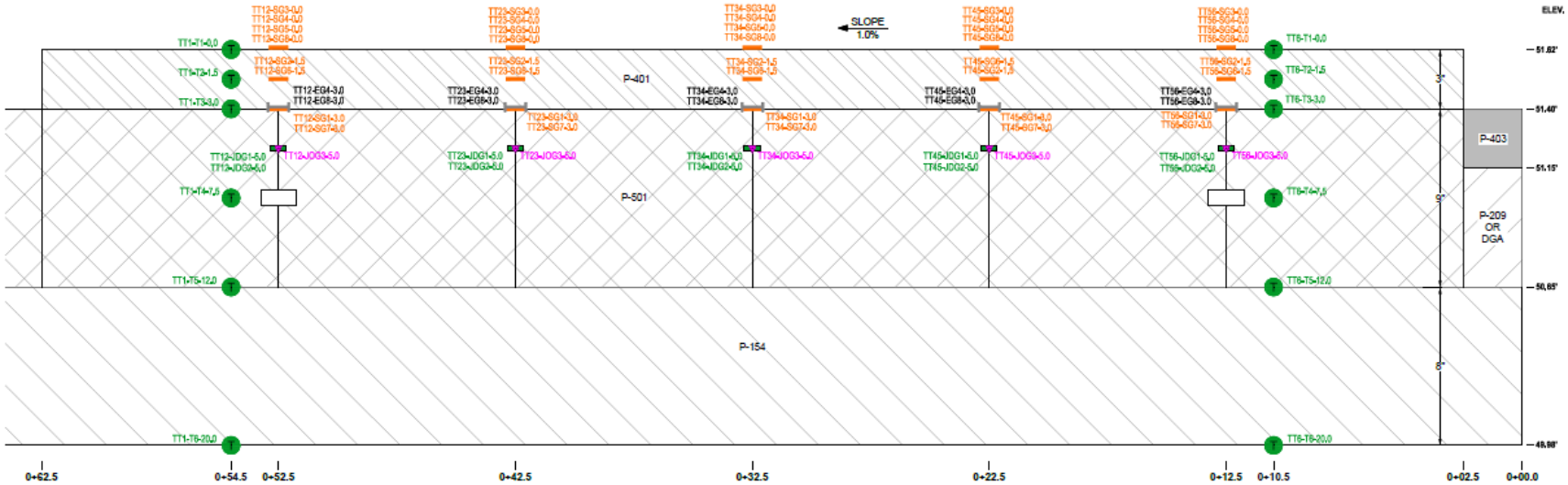

TEMPERATURE AND TRAFFIC LOADS PROFILE VIEW

INSTRUMENT KEY AND QUANTITY			
	EG	EMBEDDED DYNATEST STRAIN GAGE	5
	SG	SURFACE STRAIN GAGE	35
	JDG	JOINT DISPLACEMENT GAGE	10
	T	THERMOCOUPLE	12

(d)

Figure 5. Reflective Cracking Outdoor Phase I Instrumentation Layout (Mandal and Yin, 2019).

DESCRIPTION OF TESTING METHODS AND EQUIPMENT

TESTING EQUIPMENT.

The FAA HVS-A (Mark VI) was used to conduct traffic testing on the TT section (figure 6). The HVS-A (Mark VI) is the largest HVS of its kind, measuring 121 feet long, 16 feet wide, and 14 feet high. Equipped with enhanced control systems, it has greater wander capability than previous generation simulators and is capable of applying bi-directional or unidirectional aircraft loading via a single wheel (maximum load: 100,000 lbs) or dual wheel (maximum load: 50,000 lbs per wheel).

Figure 6. HVS-A with SWL on RC Outdoor Phase I Pavement Section.

TEST DESCRIPTION.

ESTIMATION OF WHEEL LOAD. The single wheel (SWL) was used as the Heavy Vehicle Simulator-Airfields (HVS-A) gear configuration for the traffic test on the TT section. Two threshold criteria were considered for the wheel load selection:

a. Cracking Strain (CS), i.e. Failure Strain, of 1800 microstrain was determined from previous Reflective Cracking indoor tests.
b. Cumulative Cracking Strain Energy (CCSE) of 14.31 in.-lb/in.^{3} determined from Reflective Cracking indoor tests.

As shown in figures 7 and 8, finite element based simulations suggested that both the horizontal tensile strain and the cumulative strain energy at the overlay bottom develop in a highly nonlinear fashion. The details were reported in Appendix F of the RC Outdoor Phase I Comprehensive Test

Plan (GDIT, 2019). The threshold values of CS and CCSE are marked with a solid horizontal red line. As expected, the higher the wheel load, the sooner the threshold was reached. Figure 9 shows the number of passes required for crack initiation at varying load levels (10 kip through 70 kip at 5 kip interval). Given the project timeframe (e.g., 3 years), a wheel load of 40 kip was selected for the traffic test.

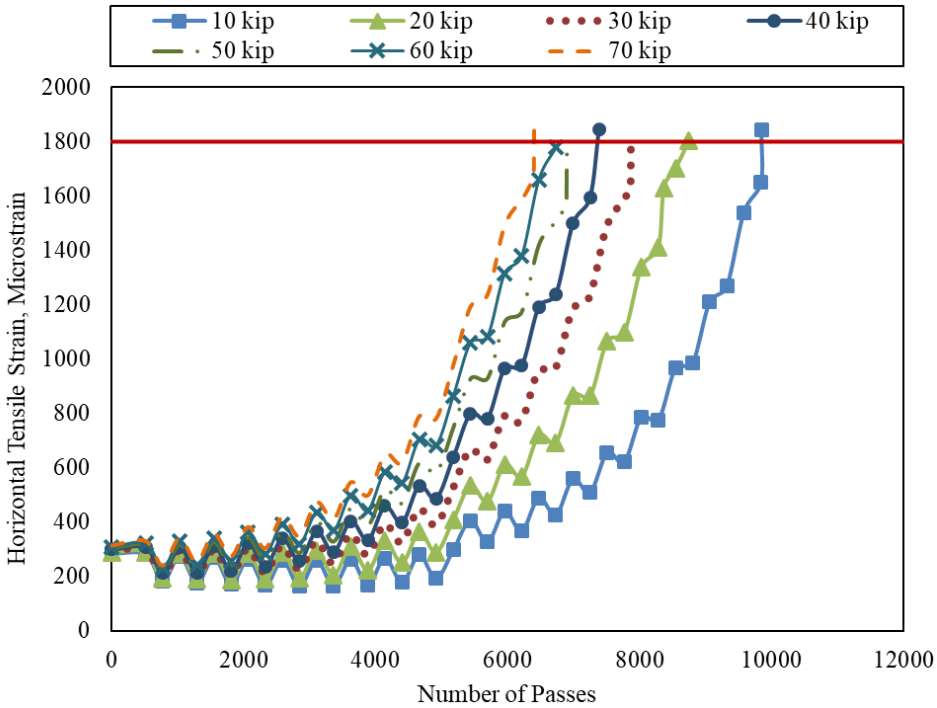

Figure 7. Horizontal Tensile Strain at HMA Overlay Bottom (Traffic & Temperature Load) (GDIT, 2019).

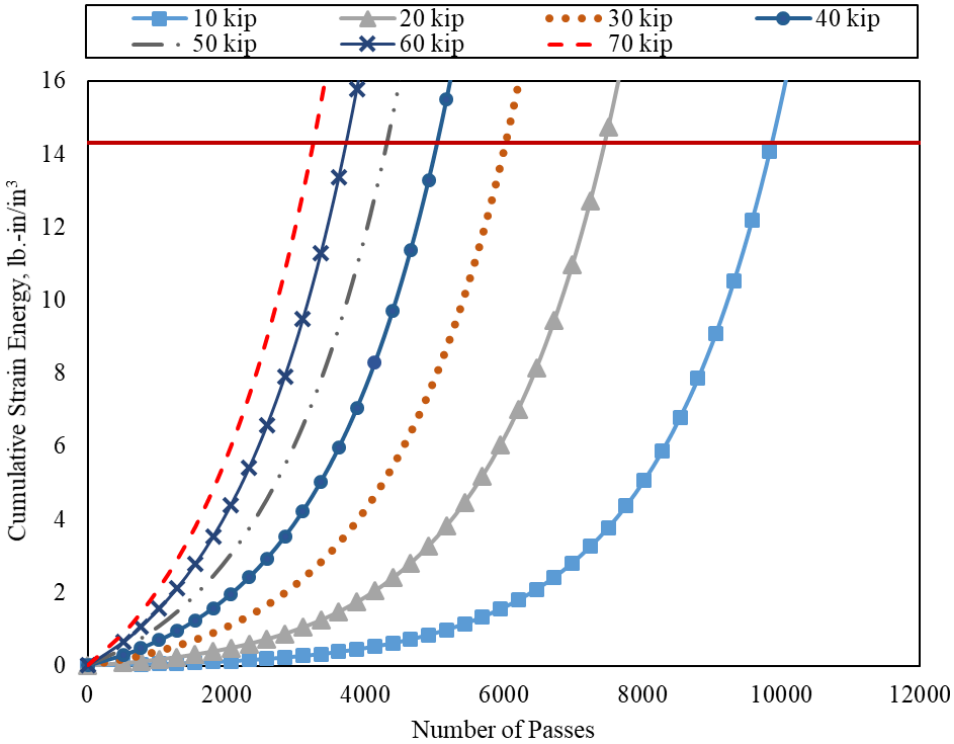

Figure 8. Cumulative Strain Energy at HMA Overlay Bottom (Traffic & Temperature Load) (GDIT, 2019).

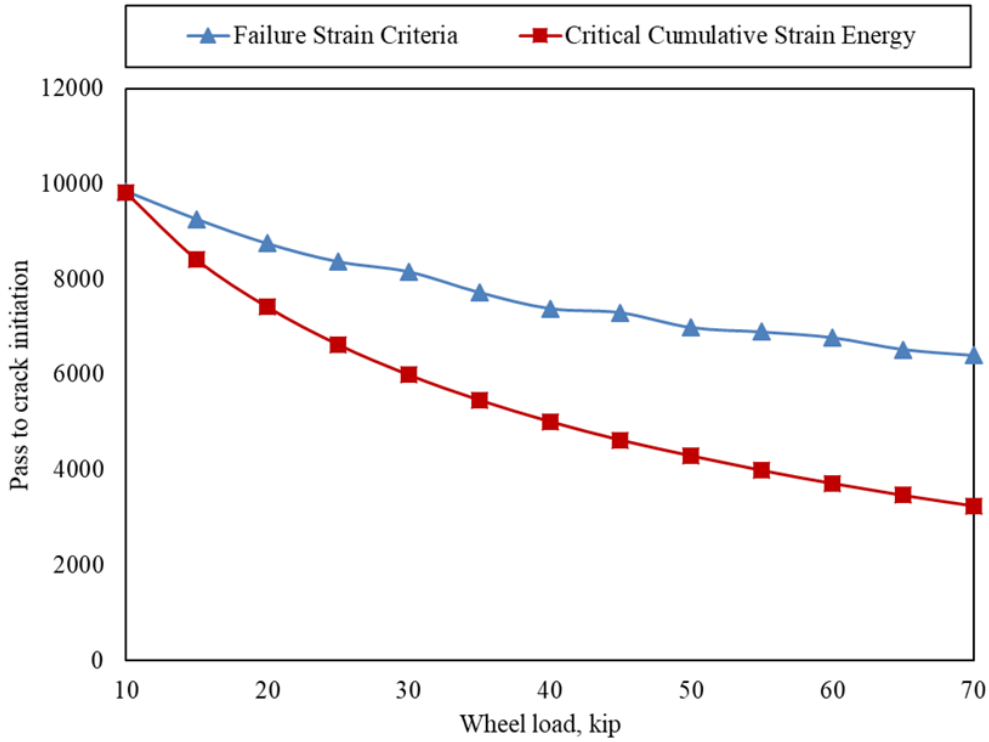

Figure 9. Pass to Crack Initiation vs. Wheel Load (Traffic & Temperature Loads) (GDIT, 2019).

TEST PROCEDURE.

a. General. All traffic was conducted at a vehicle speed of 3 mph and with a nominal tire pressure of 214 psi.
b. Wander Pattern. The wander pattern consisted of 62 passes (figure 10), with each movement of the HVS-A to the north being counted as a pass, and the return to the south counted as a second pass. These 62 passes were arranged in 11 wheel tracks, as shown in table 3.
c. Baseline Testing. Baseline HWD and LWD measurements were done at the slab centers on both TO and TT sections. The HWD testing was conducted with a four-drop loading sequence beginning with an approximate 12,000-lb seating load. The subsequent loads were approximately 6,000, 9,000, and 12,000 lbs. Lower load levels were selected to avoid damage in the thin HMA overlay. Since HWD deflections capture the overall structural integrity of a pavement system and uniformity, LWD testing was considered to determine in-situ HMA modulus, which is expected to be independent of the effect of the underlying layers. LWD tests were conducted using a 6-inch diameter loading plate and drop heights between 6 and 24 inches at 6-inch intervals.
d. Response Test. The purpose of this test was to make sure all systems were operating properly, and the gages were operational. A total of 22 passes was applied along 11 wheel tracks at a wheel load of 10,000 pounds, as shown in table 4. The condition of slabs was monitored to verify that test items were not damaged. Baseline sensor readings were recorded for both TT and TO sections.
e. Traffic Test. The wander pattern for full traffic testing consists of 62 passes arranged in 11 tracks. Traffic testing was performed at a speed of 3 mph on the TT section only. Wheel load and tire pressure were set at 40 kips and 214 psi, respectively.

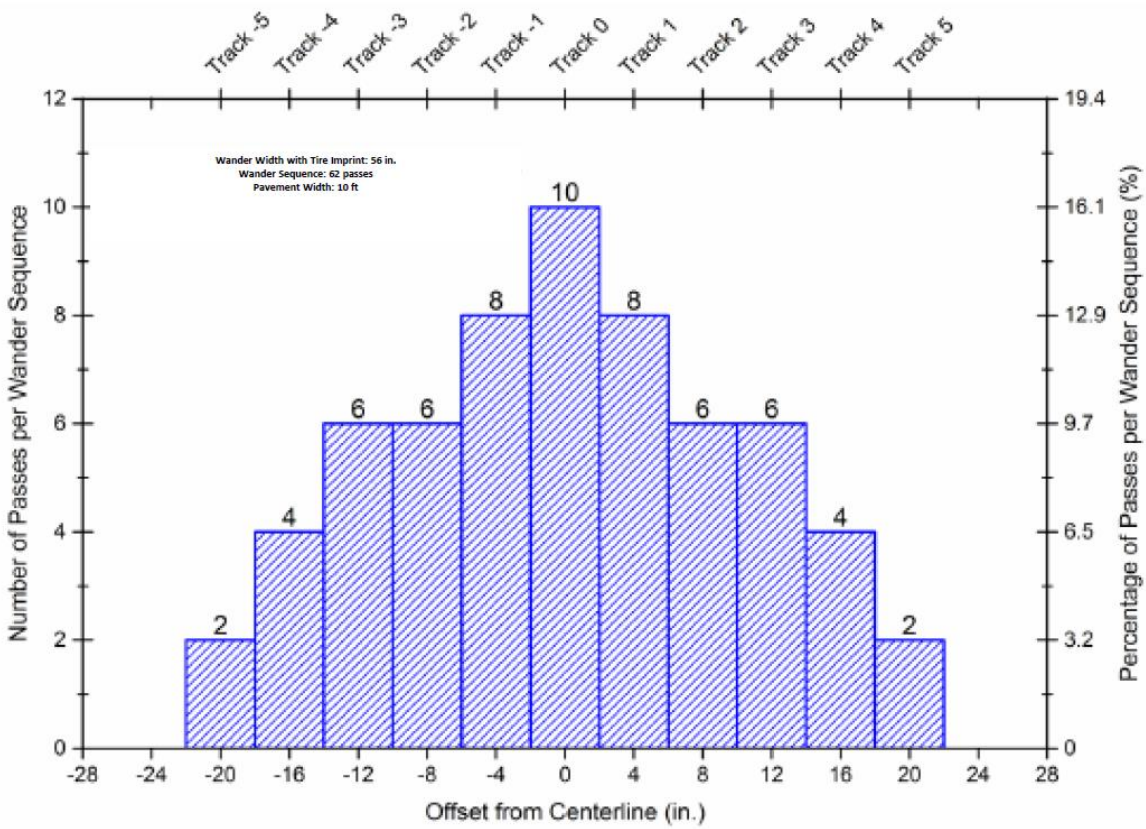

Figure 10. Wander Pattern (GDIT, 2019).

Table 3. HVS-A Carriage Positions for a Full Wander Pattern (GDIT, 2019).

Pass Sequence No.	Direction	Track No.	Carriage Centerline Location, in.
1	S → N	-5	-20
2	N → S	-5	-20
3	S → N	-3	-12
4	N → S	-3	-12
5	S → N	-1	-4
6	N → S	-1	-4
7	S → N	1	4
8	N → S	1	4
9	S → N	3	12
10	N → S	3	12
11	S → N	5	20
12	N → S	5	20
13	S → N	4	16
14	N → S	4	16
15	S → N	2	8
16	N → S	2	8

Pass Sequence No.	Direction	Track No.	Carriage Centerline Location, in.
17	S → N	0	0
18	N → S	0	0
19	S → N	-2	-8
20	N → S	-2	-8
21	S → N	-4	-16
22	N → S	-4	-16
23	S → N	-2	-8
24	N → S	-2	-8
25	S → N	0	0
26	N → S	0	0
27	S → N	2	8
28	N → S	2	8
29	S → N	4	16
30	N → S	4	16
31	S → N	3	12
32	N → S	3	12
33	S → N	1	4
34	N → S	1	4
35	S → N	-1	-4
36	N → S	-1	-4
37	S → N	-3	-12
38	N → S	-3	-12
39	S → N	-1	-4
40	N → S	-1	-4
41	S → N	1	4
42	N → S	1	4
43	S → N	3	12
44	N → S	3	12
45	S → N	2	8
46	N → S	2	8
47	S → N	0	0
48	N → S	0	0
49	S → N	-2	-8
50	N → S	-2	-8
51	S → N	-1	-4
52	N → S	-1	-4
53	S → N	1	4
54	N → S	1	4
55	S → N	0	0
56	N → S	0	0
57	S → N	-4	-16
58	N → S	-4	-16
59	S → N	-3	-12

Pass Sequence No.	Direction	Track No.	Carriage Centerline Location, in.
60	N → S	-3	-12
61	S → N	0	0
62	N → S	0	0

RESPONSE TEST. Upon the completion of instrumentation for RC Outdoor Phase I, the response test was executed with the following parameters:

- Wheel Load: 10,000 lbs. (to avoid possible shake-down deformation in the HMA layer)
- Tire pressure: 214 psi
- Wander pattern: 11 wheel tracks as summarized in table 4.
- Pass and Carriage Position: Table 4 summarizes 22 passes (distributed over all 11 tracks) and associated carriage positions. Each complete movement of the HVS-A to the north counts as one pass, and the complete return to the south counts as a second pass.

Table 4. HVS-A Carriage Positions for Response Test (GDIT, 2019).

Pass Sequence No.	Direction	Track No.	Carriage Centerline Location, in.
1	S → N	-5	-20
2	N → S	-5	-20
3	S → N	-4	-16
4	N → S	-4	-16
5	S → N	-3	-12
6	N → S	-3	-12
7	S → N	-2	-8
8	N → S	-2	-8
9	S → N	-1	-4
10	N → S	-1	-4
11	S → N	0	0
12	N → S	0	0
13	S → N	1	4
14	N → S	1	4
15	S → N	2	8
16	N → S	2	8
17	S → N	3	12
18	N → S	3	12
19	S → N	4	16
20	N → S	4	16
21	S → N	5	20
22	N → S	5	20

MONITORING.

a. Dynamic Responses. Sensors EG, SG, and JDG data were collected during trafficking to monitor traffic loading effect.

b. Static Responses. Thermocouple and JDG data were collected hourly to monitor environmental changes.

c. Pavement Condition.

1) Manual Distress Survey: Daily distress surveys on the TT section during trafficking and weekly distress surveys on both TT and TO sections when no trafficking was conducted. In accordance with ASTM D5340 (ASTM, 2012), transverse and longitudinal cracking were considered. As needed, the surveys were augmented with wire brushes, chalk markings, flashlights and other tools to ascertain the presence and pattern of very fine cracks. Cumulative plots of crack mapping were prepared and submitted to the Principal Investigator's (PI) on a daily basis. On these plots, the distresses were color-coded to separate dates/passes of distress survey on which new distresses are observed.

2) LWD Test: Weekly LWD testing on the TT section during trafficking and monthly LWD testing on both TT and TO sections when no trafficking was conducted in accordance with ASTM E2583 (ASTM, 2015).

FULL SCALE TEST

RESPONSE TEST.

A response test was conducted on October 23, 2019 to check the operation of both the DAQ and installed gages. Both the TT and TO sections were trafficked with SWL at a wheel load of 10,000 pounds, with 214 psi tire pressure. A total of 22 passes was applied along 11 tracks (table 4). Tables 5 and 6 summarize the gage responses under critical tracks.

Table 5. RC Outdoor Phase I Sensor Response Test Data Summary for TT Section

Sensor ID	Critical Pass	Critical Track	Peak strain (microstrain)		Functionality	Joint Type
			Compression	Tension		
TT12-SG1-3	21	5		9	Operational	Doweled
TT12-SG2-1.5	21	5	-41		Operational	Doweled
TT12-SG3-0	21	5	-38		Operational	Doweled
TT12-SG4-0	1	-5	-95		Operational	Doweled
TT12-EG4-3	-				Non-operational	Doweled
TT12-SG5-0	1	-5	-80		Operational	Doweled
TT12-SG6-1.5	1	-5	-70		Operational	Doweled
TT12-SG7-3	1	-5	-80		Operational	Doweled
TT23-SG1-3	21	5		5	Operational	Undoweled
TT23-SG2-1.5	21	5	-33		Operational	Undoweled
TT23-SG3-0	21	5	-75		Operational	Undoweled
TT23-SG4-0	1	-5	-101		Operational	Undoweled
TT23-EG4-3	-				Non-operational	Undoweled
TT23-SG5-0	1	-5	-74		Operational	Undoweled
TT23-SG6-1.5	1	-5	-37		Operational	Undoweled
TT23-SG7-3	1	-5		14	Operational	Undoweled
TT34-SG1-3	21	5		15	Operational	Undoweled
TT34-SG2-1.5	21	5	-30		Operational	Undoweled
TT34-SG3-0	21	5	-60		Operational	Undoweled
TT34-SG4-0	1	-5	-90		Operational	Undoweled
TT34-EG4-3	-				Non-operational	Undoweled
TT34-SG5-0	1	-5	-60		Operational	Undoweled

TT34-SG6-1.5	1	-5	-24		Operational	Undoweled
TT34-SG7-3	1	-5		16	Operational	Undoweled
TT45-SG1-3	21	5		5	Operational	Undoweled
TT45-SG2-1.5	21	5	-45		Operational	Undoweled
TT45-SG3-0	21	5	-74		Operational	Undoweled
TT45-SG4-0	1	-5	-113		Operational	Undoweled
TT45-EG4-3	1	-5		10	Operational	Undoweled
TT45-SG5-0	1	-5	-69		Operational	Undoweled
TT45-SG6-1.5	1	-5	-41		Operational	Undoweled
TT45-SG7-3	1	-5		12	Operational	Undoweled
TT56-SG1-3	21	5		18	Operational	Doweled
TT56-SG2-1.5	21	5	-83		Operational	Doweled
TT56-SG3-0	21	5	-82		Operational	Doweled
TT56-SG4-0	1	-5	-93		Operational	Doweled
TT56-EG4-3	-	-			Non-operational	Doweled
TT56-SG5-0	1	-5	-75		Operational	Doweled
TT56-SG6-1.5	1	-5	-72		Operational	Doweled
TT56-SG7-3	1	-5		25	Operational	Doweled
TT12-SG8-0	15	2	-78		Operational	Doweled
TT23-SG8-0	15	2	-119		Operational	Undoweled
TT34-SG8-0					Non-operational	Undoweled
TT45-SG8-0	15	2	-97		Operational	Undoweled
TT56-SG8-0	15	2	-83		Operational	Doweled
TT12-EG8-3	-	-			Non-operational	Doweled
TT23-EG8-3					Non-operational	Undoweled
TT34-EG8-3	15	2		3	Operational	Undoweled
TT45-EG8-3					Non-operational	Undoweled
TT56-EG8-3	15	2		18	Operational	Doweled

Failed during paving	Failed after paving	Failed before traffic	Failed during traffic

Table 6. RC Outdoor Phase I Sensor Response Test Data Summary for TO Section

Sensor ID	Critical Pass	Critical Track	Peak strain (microstrain)		Functionality	Joint Type
			Compression	Tension		
TO12-SG1-3	21	5		6	Operational	Doweled
TO12-SG2-1.5	21	5	-67		Operational	Doweled
TO12-SG3-0	21	5	-66		Operational	Doweled
TO12-SG4-0	1	-5	-84		Operational	Doweled
TO12-EG4-3	-	-			Non-operational	Doweled
TO12-SG5-0	1	-5	-60		Operational	Doweled
TO12-SG6-1.5	1	-5	-61		Operational	Doweled
TO12-SG7-3	1	-5		5	Operational	Doweled
TO23-SG1-3	21	5		38	Operational	Undoweled
TO23-SG2-1.5	21	5	-29		Operational	Undoweled
TO23-SG3-0	21	5	-71		Operational	Undoweled
TO23-SG4-0	1	-5	-127		Operational	Undoweled
TO23-EG4-3	-	-			Non-operational	Undoweled
TO23-SG5-0	1	-5	-79		Operational	Undoweled
TO23-SG6-1.5	1	-5	-43		Operational	Undoweled
TO23-SG7-3	1	-5		18	Operational	Undoweled
TO34-SG1-3	21	5		45	Operational	Undoweled
TO34-SG2-1.5	21	5	-20		Operational	Undoweled
TO34-SG3-0	21	5	-60		Operational	Undoweled
TO34-SG4-0	1	-5	-104		Operational	Undoweled
TO34-EG4-3	-	-			Non-operational	Undoweled

TO34-SG5-0	1	-5	-59		Operational	Undoweled
TO34-SG6-1.5	1	-5	-21		Operational	Undoweled
TO34-SG7-3	1	-5		28	Operational	Undoweled
TO45-SG1-3	21	5		35	Operational	Undoweled
TO45-SG2-1.5	21	5	-30		Operational	Undoweled
TO45-SG3-0	21	5	-82		Operational	Undoweled
TO45-SG4-0	-	-			Non-operational	Undoweled
TO45-EG4-3	-	-			Non-operational	Undoweled
TO45-SG5-0	1	-5	-61		Operational	Undoweled
TO45-SG6-1.5	1	-5	-31		Operational	Undoweled
TO45-SG7-3	1	-5		19	Operational	Undoweled
TO56-SG1-3	21	5		29	Operational	Doweled
TO56-SG2-1.5	21	5	-60		Operational	Doweled
TO56-SG3-0	21	5	-61		Operational	Doweled
TO56-SG4-0	1	-5	-81		Operational	Doweled
TO56-EG4-3	-	-			Non-operational	Doweled
TO56-SG5-0	1	-5	-60		Operational	Doweled
TO56-SG6-1.5	1	-5	-57		Operational	Doweled
TO56-SG7-3	1	-5		19	Operational	Doweled
TO12-SG8-0	15	2	-175		Operational	Doweled
TO23-SG8-0	15	2	-133		Operational	Undoweled
TO34-SG8-0	15	2	-94		Operational	Undoweled
TO45-SG8-0	15	2	-149		Operational	Undoweled
TO56-SG8-0	15	2	-69		Operational	Doweled
TO12-EG8-3	-	-			Non-operational	Doweled
TO23-EG8-3	15	2		3	Operational	Undoweled
TO34-EG8-3	15	2		4	Operational	Undoweled
TO45-EG8-3	-	-			Non-operational	Undoweled
TO56-EG8-3	-	-			Non-operational	Doweled

Failed during paving	Failed after paving	Failed before traffic

TRAFFIC TEST.

The traffic test was conducted on February 11-18, 2020 (5 days). The traffic test was on the TT test section only, using a single wheel load of 40,000 pounds, vehicle speed of 3.0 mph, and nominal tire pressure of 214 psi. Table 7 summarizes the traffic history. In addition to monitoring both dynamic and static instrumentation data, manual distress surveys were conducted at the end of each trafficking day. At the conclusion of traffic testing on February 18, 2020, the cumulative pass number was 2976. Then LWD testing was conducted on the overlay surface of the TT section.

Table 7. Traffic History on TT Section

Day	Date	Time	Passes	Cumulative Passes	Wander Number
1	02/11/2020	6:56AM – 12:30PM	496	496	8
2	02/12/2020	6:56AM – 1:30PM	666	1162	10
3	02/13/2020	6:46AM – 1:53PM	574	1736	10
4	02/14/2020	6:40AM – 1:08PM	620	2356	10
5	02/18/2020	6:46AM – 1:36PM	620	2976	10

OBSERVATIONS.

Daily distress surveys were conducted in accordance with ASTM D5340 (ASTM, 2012). Distresses were outlined with chalk and measured using a tape measure. The surveys recorded the changes to existing distresses and any new distresses. Visual distress surveys were documented in two ways: a scale map and a written log. The distress map shows all distresses to scale and keys each distress to a pass number/cycle number and joint ID. Figure 11 shows sample distress maps for both joints TT34 and TO34. At each joint, distresses were recorded on the top surface and on the west and east vertical edges. Distresses are numbered for reference to the written log. Appendix A and B contain all RC Outdoor Phase I distress photos and maps, respectively.

The written log records all the distress information chronologically. Figure 12 is a screenshot of part of the log. The written log records the date, pass number, type of distress, distress number (which can be cross-referenced to the distress map), the location of the distress, and any relevant notes. The notes may indicate changes to existing distresses, severity levels, merging of multiple previously identified distresses, etc. Appendix B contains the complete written log.

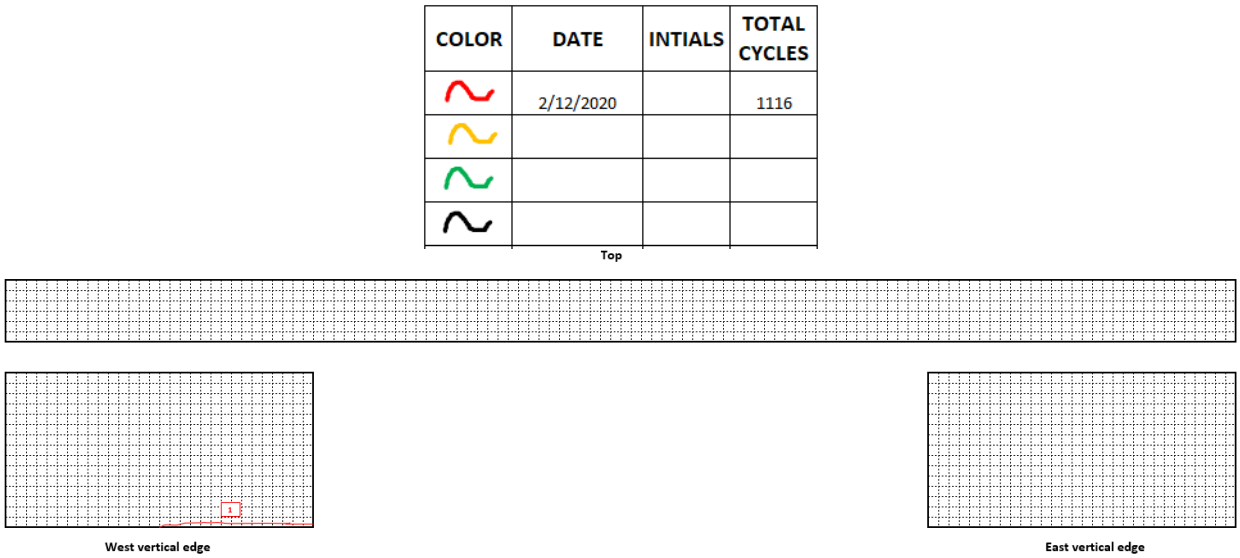

(a) TT34 Joint of TT Section

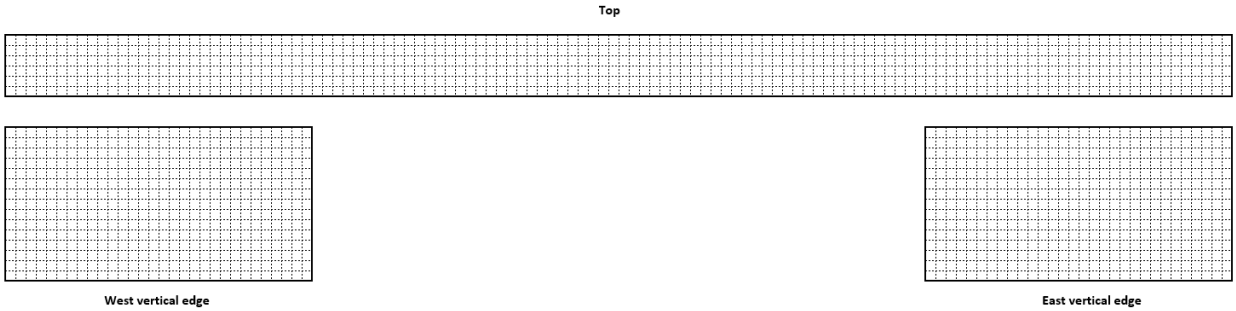

(b) TO34 Joint of TO Section

Figure 11. Sample Distress map (Portion).

DATE	TOTAL CYCLES	DISTRESS							NOTES
		DESCRIPTION	NO.	LOCATION					
				X AXIS (in.)		Y AXIS (in.)		Section	
				INITIAL	END	INITIAL	END		
2/12/2020	1116	Bottom-up crack	1	3	6	0	0.1	TT34 joint, West vertical edge	
2/12/2020	1116	Bottom-up crack	2	2.8	3	0.1	0	TT45 joint, West vertical edge	
2/12/2020	1116	Bottom-up crack	3	0	2.9	0.1	0	TT56 joint, West vertical edge	
2/12/2020	1116	Bottom-up crack	4	3.1	6	0	0.1	TT56 joint, West vertical edge	
2/12/2020	1116	Bottom-up crack	5	2.9	3	0.1	0	TT56 joint, East vertical edge	

Figure 12. Sample Log (Portion).

As shown in table 8, reflection cracks were first observed on the 2nd day of traffic testing (i.e., February 12, 2020) after cumulative pass #1162. These cracks were located on both the east and west sides along joint TT34, TT45, and TT56. After initiation, the progress of bottom-up cracks varied. For example, on the west side of joint TT45, the crack reached the 1.4-inch mark (as measured from the bottom of the overlay) as reported on February 14, 2020, after pass no. 2356. Photos of these cracks are included in Appendix A.

Table 8. Traffic History and Distress Observation on TT Section

Day	Date	Cumulative Passes	Distress Observation
1	2/11/2020	496	No crack initiated
2	2/12/2020	1162	(a) TT34 joint west side: 3 mm (approximate) vertical hairline crack, in asphalt at concrete joint, then the hairline crack moved to the right for 40 mm (approximate) parallel to the concrete surface (b) TT45 joint west side: 10 mm (approximate) vertical hairline crack, in asphalt at concrete joint at approximately 45 degrees to the left, then the hairline crack moved to the right for 40 mm (approximate) parallel to the concrete surface (c) TT45 joint east side 4 mm (approximate) vertical hairline crack, in asphalt at concrete joint at approximately 45 degrees to the left, then the hairline crack moved to the right for 40 mm (approximate) parallel to the concrete surface (d) TT56 joint west side: 2 hairline vertical cracks 4 mm each at the joint then moved 50 mm individually one to the right the other to the left of joint parallel to the concrete surface (e) TT56 joint east side: 4 mm (approximate) vertical hairline crack, in asphalt at concrete joint, then the hairline crack moved to the right for 30 mm (approximate) parallel to the concrete surface
3	2/13/2020	1736	No further propagation observed on the existing crack
4	2/14/2020	2356	(a) TT45 joint west side: Bottom up crack reaches the height of 1.4 inch (b) No further propagation observed on other joints
5	2/18/2020	2976	No further propagation observed on the existing crack

BASELINE MEASUREMENT ANALYSIS

On October 21, 2019, HWD and LWD tests were conducted on both sections (TT and TO). These measurements served as the baseline for condition monitoring and as the basis for calculating in-situ pavement layer properties.

HWD DATA.

INITIAL ANALYSIS. HWD testing locations are shown in figure 13. On October 21, 2019, the testing was conducted using a KUAB Model 150 tester with a four-drop loading sequence beginning with an approximate 12,000-pound seating load. The subsequent loads were approximately 6,000 pounds, 9,000 pounds, and 12,000 pounds. At each load level, surface deflections were measured using a total of eight geophones spaced at a regular interval of 12 inches. The positions of these geophones were: -12, 0, 12, 24, 36, 48, 60, and 72 inches, respectively. The HWD loading plate was placed at 7 feet offset from the slab ends to accommodate all the geophones within 10 × 10 foot slabs. During the test, pavement temperature remained in the range 74-75°F.

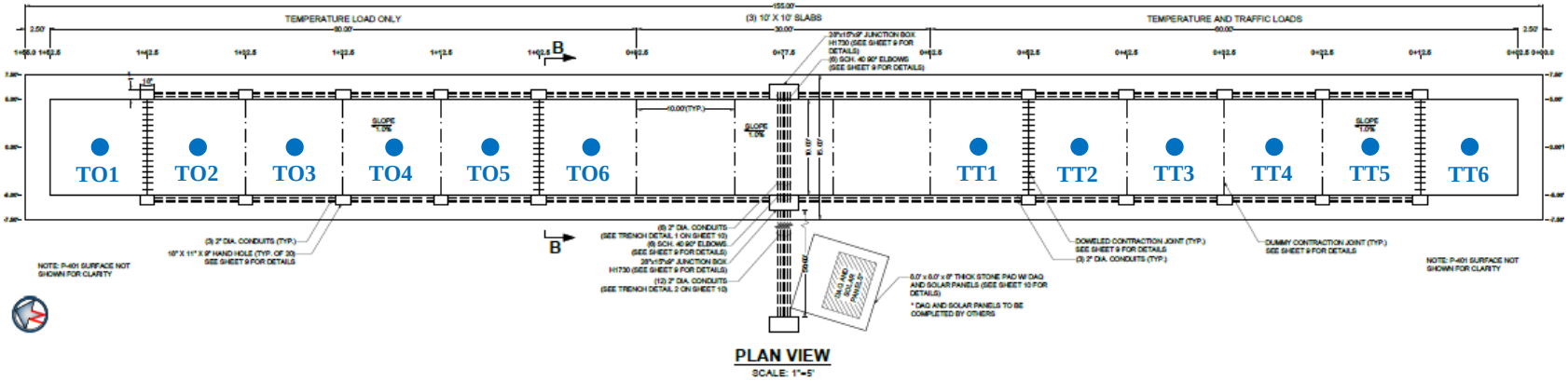

Figure 13. HWD and LWD Test Layout.

Deflection Basin. Deflection data were first normalized to a standard load (i.e., 6,000, 9,000, and 12,000 pounds). Figure 14 (a) and (b) show the deflection basins corresponding to 12,000 pounds load level. Deflection basins on the TT sections exhibited relatively higher variability compared to those on the TO sections.

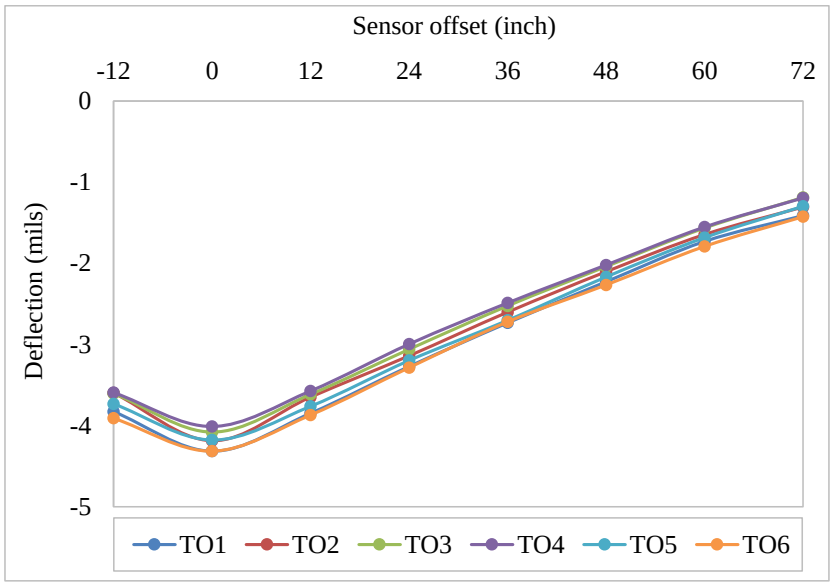

(a)

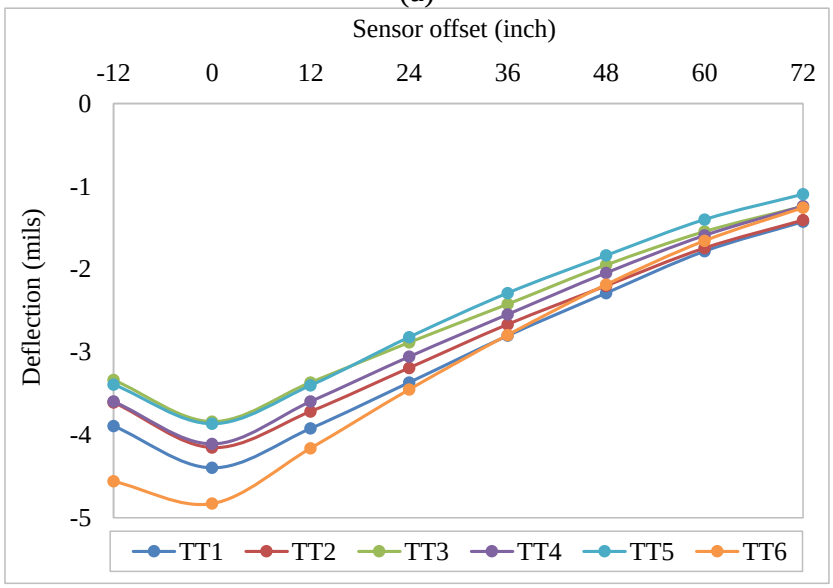

(b)

Figure 14. HWD Deflection Basin: (a) TO, and (b) TT.

Impulse Stiffness Modulus. Impulse Stiffness Modulus (ISM) was calculated from the ratio of HWD test load (P) and the maximum deflection (δ_{max}), i.e., deflection at the center of the loading plate, in response to a test load. The ISM was calculated for the maximum P at 12,000 pounds, using Equation 1:

$$ISM = \frac{P}{\delta_{max}} \qquad \text{Eq. 1}$$

Table 9 summarizes the ISM values. A good within-section uniformity was observed, and the between-section variation was small.

Table 9. Summary of ISM (TO and TT)

Test Section	Slab ID	ISM (kip/in)	Average (kip/in)	Standard Deviation	COV (%)
TO	TO1	2781	2872	84.6	2.9
	TO2	2866			
	TO3	2942			
	TO4	2992			
	TO5	2873			
	TO6	2781			
TT	TT1	2730	2877	241.6	8.4
	TT2	2890			
	TT3	3127			
	TT4	2922			
	TT5	3106			
	TT6	2485			

BACKCALCULATION OF LAYER MODULI. ISM only represents the combined stiffness of a pavement section. The modulus of each individual layer was backcalculated using BAKFAA v3.1.0. As-built layer thicknesses and seed moduli used in the backcalculation are summarized in table 10. Seed moduli were obtained from either field material characterization during construction or post-construction laboratory tests. Such details are documented elsewhere in the RC Outdoor Phase I Construction History Report and RC Outdoor Phase I Material Characterization Report (Mandal and Yin, 2019; Horizon Engineering Consulting, LLC, 2020). During the backcalculation, the iteration tolerance was set to 0.001.

Table 10. Pavement Structure and Layer Seed Moduli Used for Backcalculation

Layer	Seed Modulus (ksi)	Poisson's Ratio	Interface Condition	Thickness (in)
P-401MR	500	0.35		3
			1.0[1]	
P-501MR	4000	0.15		9
			0.0[2]	
P-154MR	30	0.35		8
			1.0	
P-152MR	11.74	0.4		-

[1] *fully-bonded*
[2] *unbonded*

Tables 11 and 12 summarize the HWD test data. TO sections exhibited greater consistency than the TT sections. The average P-401MR (HMA) modulus of the TT sections was higher than that of the TO section. The lower average modulus in the TO section was most likely due to insufficient compaction, as detailed in the Construction History Report. The average P-401MR backcalculated modulus was compared to the dynamic modulus master curve (figure 15), which was prepared from the test data obtained from RC Outdoor Phase I Material Characterization Report (Horizon, 2020). The dynamic modulus of P-401MR was 457.5 ksi, corresponding to the HWD loading frequency and pavement temperature (33 Hz and 74.3°F respectively). The HWD loading frequency was determined from the reciprocal of the loading duration, which was about 30 milliseconds at 12-kip load (Villacorta, 2012). It was necessary to verify that TO and TT sections are replicates (or can be treated as replicates for analytical purposes) to exclude any bias while comparing the results of the two sections. To verify this, an Analysis of Variance (ANOVA) test was performed on the backcalculated layer moduli (table 12). Two separate analyses were performed on backcalculated moduli, one assuming equal variances and the other assuming unequal variances. The null hypothesis assumed that all means were equal and the confidence level was set at 95%. Results from the ANOVA analysis for all four layers are summarized in table 13. In general, the *p*-Values were above 0.05, suggesting that the apparent difference in the backcalculated moduli were not statistically significant and thereby, it can be assumed that TO and TT sections are replicates.

Table 11. Summary of HWD Load and Deflection Corresponding to 12,000 lbs Load Level

Location	Load (lbs)	Deflection (mils) at varying Geophone Offset (inch)							Pavement Temperature (°F)
		D0 (at 0-in)	D2 (at 12-in)	D3 (at 24-in)	D4 (at 36-in)	D5 (at 48-in)	D6 (at 60-in)	D7 (at 72-in)	
TO1	12070	4.34	3.87	3.29	2.75	2.24	1.74	1.42	74
TO2	12039	4.2	3.66	3.15	2.61	2.11	1.65	1.31	74
TO3	12119	4.12	3.65	3.09	2.55	2.06	1.58	1.2	74
TO4	12058	4.03	3.59	3.01	2.5	2.03	1.56	1.2	74
TO5	12122	4.22	3.8	3.23	2.73	2.19	1.7	1.31	74
TO6	12126	4.36	3.91	3.32	2.75	2.29	1.81	1.44	75
TT1	12119	4.44	3.96	3.4	2.83	2.31	1.8	1.44	75
TT2	12111	4.19	3.75	3.22	2.69	2.22	1.76	1.42	75
TT3	12194	3.9	3.42	2.93	2.46	1.98	1.57	1.26	75
TT4	12213	4.18	3.66	3.11	2.59	2.08	1.62	1.26	74
TT5	12174	3.92	3.45	2.86	2.32	1.86	1.42	1.11	74
TT6	12029	4.84	4.17	3.46	2.8	2.19	1.66	1.26	74

Table 12. Summary of Backcalculated Layer Modulus

Test Item	Slab ID	P-401MR			P-501MR			P-154MR			P-152MR		
		Modulus, ksi	Average	COV (%)	Modulus, ksi	Average	COV (%)	Modulus, ksi	Average	COV (%)	Modulus, ksi	Average	COV (%)
TO	TO1	735	788	9	5931	5771	4	48	44	14	35	37	5
	TO2	752			5924			45			37		
	TO3	775			5567			46			39		
	TO4[1]	-			4571			2			96		
	TO5	761			5918			48			36		
	TO6	916			5514			33			35		
TT	TT1	1031	904	13	4981	5617	12	33	46	17	35	39	10
	TT2	773			6543			52			35		
	TT3	1001			5990			52			40		
	TT4	781			5678			45			39		
	TT5	932			4893			48			44		
	TT6[1]	-			3276			21			39		

Note-1: Layer moduli from TO-4 and TT-6 were discarded as the ratio of P-154 and P-152 moduli < 1.0

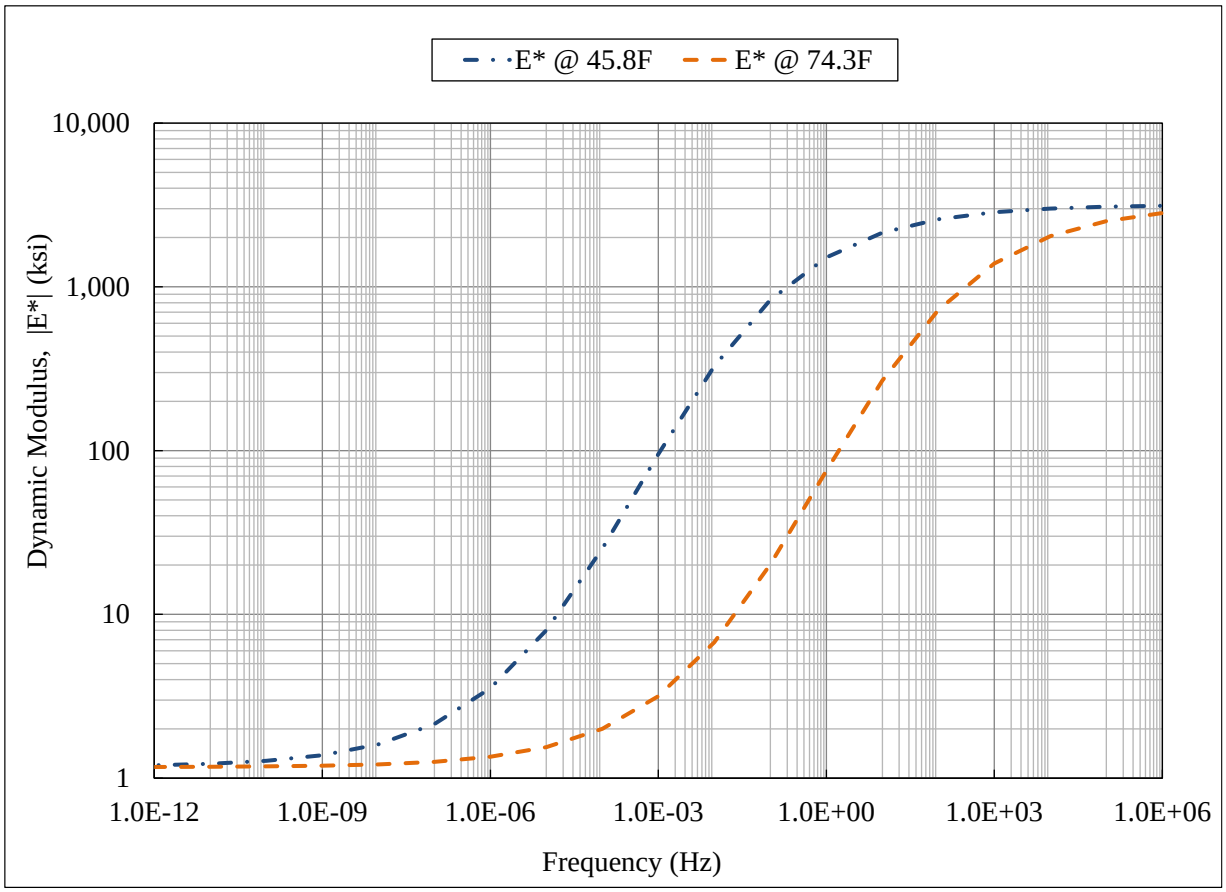

Figure 15. Dynamic Modulus of P-401MR.

Table 13. ANOVA Analysis of Backcalculated Layer Moduli

Layer	Assumption of Variance	Section ID	Mean, ksi	F-Value	p-Value	Accept Null Hypothesis (p > 0.05 ?)
P-401MR	Equal Variances	TO	787.8	3.35	0.104	YES
		TT	903.6			
	Unequal Variances	TO	787.8	3.35	0.113	YES
		TT	903.6			
P-501MR	Equal Variances	TO	5770.8	0.22	0.648	YES
		TT	5617.0			
	Unequal Variances	TO	5770.8	0.22	0.657	YES
		TT	5617.0			
P-154MR	Equal Variances	TO	44.0	0.20	0.668	YES
		TT	46.0			
	Unequal Variances	TO	44.0	0.20	0.669	YES
		TT	46.0			
P-152MR	Equal Variances	TO	36.4	1.42	0.268	YES
		TT	38.6			
	Unequal Variances	TO	36.4	1.42	0.283	YES
		TT	38.6			

LWD DATA.

Following ASTM E2583 (ASTM, 2015), LWD testing was conducted on the surface of P-401MR on October 16, 2019 (see figure 13). At each testing location, load was applied at four incremental drop heights, i.e., 6, 12, 18, and 24 inches with five replicate drops. The detailed test results are included in Appendix C. The surface deflection is the summation of deformations in all pavement layers within the influence zone, and the higher the LWD load, the more pavement layers will be captured within the influence zone. Table 14 summarizes the combined pavement modulus corresponding to a 24-inch drop height. LWD post-data processing computed the combined modulus (*E*) using Boussinesq's method as follows (Schwartz et al. 2017):

$$E = \frac{2k_s(1-\nu^2)}{Ar_0} \qquad \text{Eq. 2}$$

where k_s = stiffness $\left(= {}^{P}/_{\delta}\right)$, P = LWD load, δ = surface deflection at the center of loading plate, ν = Poisson's ratio, r_0 = radius of loading plate, and A = stress distribution factor. Both TO and TT sections had a similar value of averaged combined modulus; however, the TT section showed less uniformity. An ANOVA test was also performed on the combined modulus to verify the previous claim on the TO and TT sections being replicates. The analysis results are summarized

in table 15. The *p*-Values were above 0.05, indicating that the apparent difference in the combined moduli was not statistically significant. Therefore, this observation supports the previous claim based on HWD backcalculated layer moduli. Since the combined modulus does not represent the strength of any individual layer, a performance indicator (designated "HMA Overlay Modulus") was introduced to monitor local damage to the HMA overlay using monthly LWD test data. Details are reported in Appendix D of this report.

Table 14. Summary of Combined Modulus from LWD Test

Test Item	Section ID	Load[1], lbs	Deflection[2], mils	Combined Modulus			
				Modulus, ksi	Average	Standard Deviation	COV (%)
TO	TO1	1135.3	0.4	490.6	476.8	12.8	2.7
	TO2	1137.2	0.4	488.2			
	TO3	1125.9	0.4	483.6			
	TO4	1145.5	0.5	471.8			
	TO5	1134.2	0.4	483.7			
	TO6	1128.5	0.5	456.7			
TT	TT1	1133.5	0.5	435.3	506.7	50.5	10.0
	TT2	1139.5	0.4	567.6			
	TT3	1134.1	0.4	506.1			
	TT4	1139.0	0.4	557.4			
	TT5	1134.3	0.4	503.8			
	TT6	1136.9	0.5	470.0			

Note 1: Load level corresponding to 24 inches drop height
Note 2: Deflection at the center of the loading plate
Note 3: Pavement temperature range: 68.3-68.9 °F

Table 15. ANOVA Analysis of Combined Modulus

Assumption of Variance	Section ID	Mean, ksi	F-Value	p-Value	Accept Null Hypothesis (P > 0.05?)
Equal Variances	TO	479.1	1.69	0.223	YES
	TT	506.7			
Unequal Variances	TO	479.1	1.69	0.245	YES
	TT	506.7			

TRAFFIC DATA ANALYSIS

PRELIMINARY ANALYSIS.

Because a significant number of sensors were damaged prior to the traffic testing, only response test data were considered in the preliminary analysis.

CRITICAL TRACK. Instrumentation data collected from the response test were first processed, and the peak responses were then plotted against the track number to determine the critical track. One such example is given in figure 16. Surface gage (TT34-SG7-3.0) recorded the maximum strain whenever the SWL was traveling along Track: -5. A summary of all critical tracks is presented in table 16. Several gages along the intermediate locations of the overlay, such as TO23-SG8-0, TO34-SG8-0, TO34-EG8-3, TO34-SG8-0, TT12-SG8-0, TT23-SG8-0, TT45-SG8-0, TT56-EG8-3, were flagged due to the mismatch between the critical track and expected track, whenever the wheel was positioned right atop the gage locations. It was believed that this track

mismatch was due to the noise in dynamic strain data at 10 kip load level and/or localized effect. These tracks were used later to analyze dynamic data over pass number for crack characterization.

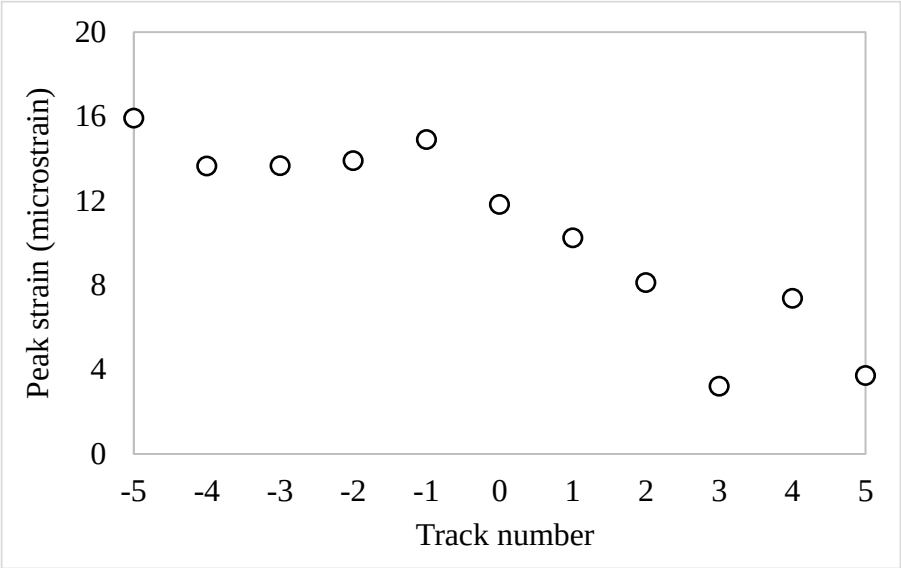

Figure 16. Determination of Critical Track from Strain Responses (TT34-SG7-3.0).

Table 16. Critical Track based on Response Test Data

Section	Joint	Gage ID	Critical Track	Section	Joint	Gage ID	Critical Track
TO	Joint #1 (TO12: Doweled)	TO12-SG1-3	5	TT	Joint #1 (TT12: Doweled)	TT12-SG1-3	5
		TO12-SG2-1.5	5			TT12-SG2-1.5	5
		TO12-SG3-0	5			TT12-SG3-0	5
		TO12-SG4-0	-5			TT12-SG4-0	-5
		TO12-SG5-0	-5			TT12-SG5-0	-5
		TO12-SG6-1.5	-5			TT12-SG6-1.5	-5
		TO12-SG7-3	-5			TT12-SG7-3	-5
		TO12-SG8-0	2			TT12-SG8-0[1]	3
		TO12-JDG1-5	5			TT12-JDG1-5	5
		TO12-JDG2-5	-5			TT12-JDG2-5	-5
	Joint #2 (TO23: Undoweled)	TO23-SG1-3	5		Joint #2 (TT23: Undoweled)	TT23-SG1-3	5
		TO23-SG2-1.5	5			TT23-SG2-1.5	5
		TO23-SG3-0	5			TT23-SG3-0	5
		TO23-SG4-0	-5			TT23-SG4-0	-5
		TO23-SG5-0	-5			TT23-SG5-0	-5
		TO23-SG6-1.5	-5			TT23-SG6-1.5	-5
		TO23-SG7-3	-5			TT23-SG7-3	-5
		TO23-SG8-0[1]	3			TT23-SG8-0[1]	4
		TO23-EG8-3	2			TT23-EG8-3	-
		TO23-JDG1-5	5			TT23-JDG1-5	5
		TO23-JDG2-5	-5			TT23-JDG2-5	-5
	Joint #3 (TO34: Undoweled)	TO34-SG1-3	5		Joint #3 (TT34: Undoweled)	TT34-SG1-3	5
		TO34-SG2-1.5	5			TT34-SG2-1.5	5
		TO34-SG3-0	5			TT34-SG3-0	5
		TO34-SG4-0	-5			TT34-SG4-0	-5
		TO34-SG5-0	-5			TT34-SG5-0	-5
		TO34-SG6-1.5	-5			TT34-SG6-1.5	-5
		TO34-SG7-3	-5			TT34-SG7-3	-5

		TO34-SG8-0[1]	3			TT34-SG8-0	-
		TO34-EG8-3[1]	-2			TT34-EG8-3	2
		TO34-JDG1-5	5			TT34-JDG1-5	5
		TO34-JDG2-5	-5			TT34-JDG2-5	-5
	Joint #4 (TO45: Undoweled)	TO45-SG1-3	5		Joint #4 (TT45: Undoweled)	TT45-SG1-3	5
		TO45-SG2-1.5	5			TT45-SG2-1.5	5
		TO45-SG3-0	5			TT45-SG3-0	5
		TO45-SG4-0	-			TT45-SG4-0	-5
		TO45-SG5-0	-5			TT45-SG5-0	-5
		TO45-SG6-1.5	-5			TT45-SG6-1.5	-5
		TO45-SG7-3	-5			TT45-SG7-3	-5
		TO45-SG8-0	2			TT45-SG8-0[1]	3
		TO45-JDG1-5	5			TT45-JDG1-5	5
		TO45-JDG2-5	-5			TT45-JDG2-5	-5
	Joint #5 (TO56: Doweled)	TO56-SG1-3	5		Joint #5 (TT56: Doweled)	TT56-SG1-3	5
		TO56-SG2-1.5	5			TT56-SG2-1.5	5
		TO56-SG3-0	5			TT56-SG3-0	5
		TO56-SG4-0	-5			TT56-SG4-0	-5
		TO56-SG5-0	-5			TT56-SG5-0	-5
		TO56-SG6-1.5	-5			TT56-SG6-1.5	-5
		TO56-SG7-3	-5			TT56-SG7-3	-5
		TO56-SG8-0[1]	4			TT56-SG8-0	2
		TO56-EG8-3	-			TT56-EG8-3[1]	3
		TO56-JDG1-5	5			TT56-JDG1-5	5
		TO56-JDG2-5	-5			TT56-JDG2-5	-5

Note-1: Critical track did not overlap the track corresponding to the position of wheel right atop the gage location

STRAIN RESPONSE. Analysis of strain gage response was focused on: (a) the strain profile in the overlay; (b) the strain distribution along the joint; and (c) a comparison of joint types (doweled vs. undoweled). After review of table 16, one undoweled joint (#3) on the TO section and one doweled joint (#5) on the TT section were selected based on criteria such as: (a) slabs on either side of a joint, i.e., doweled or undoweled, with similar end restrains, (b) gages along edges and intermediate locations of the overlay being functional to capture the full-depth and -width strain distribution in the overlay, and (c) critical track numbers being close to expected.

Strain Profile in the Overlay. Figure 17 shows the responses from TO34-SG1-3.0, TO34-SG2-1.5, and TO34-SG3-0.0 across the undoweled joint #3 (i.e., TO34). In general, responses were almost identical in both directions. Tensile strains were observed at the bottom of the HMA overlay, compressive strains were observed at the surface, with gradual transition from tensile to compressive mode. Based on strain profile, the Mode I fracture was anticipated at the overlay bottom.

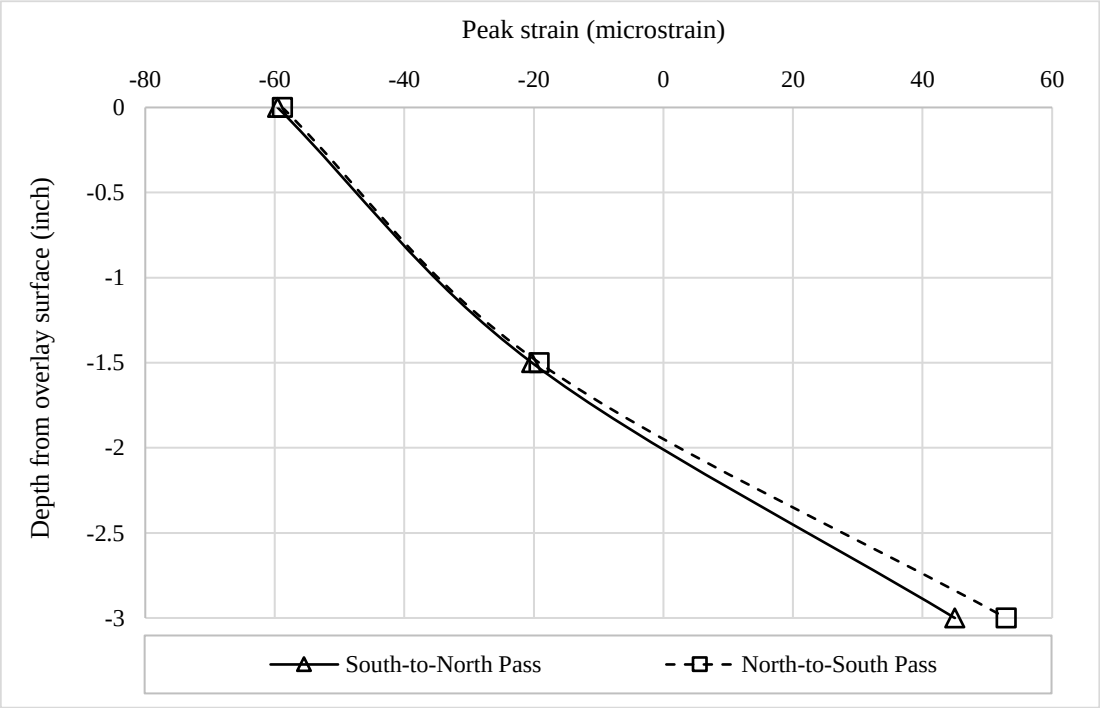

Figure 17. Strain Profile in the HMA Overlay (TO34).

Strain Distribution along Joint. Figure 18 shows the distribution of tensile strains at the overlay bottom for both undoweled and doweled joints. Strains at the vertical edges (both 60 and -60 inches from the centerline) were captured by the SGs, whereas strains in the middle of the overlay (8 inches from the centerline) were captured by the EGs. At the overlay bottom, strains were uniformly distributed above the doweled joint, while a gradual increasing strain distribution was observed towards the east vertical edge above the undoweled joint.

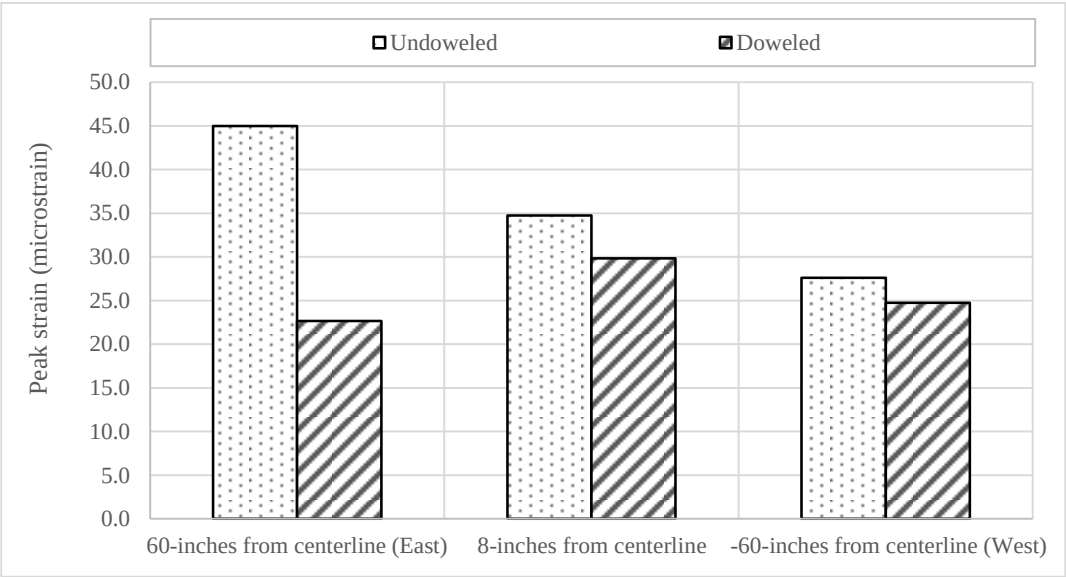

Figure 18. Strain Distribution along Joint (TO34).

Comparison of Joint Types. During the response test, the undoweled (TO34) joints showed greater movement compared to the doweled joints. For example, the maximum load-induced joint displacements for TT56 (doweled) and TO34 (undoweled) were 0.16 and 0.98 mils, respectively. Figure 19 shows the strain responses at the vertical edge for these two joints. The tensile strains at the bottom of the HMA overlay were smaller for the doweled joint. When comparing two joints in the middle of the overlay, figure 20 shows that the strain responses were almost identical.

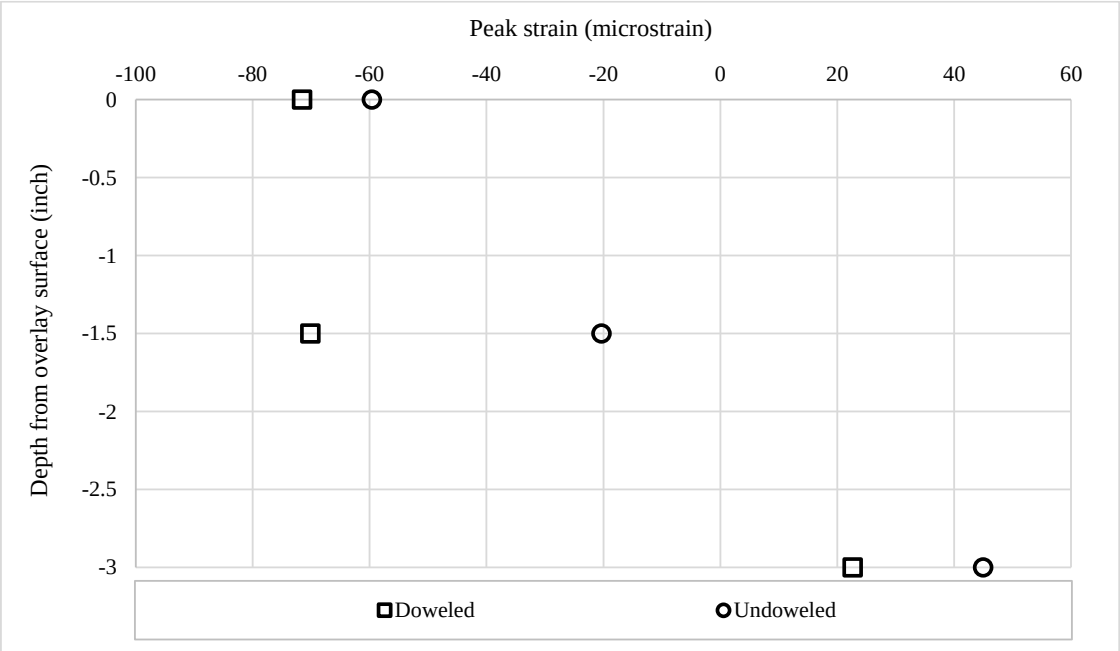

Figure 19. Strain Responses at the Overlay Edge (Doweled vs Undoweled).

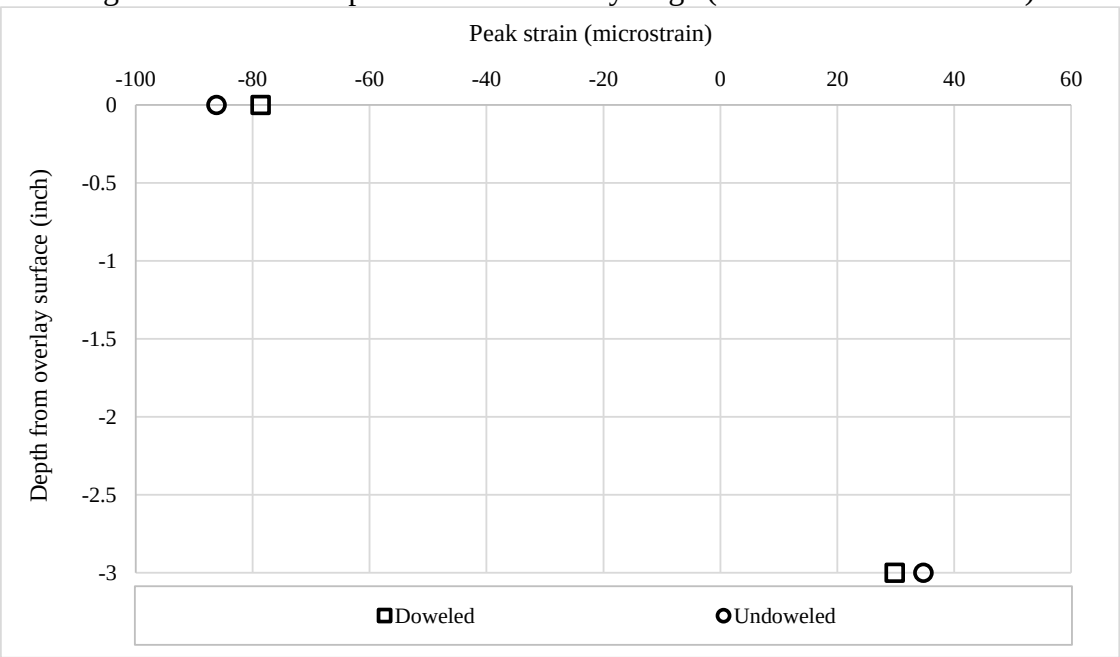

Figure 20. Strain Responses in the Middle of the Overlay (Doweled vs Undoweled).

OVERLAY TEMPERATURE. Figure 21 shows the temperature data at the top, middle, and bottom of the HMA overlay on the TO section. During daylight hours, the temperature increased until mid-afternoon (within 2:00 PM – 3:00 PM), followed by a gradual drop until the next morning. Throughout the 5-day trafficking period, the lowest overlay temperature was always at the surface. This observation is opposite to the temperature gradient from Reflective Cracking Indoor Tests, where the bottom-up cooling scheme resulted in the lowest temperatures at the overlay bottom. One such example from Indoor Phase V Test is shown in figure 22.

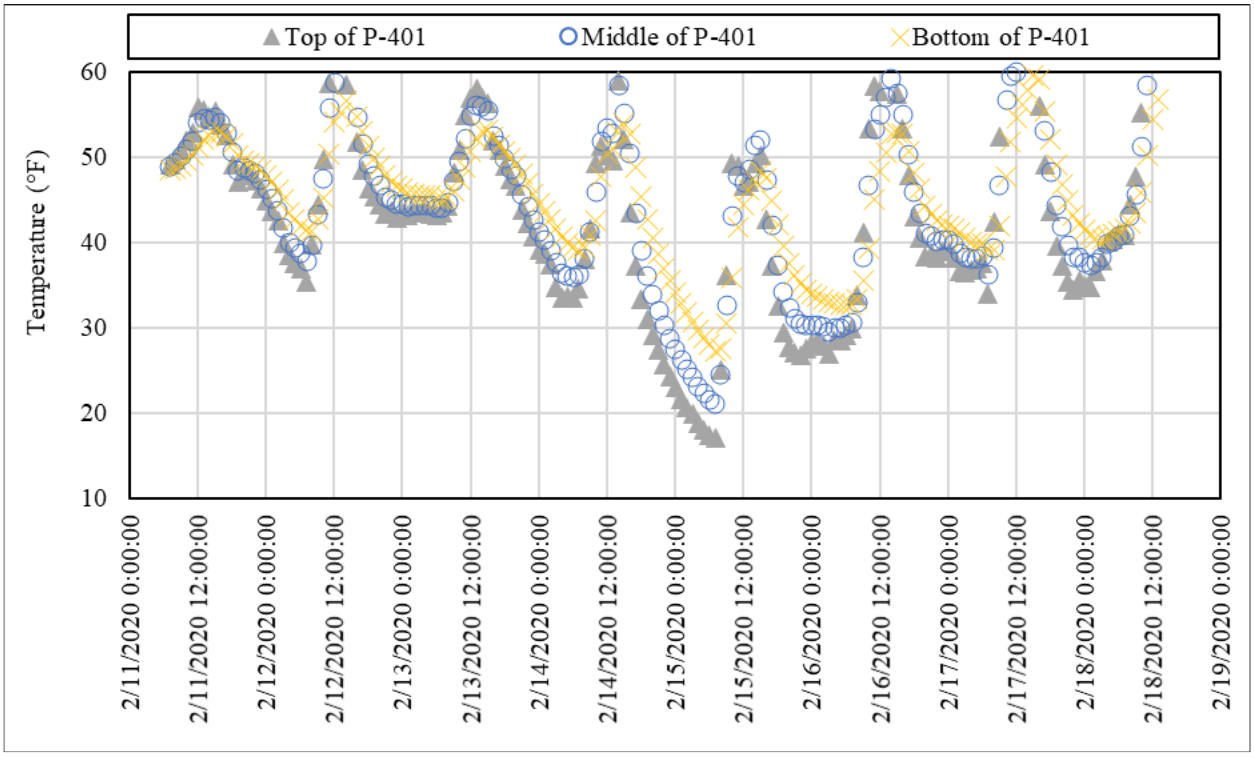

Figure 21. Temperature Variations in HMA overlay (5 day of Trafficking).

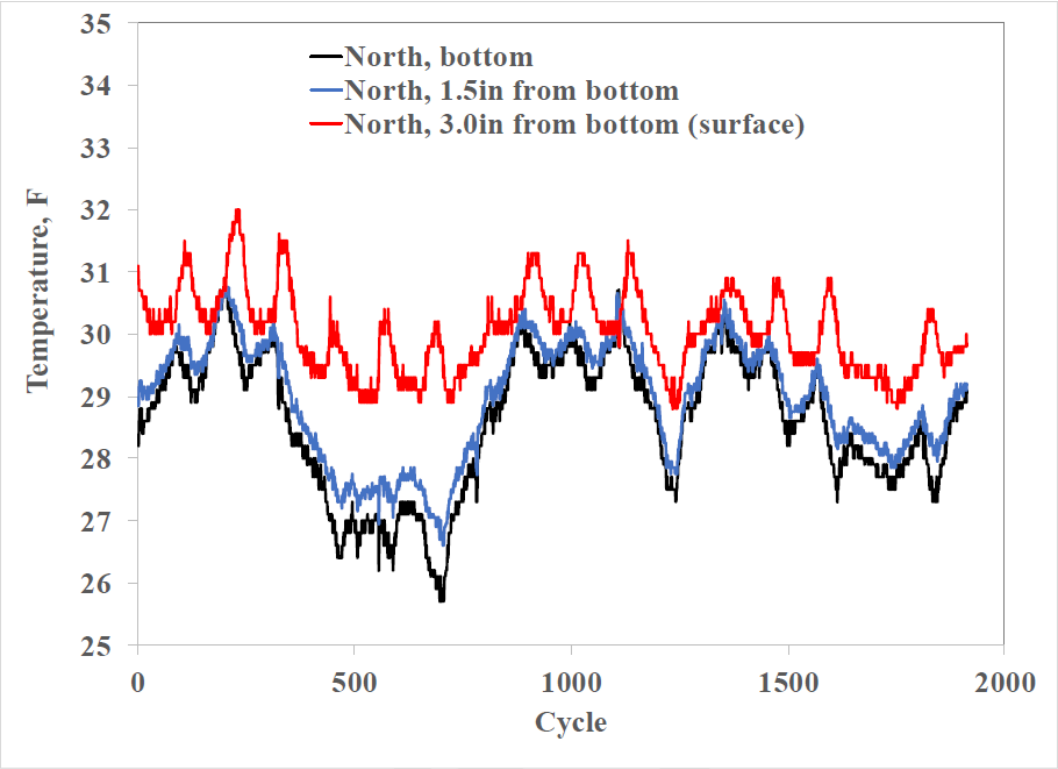

Figure 22. Temperature Variation in HMA Overlay (Yin, 2017).

ADVANCED ANALYSIS.

CRACK CHARACTERIZATION. On February 12, 2020 (2nd day of trafficking), the first bottom-up crack was observed on the west vertical edge of TT45 (undoweled joint) after cumulative pass #496 (figure 23). In figure 24, some strain fluctuation from the bottom SG first manifested at cumulative pass #507, while strains from the upper two SGs remained fairly stable. Crosscheck of joint displacement readings from TT45-JDG2-5 identified the initial jump at the same pass number (figure 25). Therefore, the pass number corresponding to the crack initiation at this location was determined to be 507. Strain and joint displacement trends from other SG, EG, and JDG are included in Appendices E and F.

Figure 23. 1st Bottom-up Crack on the West Edge of TT45 (February 12, 2020).

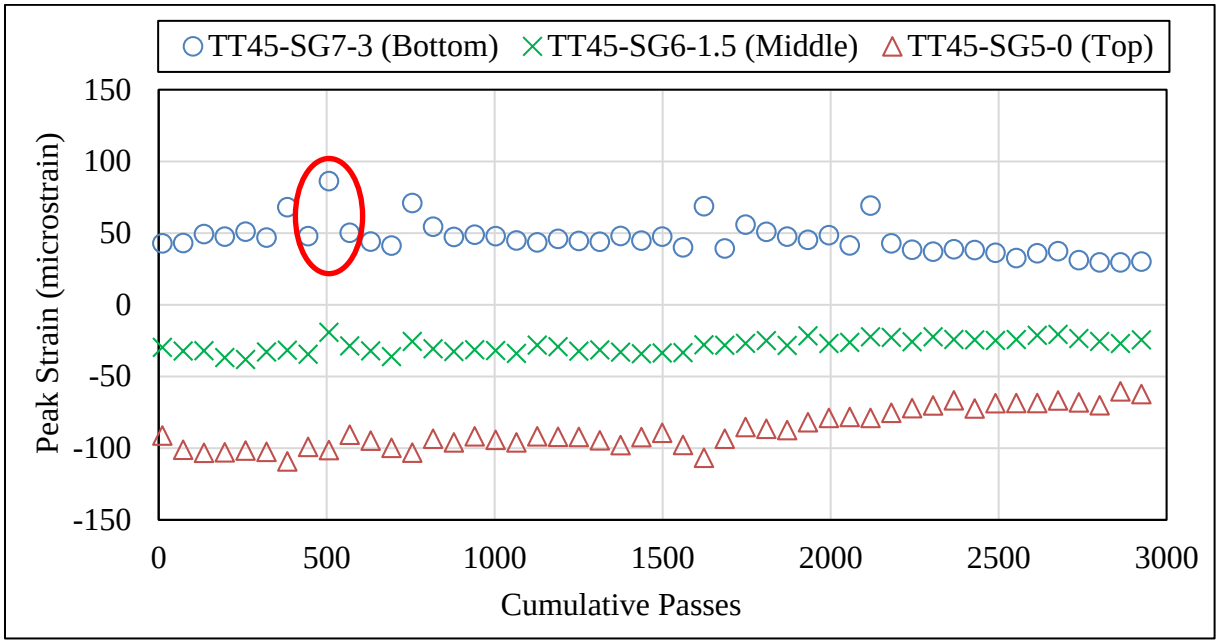

Figure 24. SG Response over Pass Number at the West Edge of TT45.

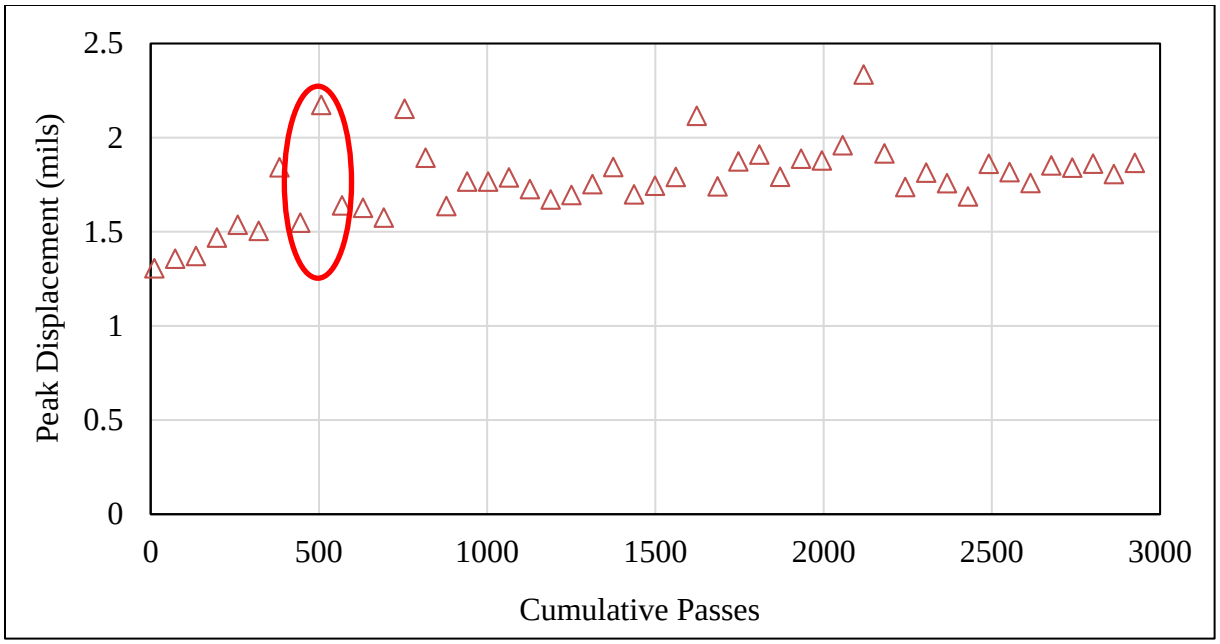

Figure 25. Joint Displacement at the West Edge of TT45.

Following the analysis of Indoor Phase VI Test data, cumulative strain energy was then calculated using the tensile strains from TT45-SG7-3.0. As shown in figure 26, there was an apparent upshift in the trend of cumulative strain energy at pass #507. This observation further confirmed the timestamp of the bottom-up crack initiation.

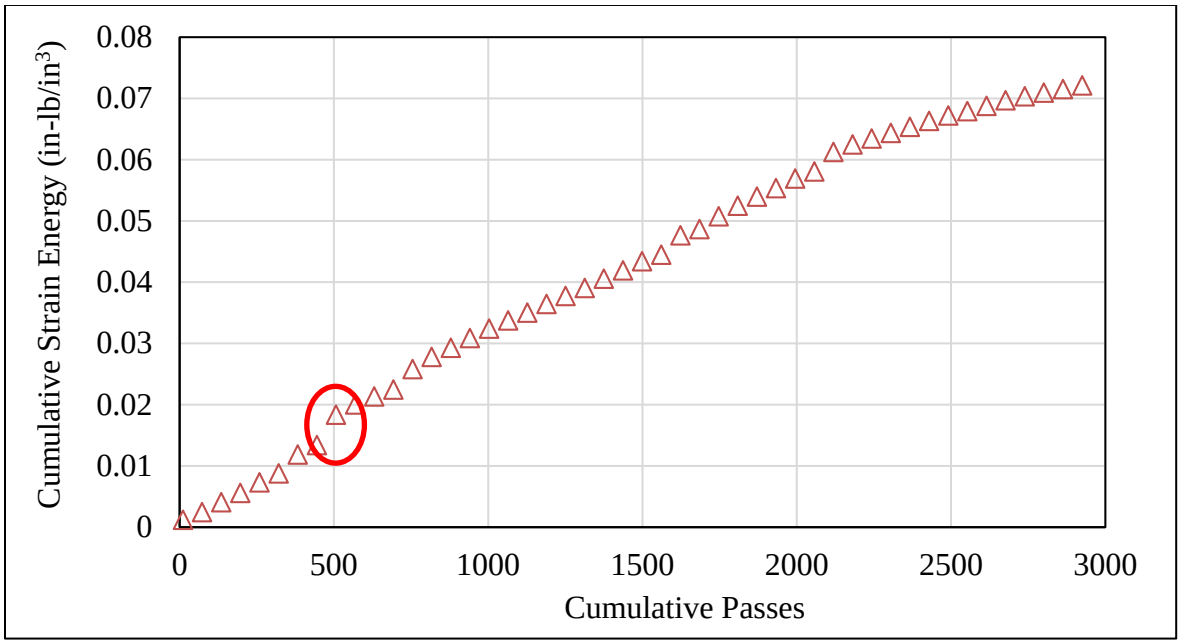

Figure 26. Cumulative Strain Energy Calculated from TT45-SG7-3.0 along West Edge of TT45.

JOINT MOVEMENT. During the traffic test, the TT section experienced a mixed loading of both traffic load using SWL and temperature variation. Hence, one doweled joint (TO12) and one undoweled joint (TO23) from the TO section were selected to study the temperature induced joint movement. Figures 27 and 28 show that the joint displacements at the doweled joint were smaller than the undoweled joint displacements.

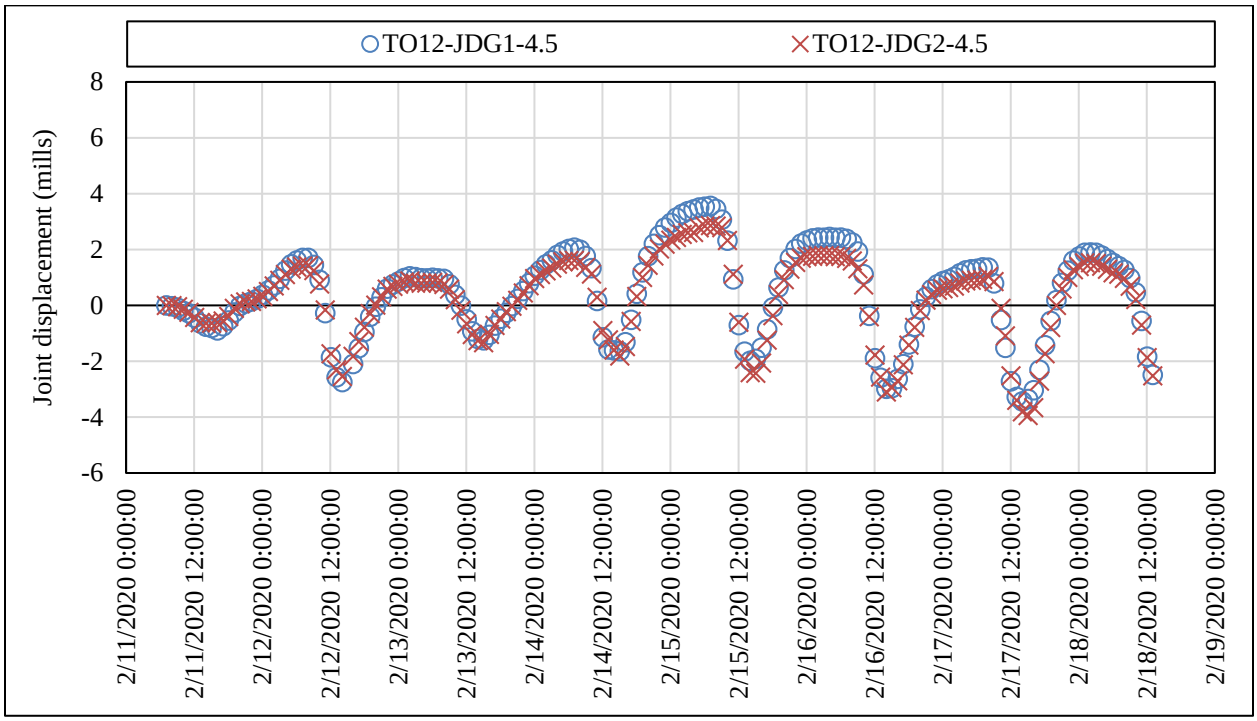

Figure 27. Joint Displacement along Doweled Joint (over 5-days of Trafficking).

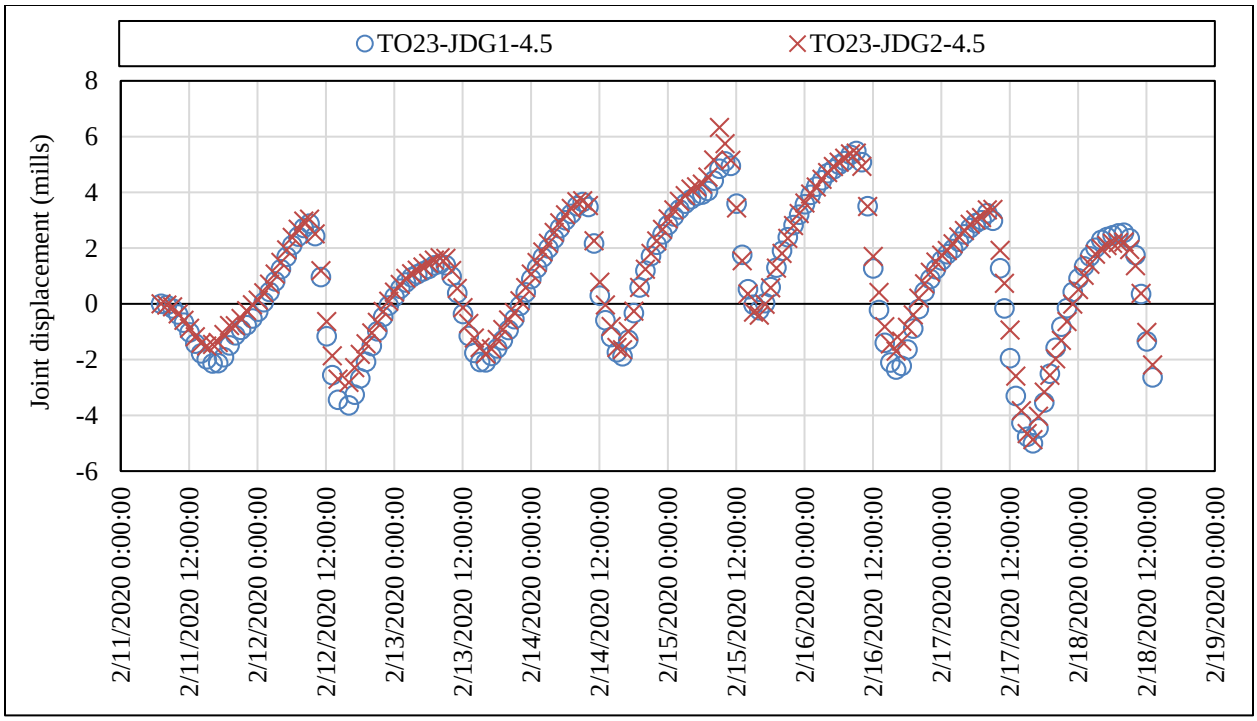

Figure 28. Joint Displacement along Undoweled Joint (over 5-days of Trafficking).

An effort was made to correlate pavement temperature and joint opening/closing. During trafficking, the temperature variation in concrete (P-501MR,) as captured by the thermocouple embedded at mid-depth of the PCC slabs, was very small (< 4°F). On the other hand, the range of temperatures in the asphalt (P-401MR) was larger (> 15°F) due to the exposed overlay edges. Figure 29 plots the joint displacement against the temperature change at the bottom of the overlay for both doweled (TO12) and undoweled (TO23) joints. In linear fashion, the PCC joint opened whenever the overlay temperature decreased and vice versa. Regardless of the joint type, the joint opening/closing was governed by both the slab contraction/expansion and the resistance from the overlay material. Thus, the bottom of the overlay underwent temperature-induced tensile stress cycles.

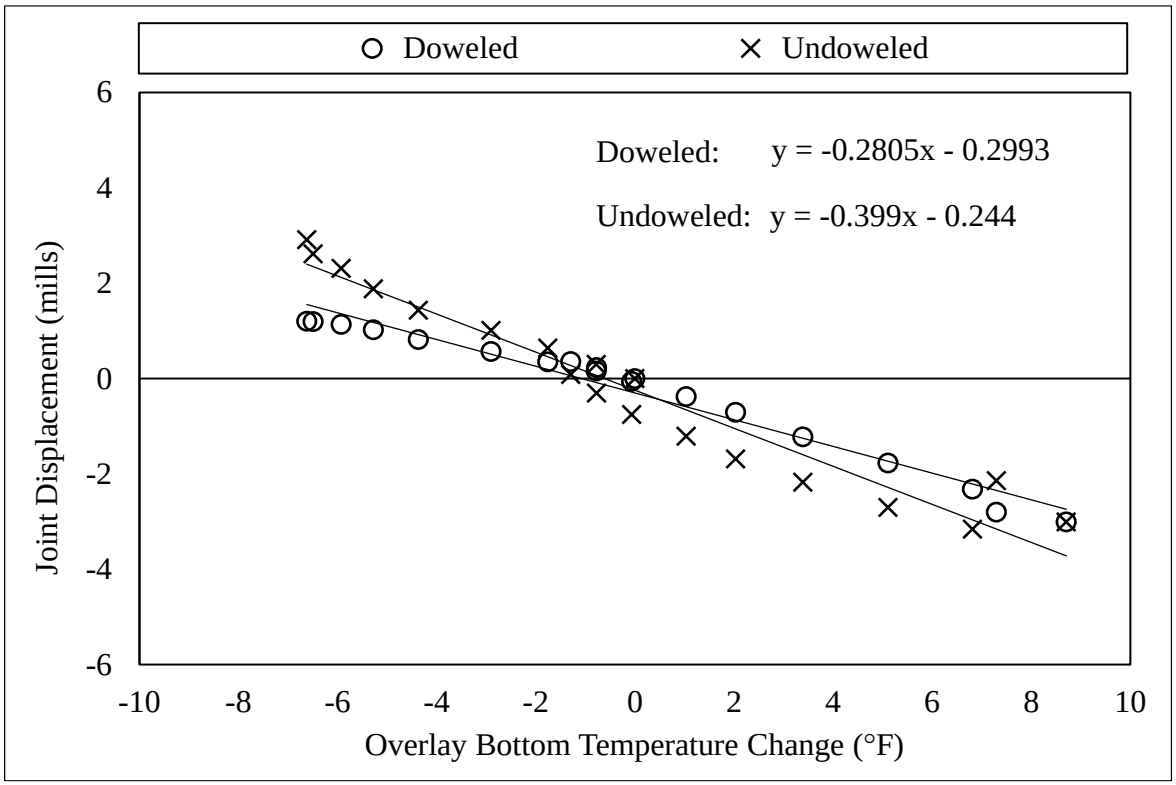

Figure 29. Joint Opening in Response to HMA Temperature Differential.

SUMMARY

The following conclusions are drawn from the Reflective Cracking Outdoor Phase I Test:

- HWD and LWD baseline measurements suggested that the structural integrity of the test overlay was relatively consistent. The average backcalculated P-401MR modulus was higher on the TT section than on the TO section. Base on statistical analysis of baseline data, the TO and TT sections can be considered replicates.
- The response test verified that most of the SGs were operational. Only three EGs in the TT section and two EGs in the TO section survived construction.
- By the end of the traffic testing, a total of 2976 cumulative passes were applied to the TT section. Several reflection cracks were observed on the east and west edges along joint TT34, TT45, and TT56.
- The 1st bottom-up reflection crack was observed on the 2nd day of traffic testing (February 12, 2020). The pass number corresponding to crack initiation was identified from strain response, joint displacement, and strain energy analysis.
- On the TO section, the lowest overlay temperature was at the surface (positive temperature gradient). This is opposite to the negative temperature gradient in the indoor tests using the NAPTF reflective cracking rig.

REFERENCES

ASTM. “Standard Test Method for Airport Pavement Condition Index Surveys,” D5340-12, American Standard for Test and Materials, West Conshohocken, PA, 2012.

ASTM. “Standard Test Method for Measuring Deflections with a Light Weight Deflectometer (LWD),” E2583-07, American Standard for Test and Materials, West Conshohocken, PA, 2015.

General Dynamics Information Technology. (2019). “Reflective Cracking Outdoor Phase I Comprehensive Test Plan,” Federal Aviation Administration., New Jersey, USA, Deliverable 4.3.3.2, Jul. 2019.

Horizon Engineering Consulting LLC. (2020). Reflective Cracking Outdoor Phase 1 Material Characterization Report. Federal Aviation Administration., New Jersey, USA, Deliverable 4.10.3.2.

Mandal, T., and Yin, H. (2019). Reflective Cracking Outdoor Phase-1 Construction History Report. Federal Aviation Administration., New Jersey, USA, Deliverable 4.10.1.

Schwartz, C. W., Afsharikia, Z, and Khosravifar, S. (2017). Standardizing Lightweight Deflectometer Modulus Measurements for Compaction Quality Assurance. Final Report, Grant No. TPF-5(285)/SP409B4P, University of Maryland, College Park, MD, USA.

Villacorta, F. L. (2012). Advanced Computing Techniques in Structural Evaluation of Flexible Pavements using the Falling Weight Deflectometer. Ph.D. Dissertation, Auburn University, AL, USA.

Yin, H. (2016). Long-term Reflective Cracking Test Plan. Federal Aviation Administration., New Jersey, USA, Deliverable 4.3.2.

Yin, H. (2017). Reflective Cracking Phase V Comprehensive Test Report. Federal Aviation Administration., New Jersey, USA, Deliverable 4.10.5.5.

APPENDIX A—DISTRESS PHOTOS

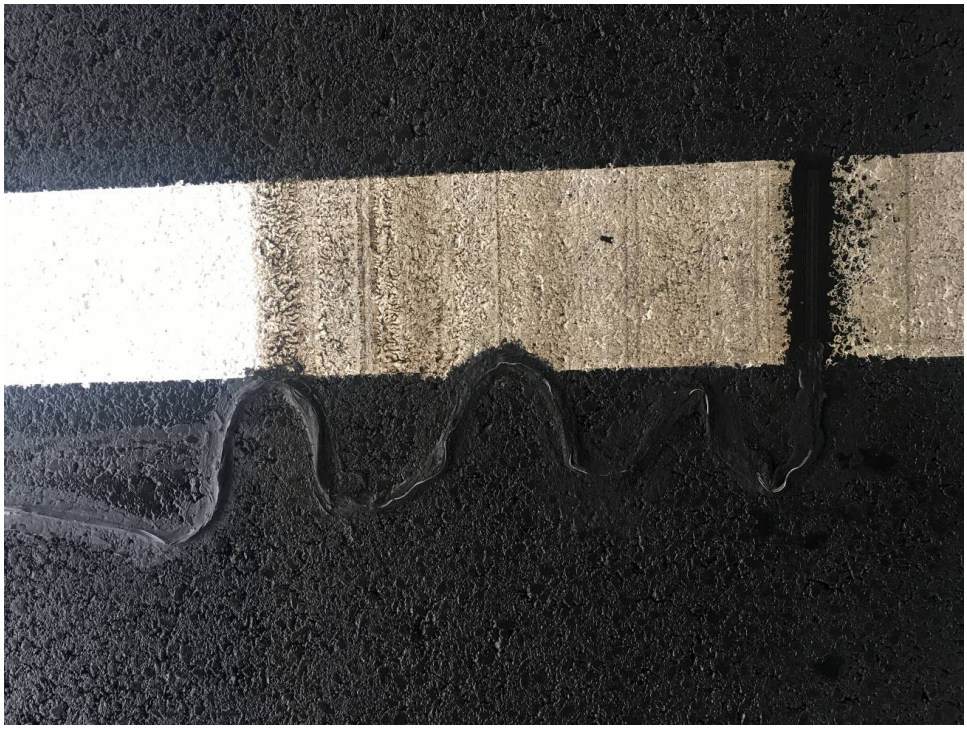

Figure A.1: TT12-SG8 (02-11-2020)

Figure A.2: TT23-SG8 (02-11-2020)

Figure A.3: TT34-SG8 (02-11-2020)

Figure A.4: Joint#3 West Side (02-11-2020)

Figure A.5: Joint#4 West Side (02-12-2020)

Figure A.6: Joint#4 East Side (02-12-2020)

Figure A.7: Joint#5 West Side (02-12-2020)

Figure A.8: Joint#5 East Side (02-12-2020)

Figure A.9: Joint#3 West Side (02-13-2020)

Figure A.10: Joint#4 West Side (02-13-2020)

Figure A.11: Joint#4 East Side (02-13-2020)

Figure A.12: Joint#5 West Side (02-13-2020)

Figure A.13: Joint#5 East Side (02-13-2020)

Figure A.14: Joint#1 West Side (02-14-2020)

Figure A.15: Joint#1 East Side (02-14-2020)

Figure A.16: Joint#2 West Side (02-14-2020)

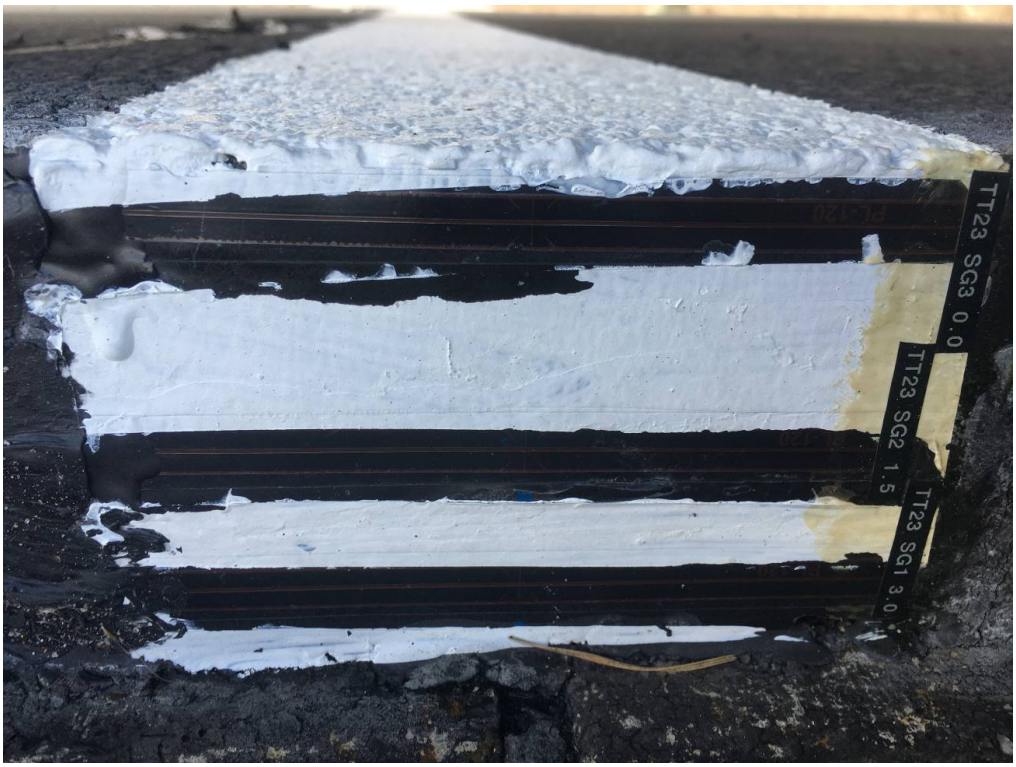

Figure A.17: Joint#2 East Side (02-14-2020)

Figure A.18: Joint#3 West Side (02-14-2020)

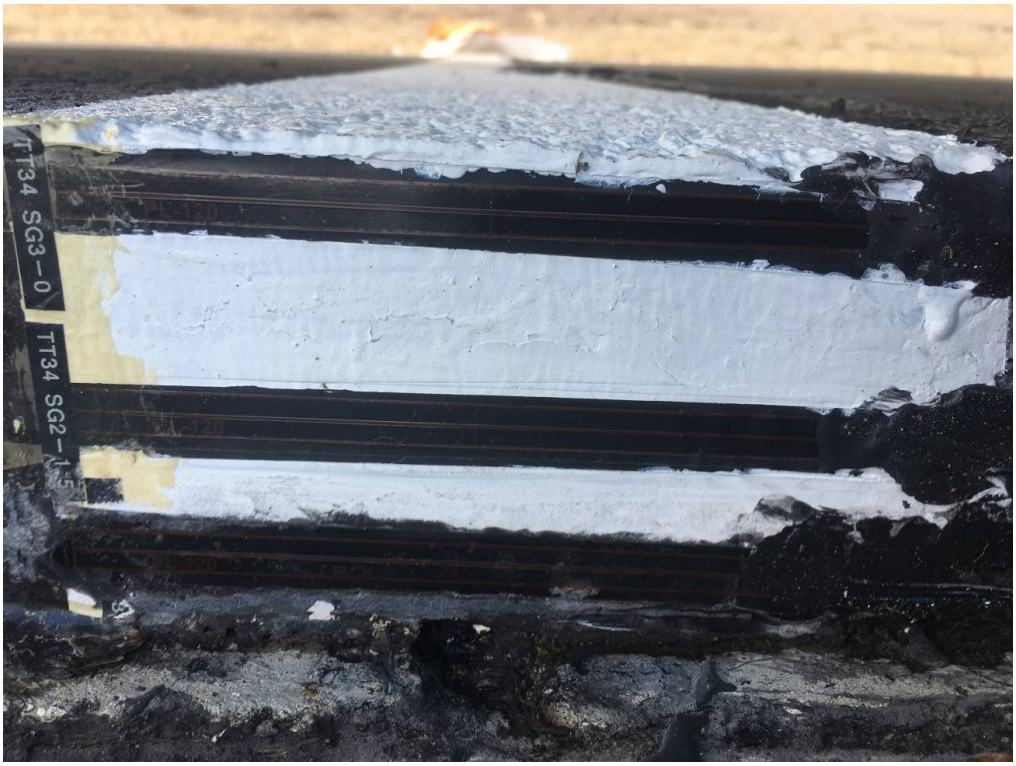

Figure A.19: Joint#3 East Side (02-14-2020)

Figure A.20: Joint#4 West Side (02-14-2020)

Figure A.21: Joint#4 East Side (02-14-2020)

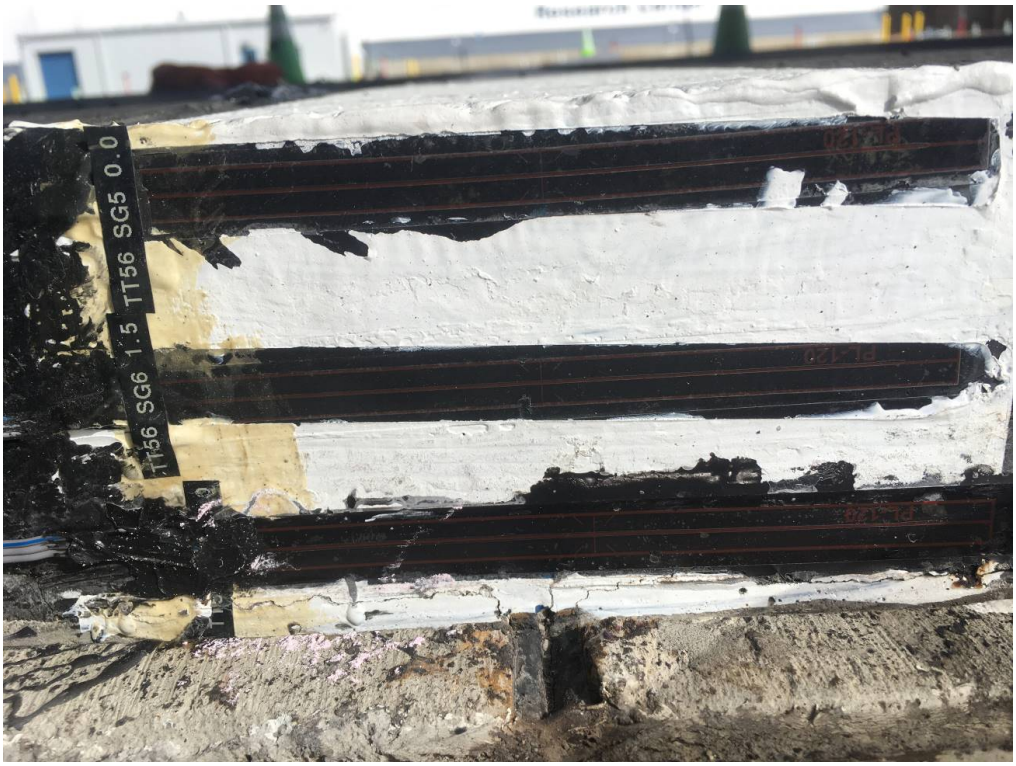

Figure A.22: Joint#5 West Side (02-14-2020)

Figure A.23: Joint#5 East Side (02-14-2020)

Figure A.24: Joint#1 East Side (02-15-2020)

Figure A.25: Joint#1 West Side (02-15-2020)

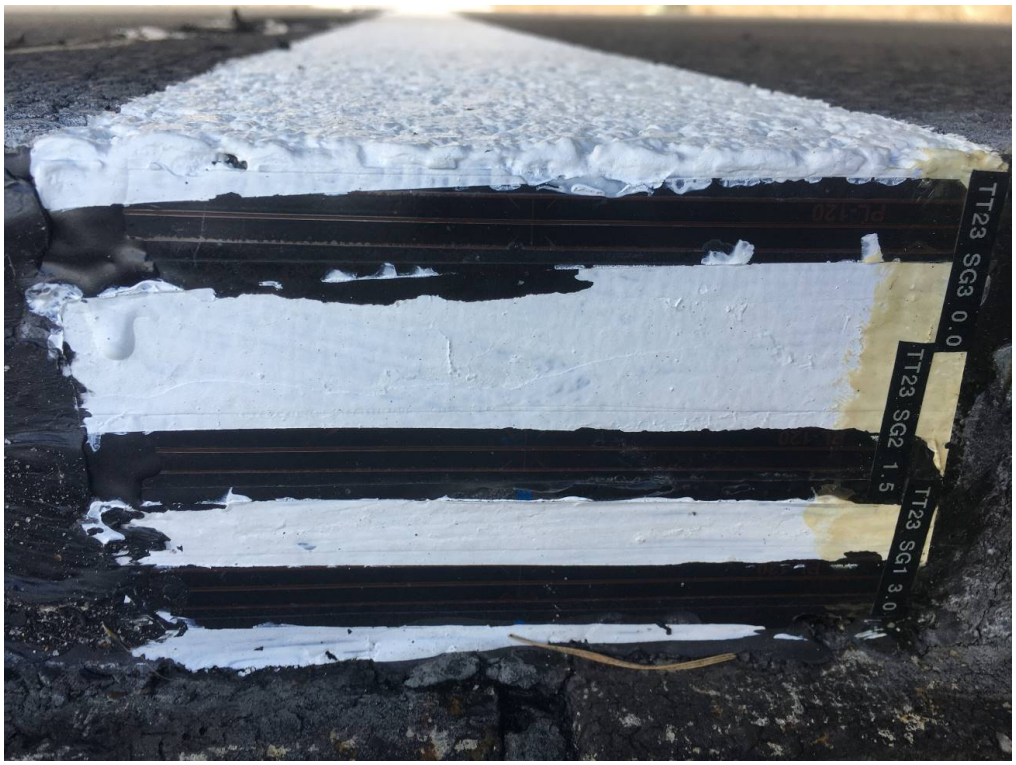

Figure A.26: Joint#2 East Side (02-15-2020)

Figure A.27: Joint#2 West Side (02-15-2020)

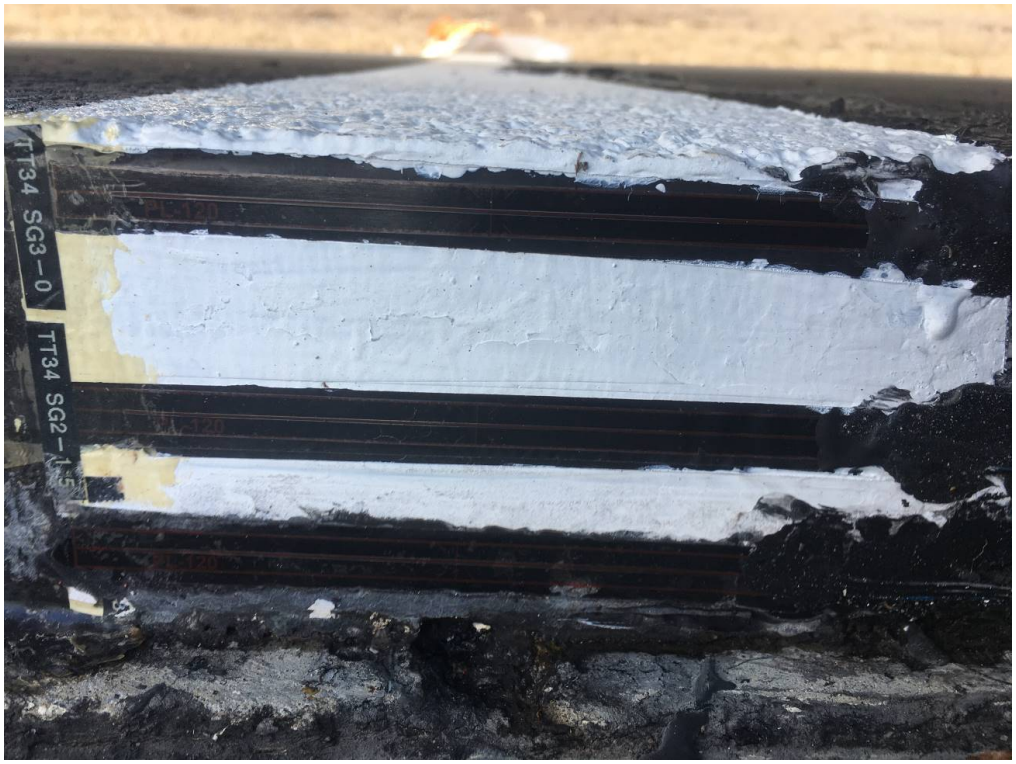

Figure A.28: Joint#3 East Side (02-15-2020)

Figure A.29: Joint#3 West Side (02-15-2020)

Figure A.30: Joint#4 East Side (02-15-2020)

Figure A.31: Joint#4 West Side (02-15-2020)

Figure A.32: Joint#5 East Side (02-15-2020)

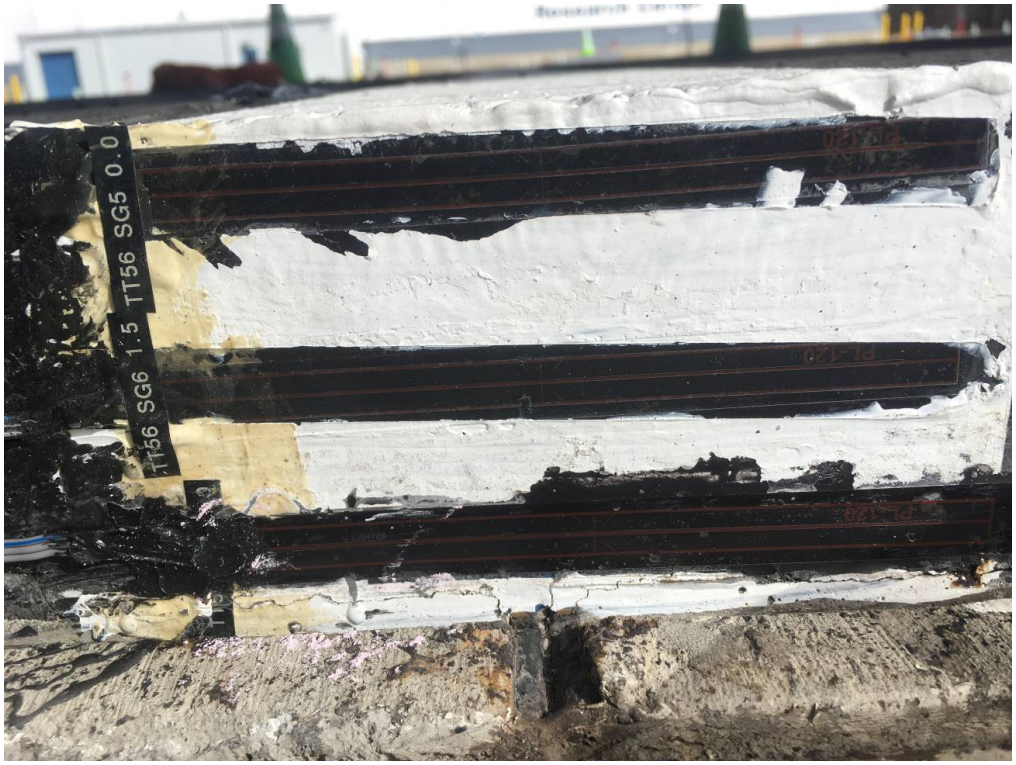

Figure A.33: Joint#5 West Side (02-15-2020)

APPENDIX B—DISTRESS MAP

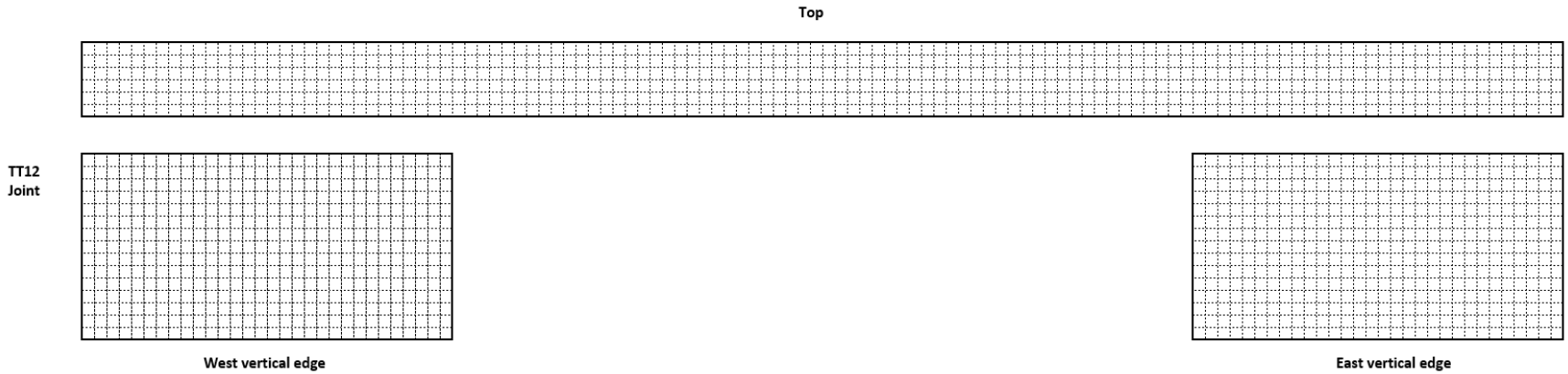

(a) 02-12-2020

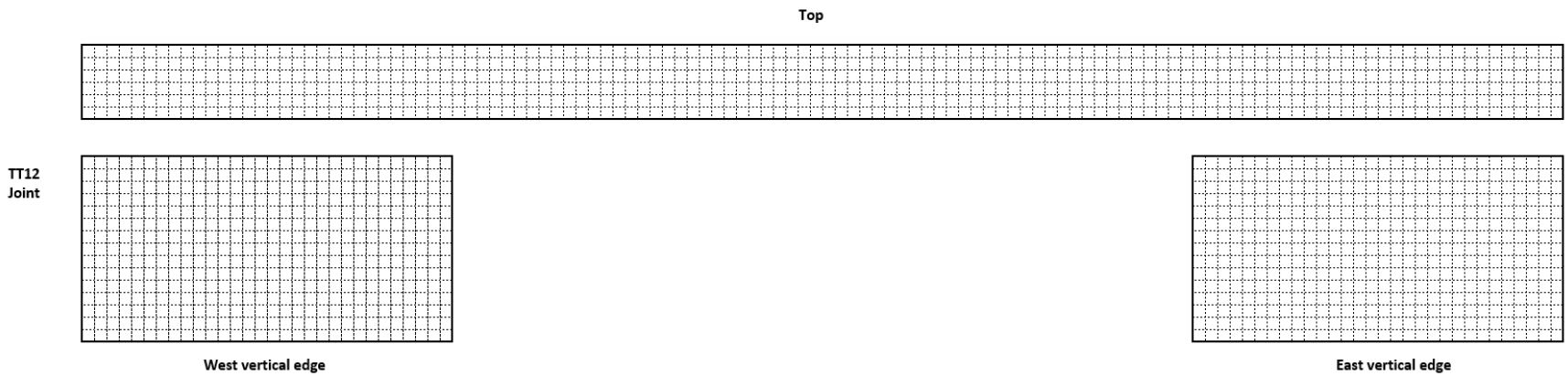

(b) 02-14-2020

Figure B.1: Joint#1 (TT12)

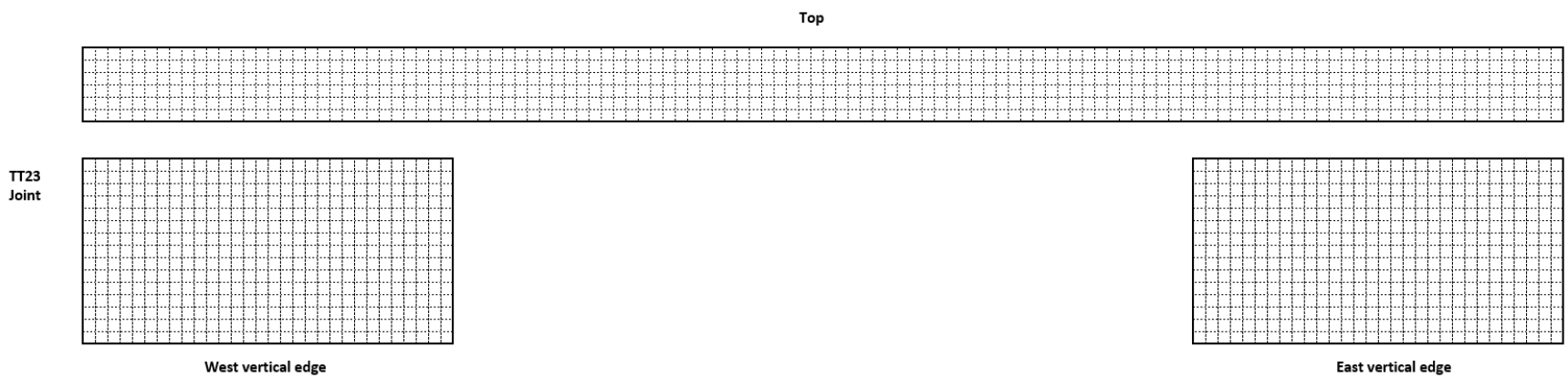

(a) 02-12-2020

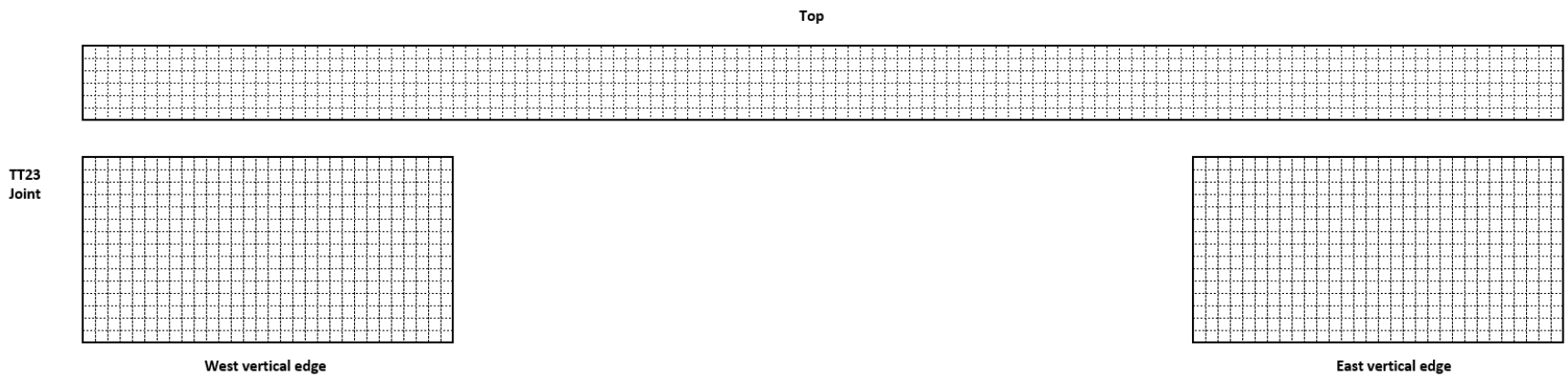

(b) 02-14-2020

Figure B.2: Joint#2 (TT23)

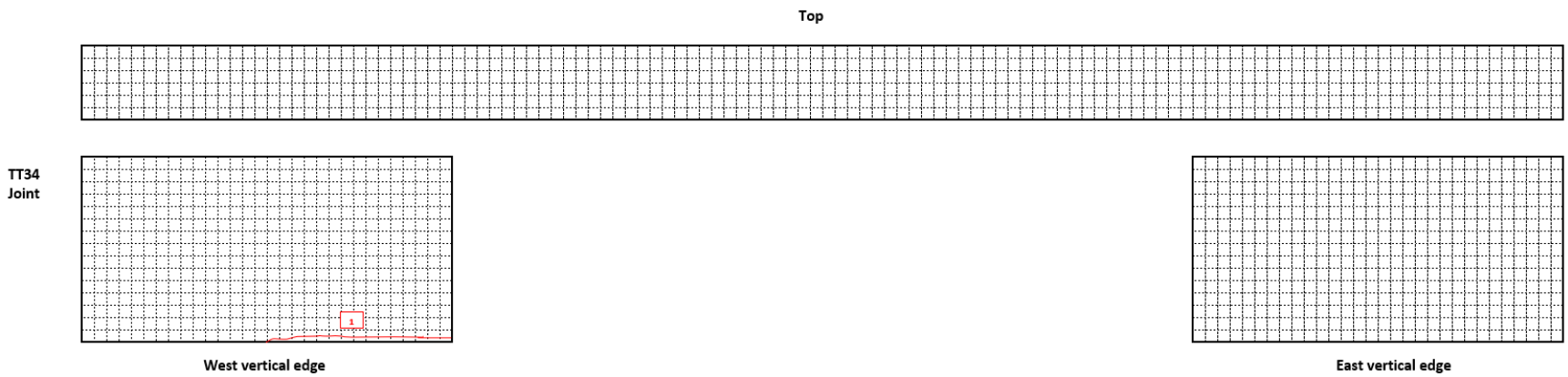

(a) 02-12-2020

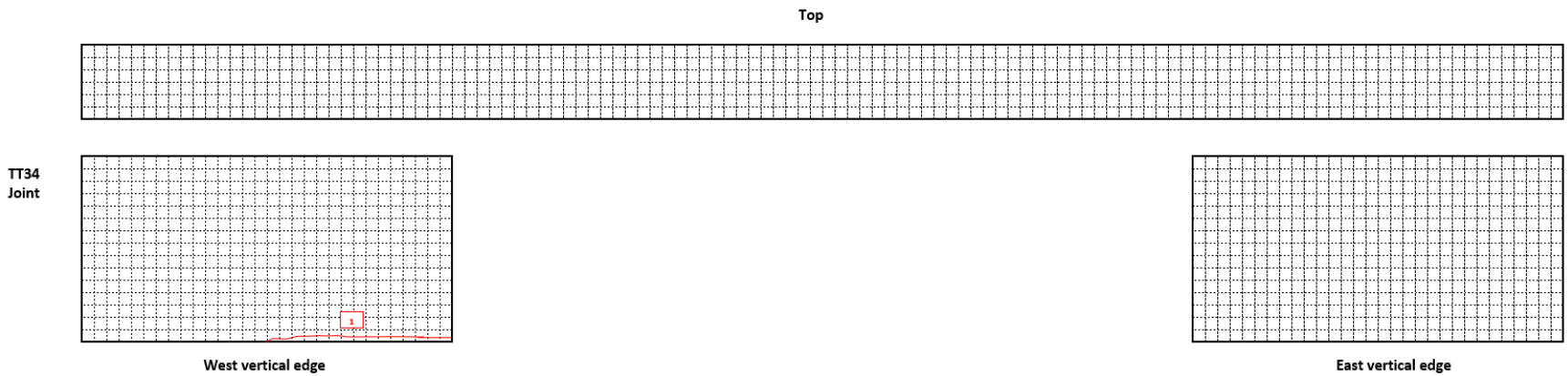

(b) 02-14-2020

COLOR	DATE	INTIALS	TOTAL CYCLES
	12-02-20		1116

Figure B.3: Joint#3 (TT34)

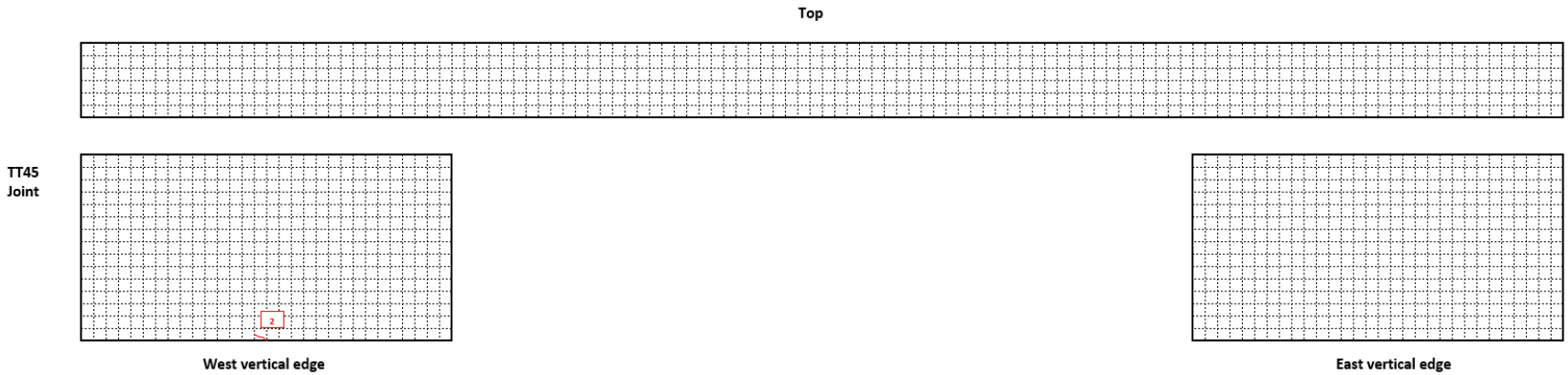

(a) 02-12-2020

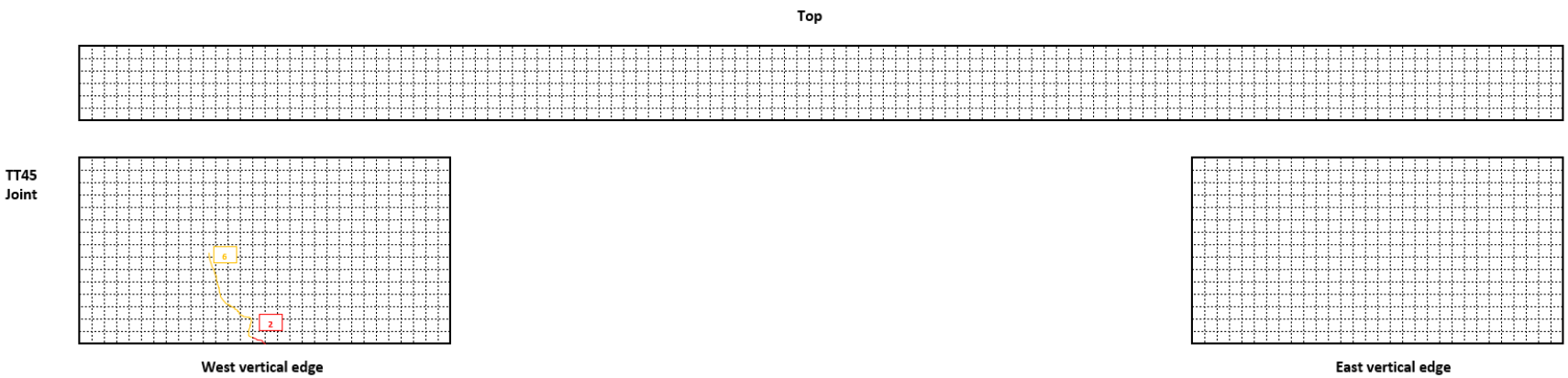

(b) 02-14-2020

COLOR	DATE	INTIALS	TOTAL CYCLES
	12-02-20		1116
	14-02-20		2356

Figure B.4: Joint#4 (TT45)

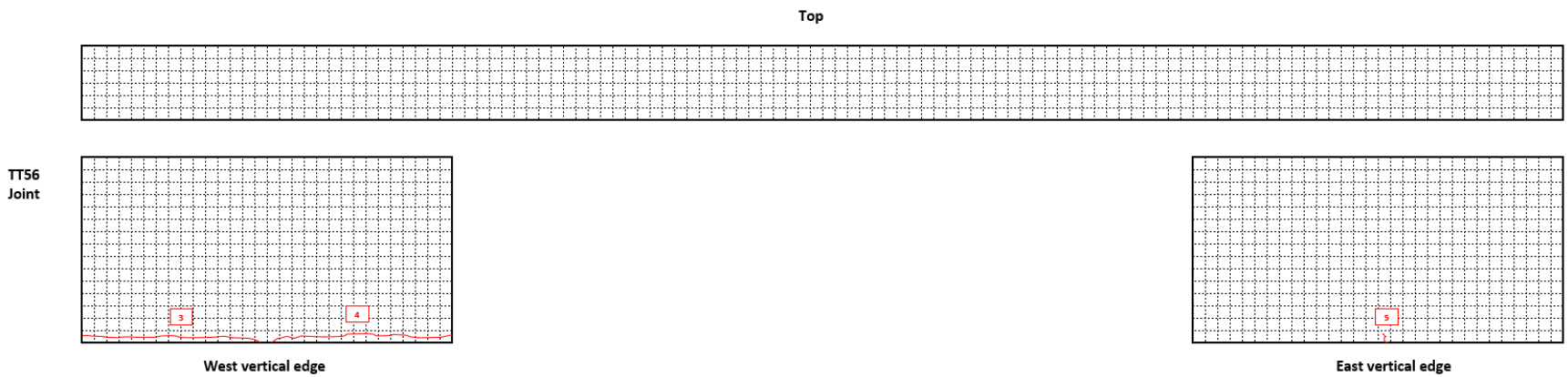

(a) 02-12-2020

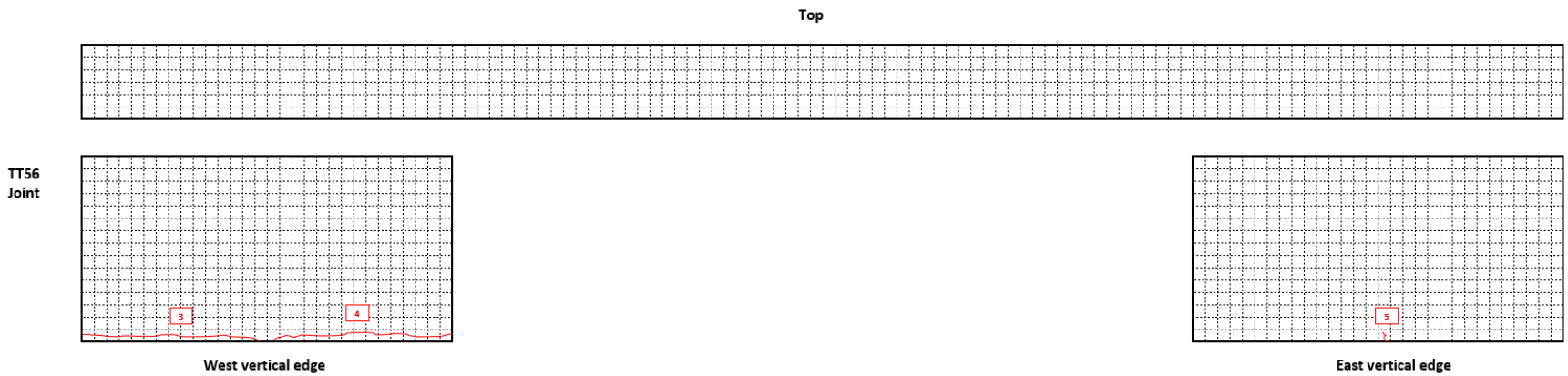

(b) 02-14-2020

COLOR	DATE	INTIALS	TOTAL CYCLES
	12-02-20		1116

Figure B.5: Joint#5 (TT56)

Table B.1: Written Log (02-14-2020)

DATE	TOTAL CYCLES	DISTRESS							NOTES
		DESCRIPTION	NO.	LOCATION					
				X AXIS (in.)		Y AXIS (in.)		Section	
				INITIAL	END	INITIAL	END		
11-02-20	496								No new crack was observed.
12-02-20	1116	Bottom-up crack	1	3	6	0	0.1	TT34 joint, West vertical edge	
12-02-20	1116	Bottom-up crack	2	2.8	3	0.1	0	TT45 joint, West vertical edge	
12-02-20	1116	Bottom-up crack	3	0	2.9	0.1	0	TT56 joint, West vertical edge	
12-02-20	1116	Bottom-up crack	4	3.1	6	0	0.1	TT56 joint, West vertical edge	
12-02-20	1116	Bottom-up crack	5	2.9	3	0.1	0	TT56 joint, East vertical edge	
13-02-20	1736								No new crack was observed.
14-02-20	2356	Bottom-up crack	6	2.1	2.8	1.4	0.1	TT45 joint, West vertical edge	
18-02-20	2976								No new crack was observed.

ASTM E2583 - Light Weight Deflectometer (LWD)

Project: TO 50 CC9
Date: 10/16/2019
Technician: Jason Alcoba
Layer Material: P-401
Test Item: TT & TO
Lift Number: 1 (Final)
Layer Thickness (in): 3
Plate Diameter (in): 6
Number of Sensors: 1

Radial Offset of Sensor (in): 0
Height of Drops (in): 6, 12, 18, 24
Falling Weight : Single Load Assembly
Buffer Type: Hard
Ground Temperature (°F): N/A
Ambient Temperature (°F): 63-69
Equipment Calibration Date: N/A

Preconditioning Drops

Load 1, lbf	Load 2, lbf	Load 3, lbf	Load 4, lbf	Load 5, lbf	% Difference <3%?
1130	1126	1127	1125	1131	Yes

Test Results

Location	Height, in	Load, lbf	Stress, psi	Deflection, mils	Stiffness, ksi	% Difference <3%?
STA 0+7.5; OFF 0.0	6	613.5	22.4	0.3	429.5	Yes
	12	782.2	28.6	0.3	435.4	Yes
	18	948.3	34.6	0.4	472.9	Yes
	24	1133.5	41.4	0.5	435.3	Yes
STA 0+17.5; OFF 0.0	6	603.5	22.1	0.3	398.8	Yes
	12	782.7	28.6	0.3	515.5	Yes
	18	963.7	35.2	0.3	540.5	Yes
	24	1139.5	41.6	0.4	567.6	Yes
STA 0+27.5; OFF 0.0	6	605.6	22.1	0.3	425.0	Yes
	12	780.4	28.5	0.3	437.5	Yes
	18	956.3	34.9	0.4	475.5	Yes
	24	1134.1	41.4	0.4	506.1	Yes
STA 0+37.5; OFF 0.0	6	608.9	22.3	0.2	488.7	Yes
	12	779.7	28.5	0.3	510.8	Yes
	18	956.9	35.0	0.3	547.9	Yes
	24	1139.0	41.6	0.4	557.4	Yes
STA 0+47.5; OFF 0.0	6	613.7	22.4	0.2	474.2	Yes
	12	783.4	28.6	0.3	455.4	Yes
	18	959.5	35.1	0.4	477.8	Yes
	24	1134.3	41.5	0.4	503.8	Yes
STA 0+57.5; OFF 0.0	6	610.3	22.3	0.3	432.8	Yes
	12	776.6	28.4	0.3	485.0	Yes
	18	952.3	34.8	0.4	487.0	Yes
	24	1136.9	41.5	0.5	470.0	Yes
STA 0+97.5; OFF 0.0	6	607.9	22.2	0.2	468.8	Yes
	12	781.4	28.5	0.3	496.1	Yes
	18	951.2	34.8	0.4	483.9	Yes
	24	1135.3	41.5	0.4	490.6	Yes
STA 1+07.5; OFF 0.0	6	616.0	22.5	0.3	444.0	Yes
	12	781.3	28.5	0.3	466.0	Yes
	18	957.8	35.0	0.3	553.9	Yes
	24	1137.2	41.5	0.4	488.2	Yes
STA 1+17.5; OFF 0.0	6	598.6	21.9	0.3	420.4	Yes
	12	779.1	28.5	0.4	403.0	Yes
	18	956.0	34.9	0.4	506.7	Yes
	24	1125.9	41.1	0.4	483.6	Yes

Comments: Results are supposed to be reviewed by GDIT engineer.

Test Performed By: Mir Shahnewaz Arefin and Jason Alcoba
Date: 10-16-19

Reviewed By:
Date:

ASTM E2583 - Light Weight Deflectometer (LWD)

Project: TO 50 CC9
Date: 10/16/2019
Technician: Jason Alcoba
Layer Material: P-401
Test Item: TT & TO
Lift Number: 1 (Final)
Layer Thickness (in): 3
Plate Diameter (in): 6
Number of Sensors: 1

Radial Offset of Sensor (in): 0
Height of Drops (in): 6, 12, 18, 24
Falling Weight : Single Load Assembly
Buffer Type: Hard
Ground Temperature (°F): N/A
Ambient Temperature (°F): 63-69
Equipment Calibration Date: N/A

Preconditioning Drops

Load 1, lbf	Load 2, lbf	Load 3, lbf	Load 4, lbf	Load 5, lbf	% Difference <3%?
1130	1126	1127	1125	1131	Yes

Test Results

Location	Height, in	Load, lbf	Stress, psi	Deflection, mils	Stiffness, ksi	% Difference <3%?
STA 1+27.5; OFF 0.0	6	605.55	22.15	0.3	448.8	Yes
	12	776.25	28.35	0.3	458.0	Yes
	18	955.8	34.9	0.4	468.6	Yes
	24	1145.5	41.8	0.5	471.8	Yes
STA 1+37.5; OFF 0.0	6	610.6	22.3	0.3	442.9	Yes
	12	784.2	28.6	0.3	465.5	Yes
	18	958.55	35	0.4	461.65	Yes
	24	1134.2	41.45	0.4	483.7	Yes
STA 1+47.5; OFF 0.0	6	609.65	22.25	0.3	445.5	Yes
	12	779.75	28.5	0.3	483.85	Yes
	18	947.2	34.6	0.5	381.5	Yes
	24	1128.45	41.2	0.5	456.7	Yes

Comments: Results are supposed to be reviewed by GDIT engineer.

Test Performed By: Mir Shahnewaz Arefin and Jason Alcoba
Date: 10-16-19

Reviewed By:
Date:

APPENDIX D – HMA OVERLAY MODULUS

HWD deflection based backcalculation of a thin surface layer is not always reliable. In the past, several researchers adopted LWD testing to evaluate HMA layer (Burhani, 2016, Commuri et al. 2012, and Guzzarlapudi et. 2016). An attempt was made to estimate the combined modulus using the LWD data. However, Odemark's multi-layered equivalent layer thickness principle was not applicable, because (a) LWD testing was not conducted atop P-501MR; and (b) inaccurate thickness transformation of four layers with highly variable material strength. An alternative performance indicator, namely 'HMA Overlay Modulus', was introduced as a part of the research effort to explore the possibility of capturing localized P-401MR damage in the future pavement condition monitoring. This indicator was computed using the ratio of stress (σ) and strain (ε). While vertical stress (σ) was readily available from the LWD load (P) and loading area (A), strain (ε) had to be carefully determined such that the LWD load was low enough and surface deflections only reflected the deformation in the HMA overlay.

During RC Outdoor Phase-I construction, HWD tests were conducted atop P-501MR at varying load levels. For demonstration purposes, figure D.1 shows an example of HWD deflections from Slab TO2. Figure D.1 clearly shows linearity in deflection trend at loads as high up to 12 kips. Above 12kip load level, it is difficult to judge a loading magnitude when the deflection trend will shift from being linear to non-linear. However, it is safe to assume that the deflection trend will follow the same linearity at loads lower than 12kip load level. A linear correlation between the HWD load and deflection suggested an HWD load of 650.06 lbs for negligible deflection. Because the LWD load corresponding to 6-inch drop height was 633 lbs, it was therefore speculated negligible deflection at and below the surface of P-501MR at this load level. Based on this speculation, the simplified formulation to determine the vertical strain in P-401MR overlay was as follows:

$$\varepsilon_{overlay} = \frac{\delta}{h_{overlay}} \qquad \text{Eq. 1}$$

where $\varepsilon_{overlay}$ = vertical strain in P-401MR overlay; δ = deformation in P-401MR equal to LWD deflection; and $h_{overlay}$ = thickness of P-401MR overlay.

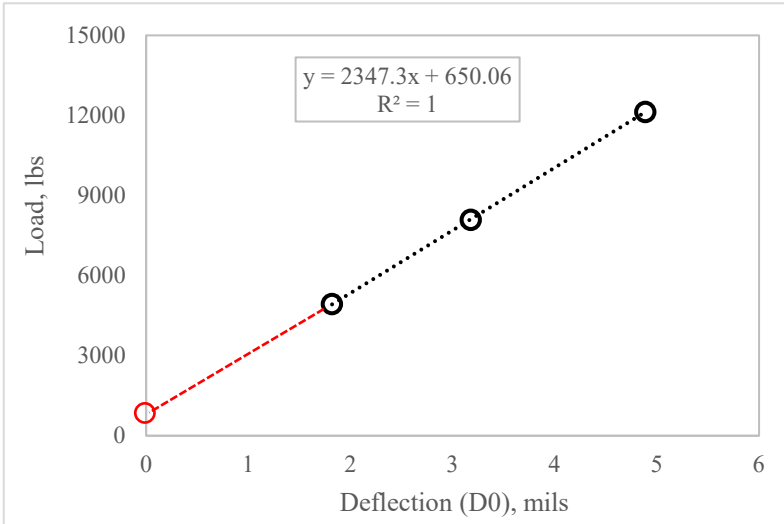

Figure D.1: Correlation between HWD Load and Deflection.

Based on the above simplified formulation, strain (ε) was first calculated from the LWD deflections corresponding to 6-inch drop height and overlay thickness, then 'HMA Overlay Modulus' of P-401MR was obtained using the following relationship:

$$HMA\ Overlay\ Modulus = \frac{\sigma_{LWD}}{\varepsilon_{overlay}} \qquad \text{Eq. 2}$$

where σ_{LWD} = vertical stress, derived from LWD testing atop P-401MR surface. As tabulated in table D.1, the overlay modulus was more consistent within the TO section compared to the TT section.

Table D.1: Summary of HMA Overlay Modulus from LWD Test

Test Item	Slab ID	Load[1], lbs	Deflection[2,3], mils	HMA Overlay Modulus (ksi)	Average	Standard Deviation	COV (%)
TT	TT1	613.5	0.3	224.0	259.9	58.4	22.5
	TT2	603.5	0.3	221.0			
	TT3	605.6	0.3	221.0			
	TT4	608.9	0.2	334.5			
	TT5	613.7	0.2	336.0			
	TT6	610.3	0.3	223.0			
TO	TO1	607.9	0.2	333.0	240.7	45.3	18.8
	TO2	616.0	0.3	225.0			
	TO3	598.6	0.3	219.0			
	TO4	605.6	0.3	221.5			
	TO5	610.6	0.3	223.0			
	TO6	609.7	0.3	222.5			

Note 1: Load level corresponding to 6-inches drop height, at which HMA Overlay Modulus was computed
Note 2: Deflection at the center of the loading plate
Note 3: All LWD measured deflections were assumed to be contributed by the deformation in HMA overlay
Note 4: Pavement temperature range: 68.3-68.9 °F

REFERENCES

Burhani, A. (2016). Correlation Study on the Falling Weight Deflectometer and Light Weight Deflectometer for the Local Pavement Systems. M.Sc. Thesis, Ohio University, Ohio, USA.

Commuri, S., Zaman, M., Beainy, F., Singh, D., Nazari, M., Imran, S., and Barman, M. (2012). Pavement Evaluation Using a Portable Lightweight Deflectometer. Oklahoma Transportation Center, Report Numbers: OTCREOS11.1-14-F, Oklahoma, USA.

Guzzarlapudi, S. D., Adigopula, V. K., and Kumar, R. (2016). Comparative Studies of Lightweight Deflectometerand Benkelman Beam Deflectometer in Low Volume Roads. Journal of Traffic and Transportation Engineering, 3(5), 438-447.

APPENDIX E—JOINT DISPLACEMENT GAGE PLOTS

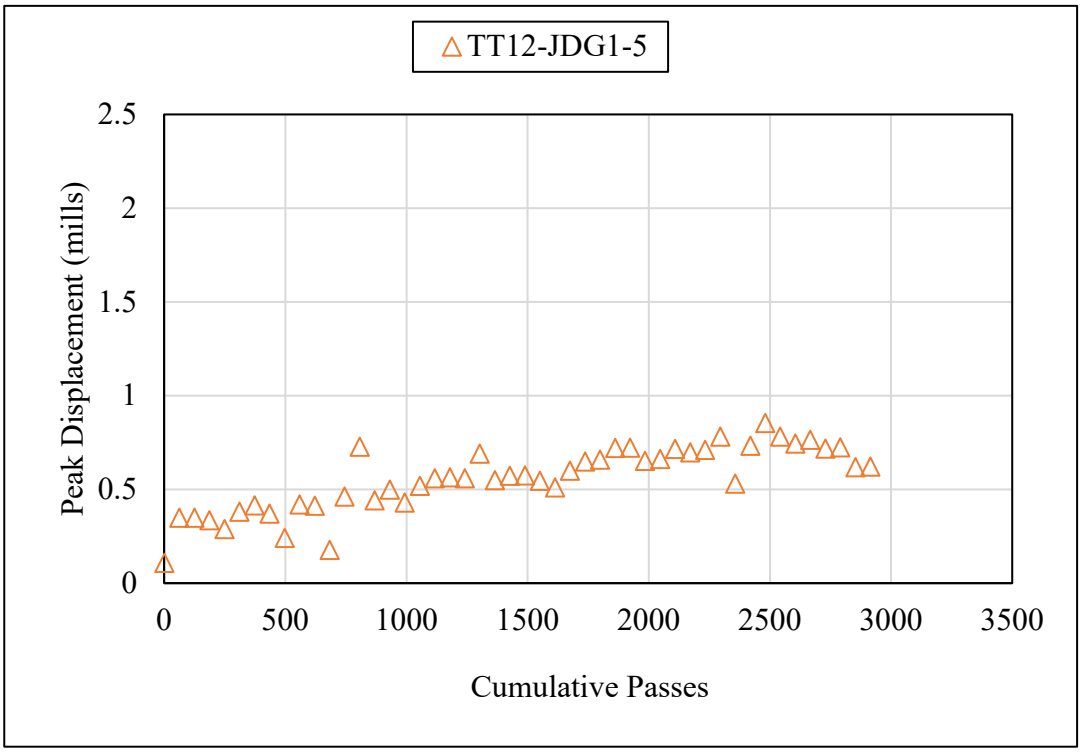

Figure E.1: TT12 East Side JDG Plots

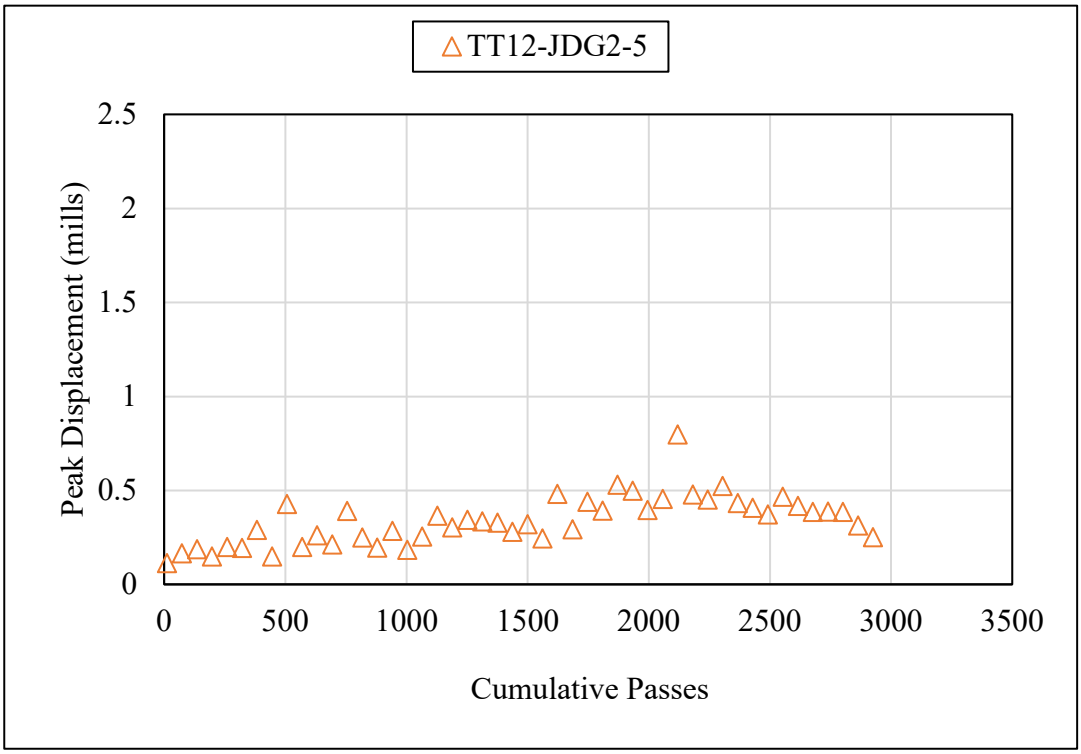

Figure E.2: TT12 West Side JDG Plots

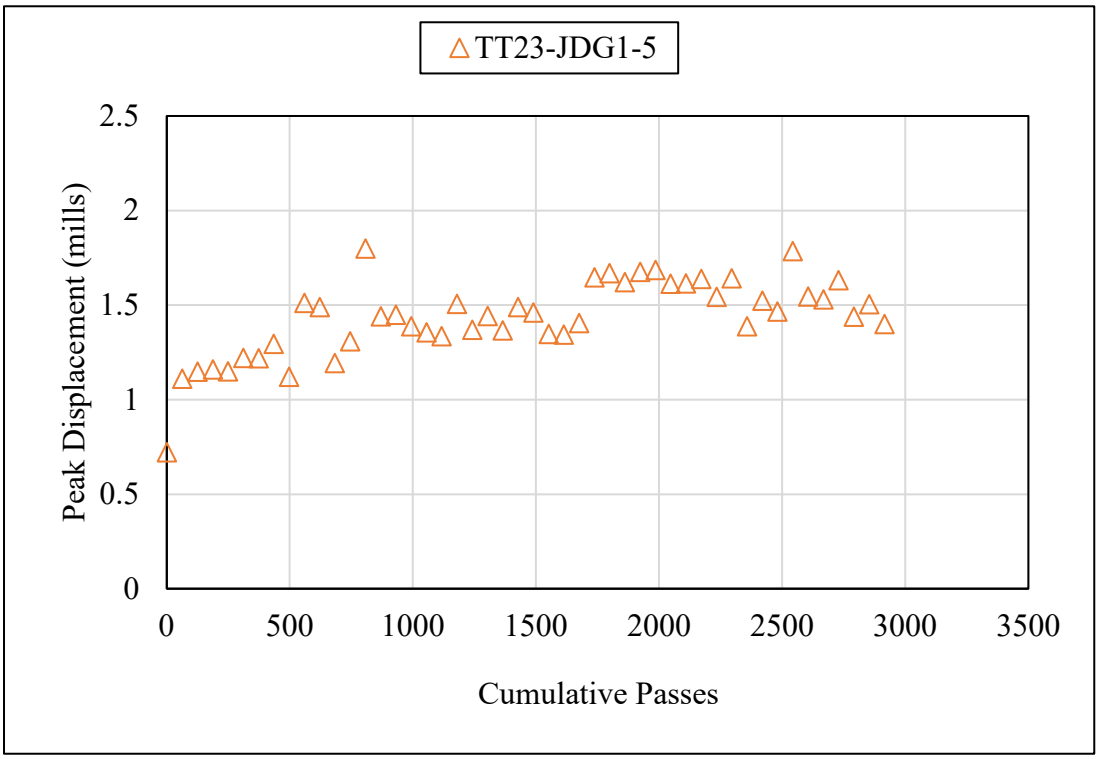

Figure E.3: TT23 East Side JDG Plots

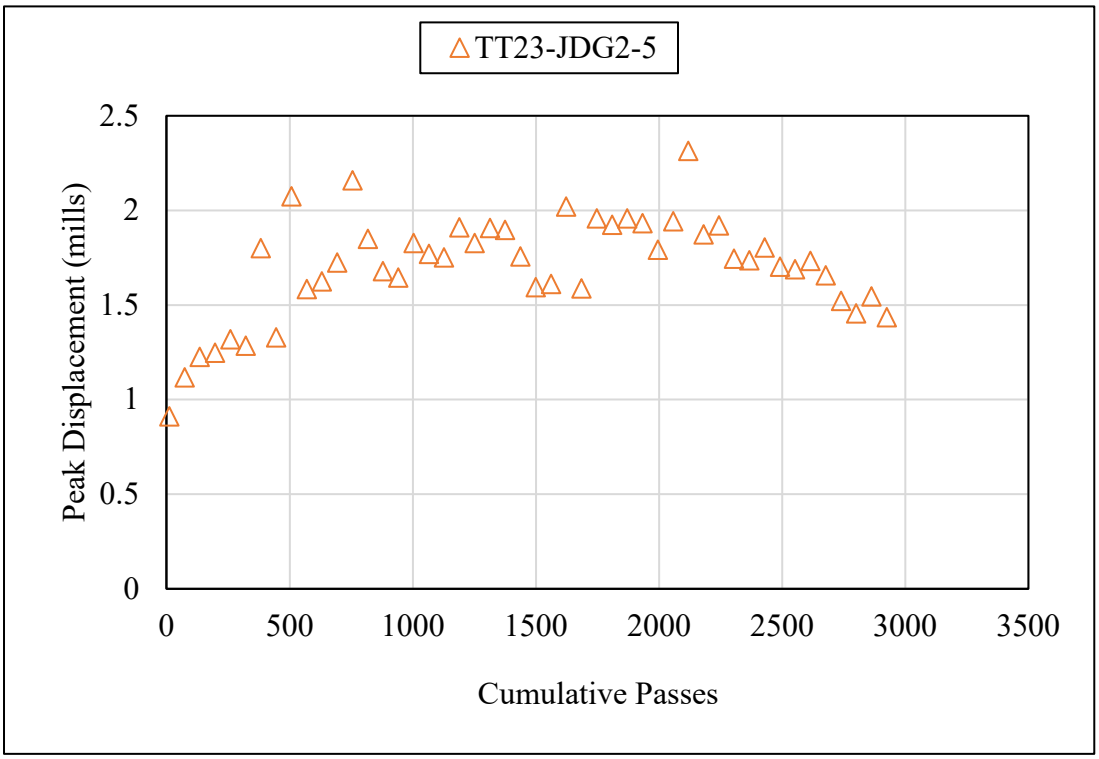

Figure E.4: TT23 West Side JDG Plots

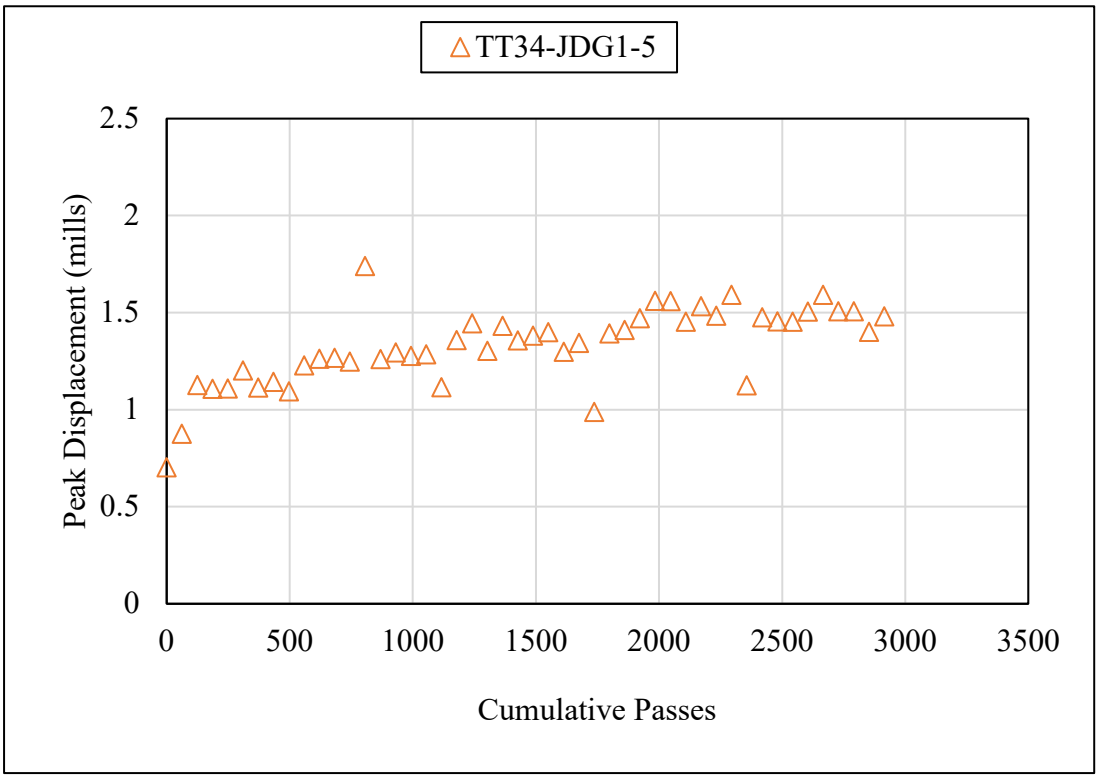

Figure E.5: TT34 East Side JDG Plots

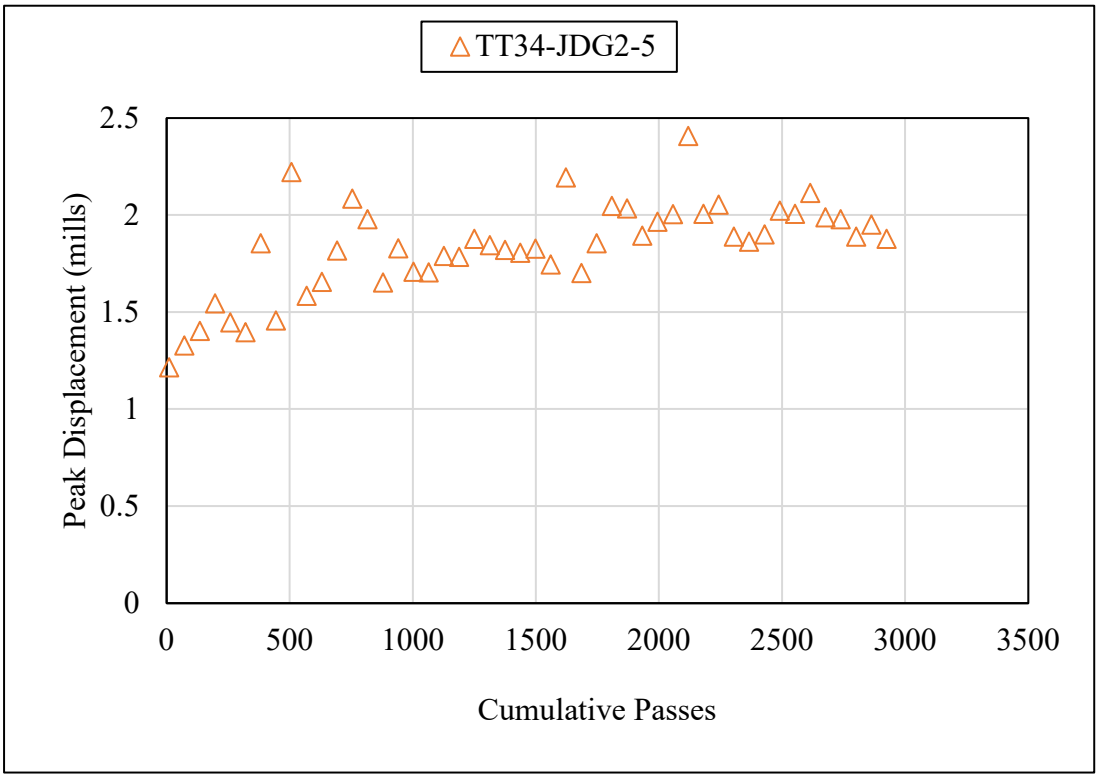

Figure E.6: TT34 West Side JDG Plots

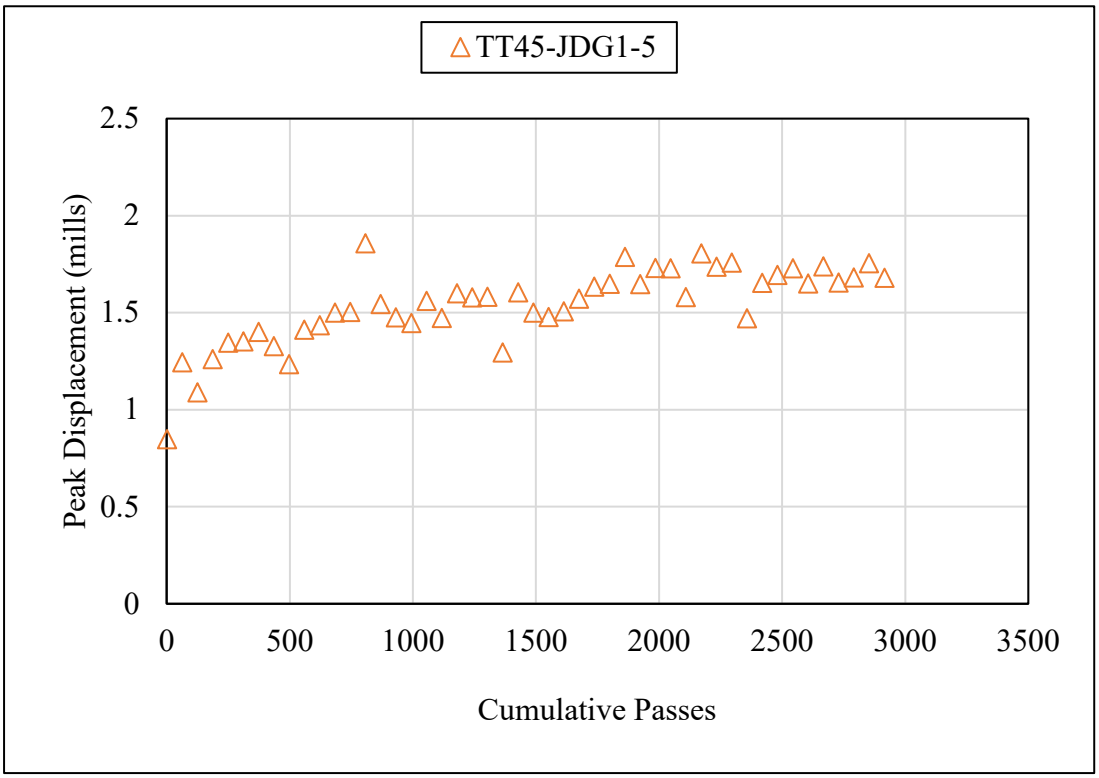

Figure E,7: TT45 East Side JDG Plots

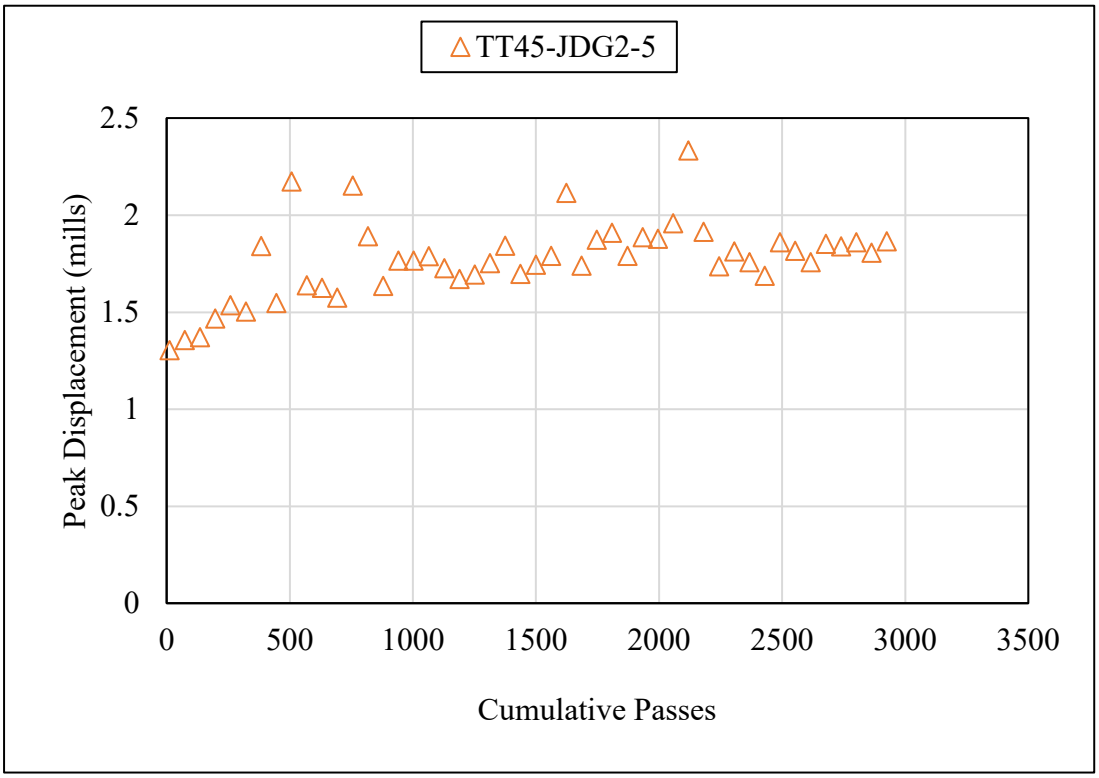

Figure E.8: TT45 West Side JDG Plots

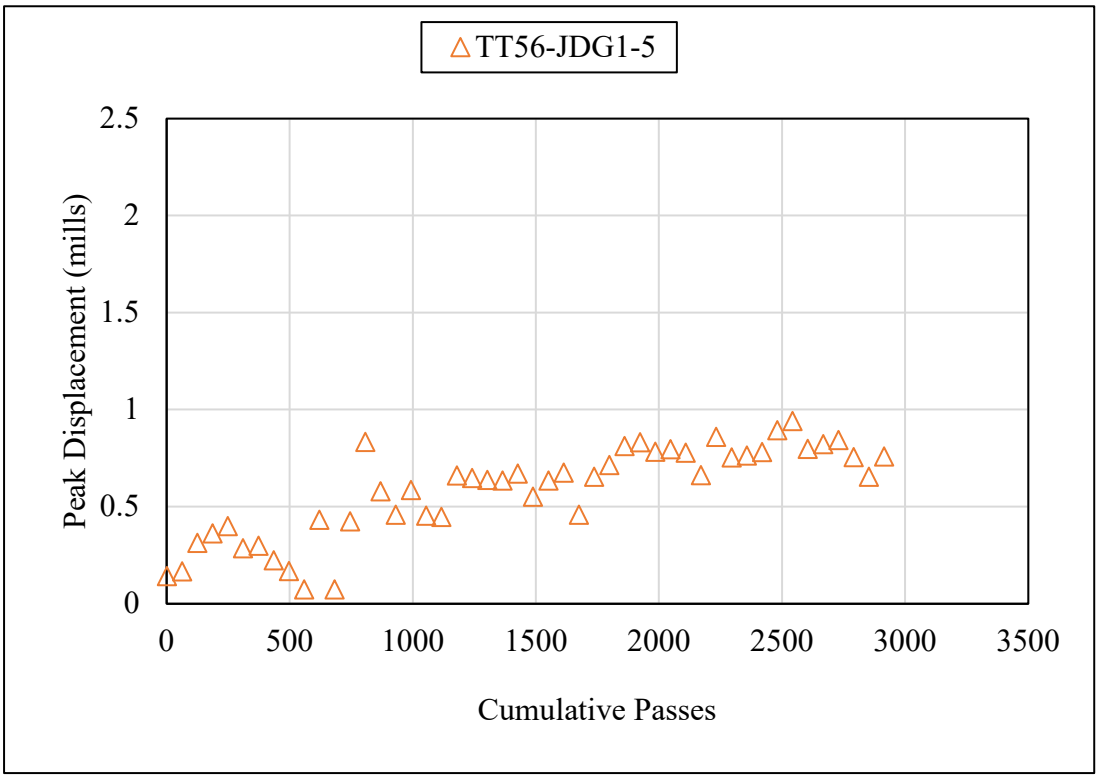

Figure E.9: TT56 East Side JDG Plots

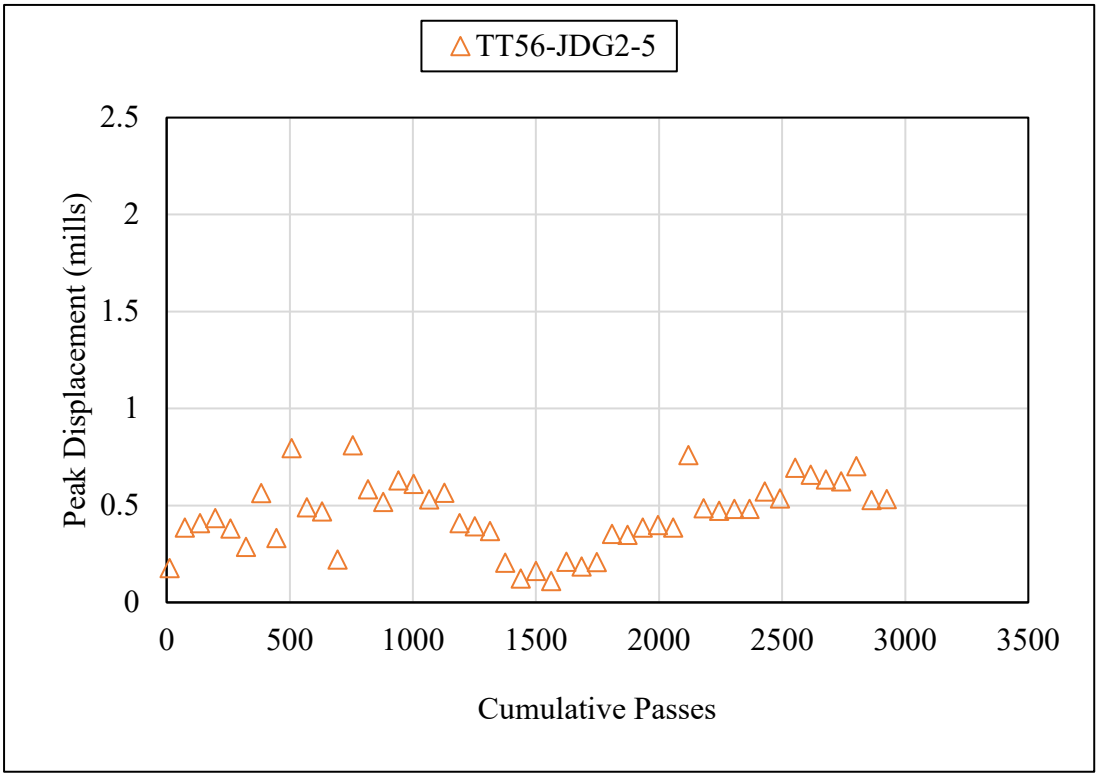

Figure E.10: TT56 West Side JDG Plots